Title
Effects of vibrational strong coupling on ground-state chemical kinetics

Permalink
https://escholarship.org/uc/item/6062v5fz

Author
Campos Gonzalez Angulo, Jorge Arturo

Publication Date
2021

Peer reviewed|Thesis/dissertation

UNIVERSITY OF CALIFORNIA SAN DIEGO

Effects of vibrational strong coupling on ground-state chemical kinetics

A dissertation submitted in partial satisfaction of the
requirements for the degree
Doctor of Philosophy

in

Chemistry

by

Jorge Arturo Campos Gonzalez Angulo

Committee in charge:

    Professor Joel Yuen-Zhou, Chair
    Professor Richard Averitt
    Professor Patricia Jennings
    Professor Katja Lindenberg
    Professor Francesco Paesani

2021

The dissertation of Jorge Arturo Campos Gonzalez Angulo is approved, and it is acceptable in quality and form for publication on microfilm and electronically:

_____

_____

_____

_____

_____

Chair

University of California San Diego

2021

EPIGRAPH

Clarity is a fair distribution

of light and shadow.

—Johann Georg Hamann

TABLE OF CONTENTS

LIST OF FIGURES

LIST OF TABLES

Chapter 5, in full is currently being prepared for submission for publication of the material. "Generalization of the Tavis-Cummings model for multi-level anharmonic systems". Campos-Gonzalez-Angulo, Jorge A.; Ribeiro, Raphael F.; Yuen-Zhou, Joel. The dissertation author was the primary investigator and author of this material.

VITA

2009	B. Sc. in Chemistry *Mención Honorífica*, Universidad Nacional Autónoma de México
2011-2014	Lecturer, Universidad Nacional Autónoma de México
2012	M. Sc. in Chemical Sciences *Mención Honorífica*, Universidad Nacional Autónoma de México
2014-2015	Graduate Student Instructor, University of California Berkeley
2016	Main Instructor, Colegio Internacional de Líderes
2016-2017	Graduate Teaching Assistant, University of California San Diego
2019-2020	Graduate Writing Consultant, University of California San Diego
2021	Ph. D. in Chemistry, University of California San Diego

PUBLICATIONS

Campos-Gonzalez-Angulo, J. A., Wiesehan G., Ribeiro, R. F. & Yuen-Zhou, J. (2020)"Computational method for highly-constrained molecular dynamics of rigid bodies: coarse-grained simulation of auxetic two-dimensional protein crystals.", *The Journal of Chemical Physics*, *152*(23), 244102.

Campos-Gonzalez-Angulo, J. A., & Yuen-Zhou, J. (2020)"Polaritonic normal modes in transition state theory.", *The Journal of Chemical Physics*, *152*(16), 161101.

Campos-Gonzalez-Angulo, J. A., Ribeiro, R. F., & Yuen-Zhou, J. (2019). "Resonant catalysis of thermally activated chemical reactions with vibrational polaritons." *Nature communications*, *10*(1), 1-8.

Ribeiro, R. F., Martínez-Martínez, L. A., Du, M., Campos-Gonzalez-Angulo, J., & Yuen-Zhou, J. (2018). "Polariton chemistry: controlling molecular dynamics with optical cavities." *Chemical science*, *9*(30), 6325-6339.

Martínez-Martínez, L. A., Ribeiro, R. F., Campos-González-Angulo, J., & Yuen-Zhou, J. (2017). "Can ultrastrong coupling change ground-state chemical reactions?" *ACS Photonics*, *5*(1), 167-176.

Campos, J. A., & Hirsch, J. G. (2011). "Single-molecule magnets and the Lipkin-Meshkov-Glick model." *Rev. Mex. Fıs. S*, *57*(3), 56-61.

Campos, Jorge A. (2013). "Sistemas cuánticos individuales." *Educación química*, *24*(1), 82-85.

Ruiz Herrera, Brenda Lizette, Jorge Arturo Campos González Angulo, & Norah Barba Behrens. (2008)."Cofactor FeMco (M= Mo, V, Fe) en la nitrogenasa." *Educación química*. *19*(1), 34-41.

Navarrete, J. M., J. Campos, T. Martínez, and L. Cabrera. (2005). "Determination of potassium traces in foodstuffs by natural 40K radiation." *Journal of Radioanalytical and Nuclear Chemistry*. *265*(1) 133-135.

ABSTRACT OF THE DISSERTATION

Effects of vibrational strong coupling on ground-state chemical kinetics

by

Jorge Arturo Campos Gonzalez Angulo

Doctor of Philosophy in Chemistry

University of California San Diego, 2021

Professor Joel Yuen-Zhou, Chair

The energy of an electromagnetic field can be stored with the help of confining devices, known as optical cavities, that localize it temporarily. If a dielectric material with a high dipole moment shares space with the confined field, the optical properties of the system correspond to neither of its components but rather to a light-matter hybrid, whose excitations are called polaritons. While experimental realizations of this phenomenon date back to decades ago, it was not until the last decade when advances in sample preparation technologies enabled the investigation of the consequences of polariton formation on the observables related to the material. In this regard, a particularly active area of interest is the study of chemical reactivity under strong-light matter coupling. A striking development in the area is the observation that reactions inside infrared

cavities, which couple to bond vibrations, experience a change in their rate even without any energy source other than room temperature. This effect has been observed in various reactions, including organometallic and carbonyl substitutions, and even in enzymatic processes. Consistently, these experiments show that rate modification is subject to the same conditions as polariton formation: the requirement of resonance between cavity and vibration and the intensification of the effect with the concentration of the sample. However, cavity quantum electrodynamics (CQED), the same theory that has successfully explained and predicted the optical properties of polaritons for decades, at first glance suggests that a local process such as a chemical reaction should not be affected by an essentially delocalized phenomenon such as light-matter coupling. This dissertation presents how CQED combines with two approaches to chemical rate theory: adiabatic reactions described within transition state theory (TST), and non-adiabatic processes, described by Marcus' theory of charge transfer. In the first case, it is found that under typical experimental conditions, a description at the level of TST predicts that vibrational strong light-matter coupling should produce no effect on the chemical rate. In contrast, for non-adiabatic processes, it is possible to conceptualize rate alteration in terms of a modified distribution of activation energies that accounts for the presence of polariton modes. Additionally, this work presents a group-theoretical method to simplify the description of a collective of identical oscillators with an arbitrary structure to a cavity mode, which may have applications to understanding chemical processes and non-linear response phenomena.

Chapter 1

Introduction

The shape of the contemporary world could not be understood without the ability of humankind to artificially modify substances. From the materials in our everyday items to the medicines with which we intend to alleviate our ailments, the ever-increasing landscape of chemical synthesis defines how people go about their lives and interact among themselves and their surrounding world. In many instances, the complexity of the compounds to prepare creates a demand for highly tailored processes that maximize the yield of a desired product while minimizing the formation of subproducts. In this regard, electromagnetic (EM) radiation, given the high specificity with which it interacts with the energetics of atoms and molecules, emerges as an obvious tool to manipulate the outcome of a chemical transformation. Thus, mode-selective photochemistry and optimal quantum control were developed with the aim of promoting or hindering bond dissociation through laser-induced excitations [1, 2].

Among the many phenomena related to the interaction between matter and light, those due to vacuum fluctuations stand out. Early developments in the research of those phenomena include the correction to the energy levels observed by Willis Lamb in the hydrogen spectrum [3], the realization by Edward Mills Purcell that the rate of spontaneous emission by a quantum emitter should be enhanced when coupled to a tuned resonant electric circuit [4], as well as

1

the examination by Hendrik Casimir and Dirk Polder of the force that these fluctuations induce between an atom and a conducting plane [5]. These advancements helped cement the area of cavity Quantum Electrodynamics, which deals with describing the properties resulting from the reciprocal action between the distribution of electric charges in a material and a long-lived spatially confined electromagnetic field [6].

Through its electric dipole moment, a material can absorb the energy stored in the EM field. This process results in the population of the excited states of the material. The interaction is considered weak when either component loses energy at a rate such that the system quickly reaches thermalization after a single occurrence of absorption followed by emission. In these circumstances, the properties of the system are mostly those of the material, and the EM field plays only a perturbative role [7]. In contrast, under conditions where energy dissipation is minimized or the interaction is enhanced several absorption/emission cycles occur before the system equilibrates; thus, the population in the excited states oscillates at the so-called *Rabi frequency* [8,9]. In this *strong coupling* regime, the system displays an energy spectrum that corresponds with neither of its components; this observation is interpreted as the formation of hybrid entities in which the contributions from both material and field are comparable. The excitations resulting from the mixture of light and matter come from the polarization field; hence, they receive the name of *polaritons* [10]. As first observed with Cs atoms at cryogenic temperatures [11], a signature of polariton formation is the bifurcation of the absorption –or transmission– signal corresponding to the frequencies at which the material and the confined light are in resonance. The difference in frequency between the straying signals corresponds to the Rabi frequency; for this reason, this quantity is also usually referred to as *Rabi splitting*.

From the perspective of the EM field, there are two ways to control the properties of the system to increase the light-matter interaction intensity. First, since the dipolar interaction is proportional to it, the field intensity ought to be amplified. The electric field amplitude is inversely proportional to the square root of the so-called mode volume; therefore, this amplification occurs

2
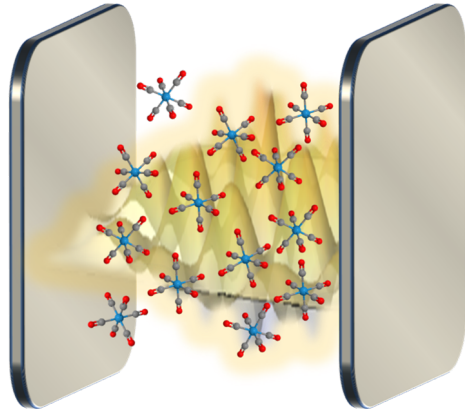
Figure 1.1: Fabry Perot resonator hosting organic molecules.

when the field is highly localized in space. Second, losses need to be minimized, which can be achieved by forcing the field to reside within the mode volume as long as possible. Devices that incorporate both approaches to various extents are known as resonators or cavities; there are several kinds of them, and their particular features are widely discussed elsewhere [12–14]. Two of particular interest are plasmonic resonators and Fabry-Perot (FP) interferometers. In a plasmonic cavity, an external source of light excites the electron density of a conductor, i.e., a plasmonic mode, creating a highly intense evanescent EM field at the surface of the conductor, thus achieving the sought-out mode confinement. In contrast, a FP resonator (fig. 1.1) is composed of two highly reflective surfaces parallel to each other separated by a dielectric medium [15]. Although the mode volumes in these devices are relatively large, the reflective surfaces act as a photon trap, effectively storing the EM energy for as long as 100 fs [16].

From the viewpoint of the material, energy losses can be reduced by lowering the temperature. Additionally, the dipolar interaction intensity scales as the square root of the number of dipoles within the mode volume. This fact implies that the strong coupling regime can be achieved simply by increasing the concentration of quantum emitters inside the active volume of a resonator [17]. Beyond atoms, polaritons have been fabricated from inorganic semiconductors [18], quantum dots [19], color centers [20], superconducting circuits [21], and Van der Waals materials [22]. Of particular interest are organic semiconductors, which offer high

3

photoluminescence quantum yields, large transition dipole moments, narrow linewidths, and a vast flexibility to build photonic devices [23, 24].

The peculiarities of polaritonic systems, such as a modified energy spectrum and the impregnation of photonic character to material degrees of freedom, have been exploited for purposes as diverse as Bose-Einstein condensation [25], quantum computing [26], room temperature lasing [27, 28], nonlinear optical responses [29, 30], reversible optical switching [31], enhanced charge conductivity [32] and long-range excitation energy transfer [16, 33]. Theoretical considerations on the latter phenomenon [34, 35] have led to the proposal of the innovative idea of remote catalysis [36].

Of utmost interest are the efforts in the direction of employing cavity resonances to control chemical reactivity [37–43]. In [44], Hutchison and co-workers demonstrated for the first time an observable effect of strong light-matter coupling on a chemical reaction. Specifically, the authors observed a Rabi-splitting-dependent slowdown in the photoisomerization of spiropyran to merocyanine when the latter is coupled to the cavity. Another example of cavity-modified excited-state chemistry can be found in [45], where Munkhabat and collaborators observe suppression of photo-oxidation for a dye aggregate by tuning the cavity to the exciton frequency of the sample. These and other excited-state chemical processes [46, 47] have motivated an intense theoretical interest in the field of polaritonic chemistry [48–53], and can be generally understood based on how light-matter coupling modifies the relaxation channels available during the processes.

Most of the works referenced so far regarding chemical modifications focus on exciton-polaritons, i.e., the molecular degree of freedom resonant with the cavity mode is an electronic excitation. However, in the pursuit of mode selective chemistry, it is reasonable to explore the scenarios where the excitations engaging with the EM field are those in bond vibrations. Conveniently, strong coupling in the infrared has been observed for a variety of substances, such as polymers [54, 55], proteins [56],organometallic complexes [57, 58], and, remarkably, organic solutes [59], and others [60]. Vibrational strong coupling has been extensively investigated

from both theoretical and experimental fronts. Among the developments along this line research there is enhanced Raman scattering [61–63], mode hybridization [64, 65], two-dimensional spectroscopy [66, 67] and non-linear response [68–70].

The most striking finding regarding molecules and cavities in the infrared is the observation that performing a chemical reaction inside a resonator can modify the rate of the process even in the absence of external stimuli [41, 43]. This phenomenon is the central topic of the present dissertation.

1.1   Cavity-induced modifications of ground-state chemical kinetics: Experimental observations

Since 2016, the Nanostructures Laboratory at the Université de Strasbourg, directed by Prof. Thomas Ebbesen, has led the charge of producing a series of experimental evidence that, when it takes place inside a FP microcavity, the kinetics of a chemical reaction is modified under conditions consistent with strong-light matter coupling.

In [71], Thomas and co-workers observed that the deprotection of 1-phenyl-2-trimethyl-silylacetylene experiences slowdown when performed in a FP cavity with inter-mirror separation tuned to produce the maximum Rabi splitting over the peak at $860\,\mathrm{cm}^{-1}$, which is arguably assigned to the stretching mode of the $\mathrm{Si-C}$ bond that brakes during the reaction [72]. They found that varying the length of the cavity gap reduces the deviation between the rates measured inside and outside of the cavity following a trend reminiscent of the absorption peak, i.e., the effect is maximum at resonance, and it decreases with the detuning following the absorption line shape. Furthermore, they found a positive correlation between the magnitude of the deceleration and the reactant concentration; this observation is interpreted as the effect on the rate being dependent on the Rabi splitting. They extracted kinetic parameters and calculated an increase in activation enthalpy and an increase in activation entropy. The latter suggests a change in the mechanism,

going from a bimolecular to a unimolecular slow-step [73].

Ebbesen's research group built upon these findings and published a study with a similar reaction but in which the reactant, *tert*-butyldimethyl{[4-(trimethylsilyl)but-3-yn-1-yl]oxy}silane, has two liable sites: a $Si\!-\!C$ ($842\,cm^{-1}$) and a $Si\!-\!O$ ($1110\,cm^{-1}$) [74]. Moreover, this time they tuned the cavity to the bending mode of $Si\!-\!CH_3$ ($1250\,cm^{-1}$) and the stretching of $C\!-\!O$ ($1045\,cm^{-1}$); these bonds do not break during the reactions. Unsurprisingly, they found that coupling to the $C\!-\!O$ bond does not affect the rate. In contrast, the results indicate that, among the remaining ones, the identity of the mode engaging with the cavity is irrelevant for retardation to be observed, although it slightly impacts the magnitude of the effect. Furthermore, the scission of the $Si\!-\!C$ is more affected than that of $Si\!-\!O$ independently of the coupled mode. This imbalance in retardation affords to invert the bare branching ratio. Despite not providing the desired selectivity, in the sense that tuning the cavity to a mode does not necessarily imply that that mode is affected above the others, the findings of this study enable the development of strategies for mode selective chemistry.

Resonant retarding effects that increase with the Rabi splitting have also been observed in prins cyclization [75] and the proteolytic activity of pepsin [76]. Later investigations had shown catalytic activity when solvent molecules couple resonantly to the cavity. Carbonyl group [77], a variety of reactions are performed under the so-called ultrastrong coupling regime, i.e., with Rabi splitting larger than 10 % of the resonant frequency. Additions and carbonyl exchanges exhibit moderate rate increases, while hydrolysis accelerates up until four orders of magnitude. Carboxyl hydrolysis, in turn, shows a more moderate enhancement when the nucleophile, ethyl acetate, is strongly coupled [78]. Interestingly, replacing the solvent with its enriched with its version enriched in the ^{13}C in the carbonyl position negates any modification induced by the cavity. Table 1.1 summarizes these results.

Table 1.1: Chemical reactions modulated by vibrational strong coupling. Ω is the Rabi frequency, ω is the frequency of the coupled mode, k_{VSC} is the rate under VSC, and k_{bare} is the rate outside of the cavity. Adapted from [43, 77].
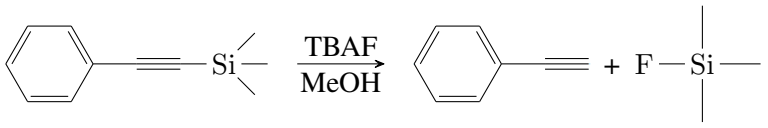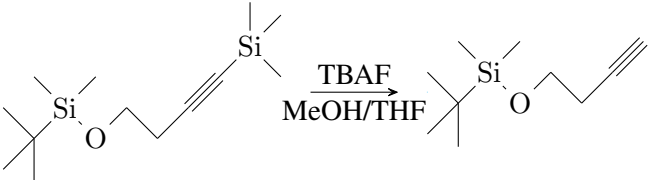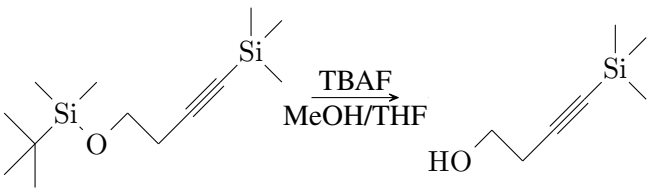
Coupled vibrational mode	Ω/ω	k_{VSC}/k_{bare}	Ref.
Si—C	0.081	0.25	[71]
Si—CH$_3$	0.034		
Si—C	0.083	0.27	[74]
Si—O	0.077	0.25	
Si—CH$_3$	0.034		
Si—C	0.083	0.65	[74]
Si—O	0.077	0.49	

Table 1.1 Chemical reactions modulated by vibrational strong coupling. Continued
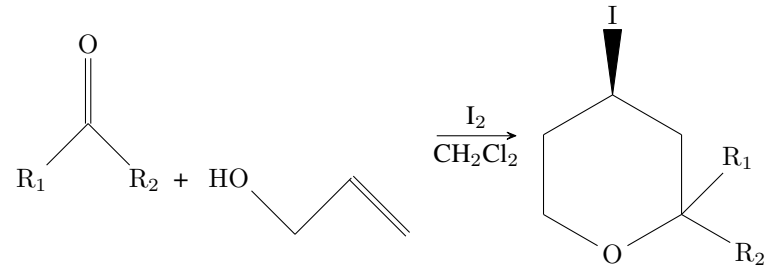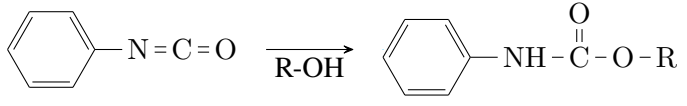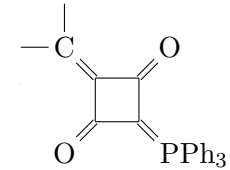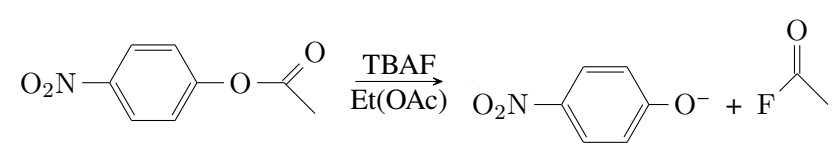
Coupled vibrational mode	Ω/ω	$k_{\mathrm{VSC}}/k_{\mathrm{bare}}$	Ref.

		0.26 Acetaldehyde	
		0.23 Propionaldehyde	
$(C{=}O)$	≈ 0.061	0.28 Acetone	[75]
		0.19 Cyclohexanone	

$$2H_2O + OCN^- \longrightarrow CO_3^{2-} + NH_4^+ \qquad 2D_2O + OCN^- \longrightarrow CO_3^{2-} + ND_4^+$$

| O—H | 0.22 | 110 | |
| O—D | 0.22 | 31 | [77] |

$$2H_2O + NH_3BH_3 \longrightarrow NH_4^+ + BO_2^- + 3H_2$$

| O—H | 0.22 | 1×10^4 | [77] |

| | | 1.56 R: CH_3 | |
| $N{=}C{=}O$ | 0.046 | 1.90 R: $CH(CH_3)_2$ | [77] |

8

Table 1.1 Chemical reactions modulated by vibrational strong coupling. Continued

Coupled vibrational mode	Ω/ω	k_{VSC}/k_{bare}	Ref.

$$K^+[O\!=\!C\ N^-]\ +\ NH_4Cl\ \longrightarrow\ (H_2N_2)CO\ +\ KCl$$

| $O\!=\!C\!=\!N$ | 0.070 | 2.41 | [77] |

$$Ph_3P\!=\!C\!=\!C\!=\!O\ \xrightarrow{\text{acetone}}$$

| $C\!=\!O$ | 0.064 | 1.55 | |
| $C\!=\!C\!=\!O$ | 0.062 | 1.29 | [77] |

| $S\!=\!C\!=\!S$ | 0.036 | 3.01 | |
| $C\!=\!C\!=\!O$ | 0.054 | 2.12 | [77] |

| $^{12}C\!=\!O$ | 0.089 | 12.5 | |
| $^{13}C\!=\!O$ | 0.091 | 1 | [78] |

$$R_1NHCOR_2\ \longrightarrow\ R_1NH_3^+\ +\ R_2COOH$$

| $O\!-\!H$ | 0.21 | 0.22 | [76] |

A prominent step forward towards the utilization of VSC in mode selective chemistry can

be found in [79]. Pang and collaborators coupled several vibrational modes of mesitylene and other charge transfer donors to resonant cavity modes and measured the equilibrium constant of the complexation reaction with iodine. They found that coupling to modes with the A' irreducible representation of the C_{3h} symmetry group resulted in deceleration, while coupling to E' modes produced acceleration.

More recently, similar results have been obtained in laboratories with no relation to Ebbesen's group [80]. All these results indicate that the EM mode is effectively modifying the energetic landscape of the ground-state in a way that must be consistent with some of the notions of polariton formation. The next section presents the efforts to provide a theoretical explanation for these phenomena.

1.2 Theoretical approaches to VSC modified chemical kinetics.

In contrast with excited-state reactions, a successful conceptualization of how light-matter coupling modifies the observed rates in thermally driven reactions has evaded the scientific community for as long as these experimental results have been made public. This situation can be understood because the theoretical frameworks that have been successful at explaining and predicting the optical properties of vibrational polaritons suggest that the material properties involved in chemical transformations should not experience an observable modification inside infrared microcavities [41].

The argument is as follows: the collective effects that allow the polaritonic coupling to overcome the dissipative process also produce normal modes that exclude any interaction with the EM field and can therefore be regarded as bare molecules. Moreover, these *dark* modes overwhelmingly outnumber the polaritons. To be exact, if there are N molecular dipoles coupling to one cavity mode, by "conservation of the number of modes," these $N + 1$ modes end up as
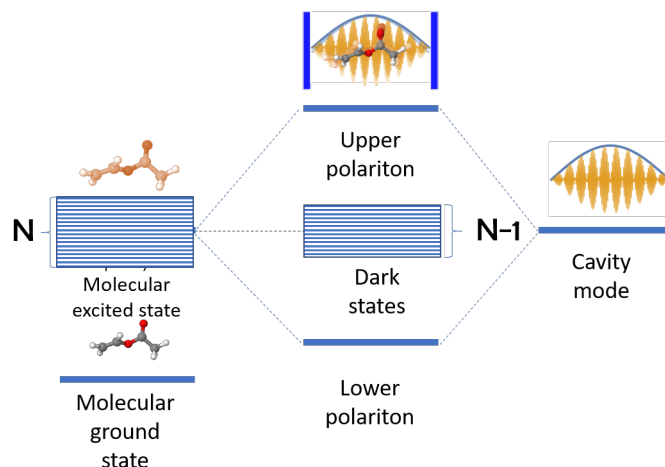
Figure 1.2: Correlation diagram of polaritonic energy levels.

one upper polariton with higher frequency, one lower polariton with lower frequency, and $N-1$ degenerate dark modes at the original frequency of vibration (fig. 1.2). The estimates of the number of dipoles that couple together to produce the experimentally observed Rabi splittings go from 1×10^7 to 1×10^{12} per cavity mode [81, 82]. The proportion between polaritonic and dark modes clearly indicates that thermodynamic averages are governed by the dark bundle, suggesting that most observables at equilibrium will be indistinguishable whether measured inside or outside a resonator.

Another argument against VSC effects is that a chemical transformation is (not referring to the reaction mechanism) a single-molecule event, i.e., only a single dipole is removed from the polaritonic ensemble. This picture implies that at a given instant during the reaction, the transition to consider is from N to $N-1$ coupled molecules. Given the orders of magnitude for N in VSC, this change is negligible in the coupled ensemble. The constrains imposed by these reasons have produced that several of the attempts to rationalize the changes to the kinetics are focused on the single-molecule limit. These efforts are discussed next.

The group of Johannes Feist at the Universidad Autónoma de Madrid put forward the first theory of cavity induced modification of ground-state reaction rates. Galego and co-workers presented a detailed discussion of how light-matter interaction, as described by a minimal coupling

Hamiltonian [7], can affect adiabatic reactions [83]. The authors worked through a hierarchy of formalisms, starting from a full-quantum first-principles description and then simplifying within the frame of the cavity Born-Oppenheimer approximation [51, 52], which allowed them to apply transition state theory to their analysis. They found that coupling between a confined EM mode and the reactive coordinate can reshape the potential energy surface governing the nuclear motion, thus modifying the activation barriers for a reaction. They showed that, within this approach, the molecularity of the transition state could be modified, consistently with the thermodynamic parameters extracted from experiments [84]. However, their formalism results in rates that are independent of the cavity frequency, i.e., it does not describe a resonant effect. Moreover, the coupling relies on the molecular permanent dipole moment. This quantity averages to zero in a collective ensemble with isotropically distributed molecular orientations, as expected in a liquid solution. Consequently, in the collective regime, the formalism predicts no effect on the rate. References [85, 86] and chapter 3 of this dissertation discuss the shortcomings of this approach.

Inspired by the work of Galego and Climent, the group of Pengfei Huo at the University of Rochester took a modified approach considering dynamical effects [87]. By giving the cavity mode the role of a solvent mode in Kramers-Grote-Hynes theory [88–90], they were able to recover the dependence on cavity frequency. Additionally, their approach produces changes in the free energy of activation with similar trends as the experimentally observed. However, this formalism introduces a pseudo-resonant condition not with those at equilibrium but with the unstable mode. Furthermore, in the collective regime, the $N \rightarrow N - 1$ argument defeats this theory.

Considering that the nuclear motion along the reaction coordinate is not harmonic, the group of Felipe Herrera at the Universidad de Santiago de Chile studied the coupling between a photon mode and a single anharmonic oscillator [91, 92]. In the case of a Morse potential [93] Herrera and coworkers found a shortening effect of the bond length. They interpret this observation as the excited states having a significant photon component that ingrains them with a harmonic

character. Later, Triana and collaborators concluded that, for more realistic molecular oscillators, the nuclear dynamics inside the cavity depends mostly on the shape of the dipole moment function; therefore, both a bond length enlargement and shortening are possible. In chapter 5, this dissertation introduces an argument that makes the extension of their findings to the many-molecules case unlikely. To be specific, collective coupling only produces permutationally invariant observables. During a chemical reaction, it is expected that the reactive molecule breaks this symmetry, and therefore no longer participates in the polaritonic ensemble.

The group of Angel Rubio at the Max Planck Institute assessed whether discarding the usual approximations incorporated in the minimal coupling Hamiltonian could provide more robust explanations of the modified kinetics. In [94], Hoffman and collaborators considered the interaction of a single molecule with multiple cavity modes. They found that the nuclear dynamics strongly changes as the number of considered photon modes increases. Adversely, this approach suffers from the same downsides as the one by Herrera's group when intended to be applied in the collective regime. On the other hand, Schäfer and coworkers contrasted the implications of including and excluding the often-neglected self-interacting terms [95]. They concluded that their absence leads to unphysical situations; moreover, its inclusion might alleviate the incompatibilities between the local nature of a chemical reaction and the delocalized essence of light-matter coupling.

As argued in chapter 4 of this dissertation, the non-adiabatic perspective of charge transfer processes allows formalizing a rate theory that circumvents all the hindrances endured by the approaches detailed earlier [96]. To be specific, considering the intramolecular degrees of freedom as quantum while approximating the solvent contribution to the reaction coordinate as classical enables to imprint the structure of the polaritonic energy spectrum in the frame of Marcus theory as upgraded by Levich and Jortner [97–99]. In this approach, the thermodynamic average of reaction channels, which the dark modes usually dominate, accounts for the polaritonic energies with exponential weights. Consequently, polaritonic channels are accessible that can outcompete

the dark channels by virtue of reduced activation energies, and thus the reaction experiences catalysis. This theory is the first to successfully incorporate collective and pseudo-resonant effects consistent with the experimental observations. Although limited in its application to real systems [100], this formalism has expanded the general understanding of the phenomena and is the basis for promising works with the potential of a more accurate explanation [101].

On the flip side, other theoretical studies have been recently published that discard other intuitive lines of thought about this problem. For instance, Vurgaftman and collaborators at the U. S. National Laboratory argue that rationalization in terms of activation energies located at the polariton resonances is inoperant under realistic experimental conditions [100]. The reason is that the natural broadening of the dark modes implies that their density of states is vastly more extensive than that of the polariton modes even at the energies of the polariton themselves. Additionally, Li and coworkers at the University of Pennsylvania analyzed the potential of mean force derived from the minimal coupling Hamiltonian [102], and concluded that a classical treatment of nuclear dynamics, such as transition state theory, cannot account for collective coupling of nuclear degrees of freedom to a cavity mode.

This dissertation compiles the contributions from Joel Yuen-Zhou's research group at the University of California San Diego to understand the cavity-induced modification of thermally driven chemical kinetics.

1.3   Summary of contents

Chapter 2 the formalism of cavity Quantum Electrodynamics is introduced to describe the general features of light-matter interaction. The approximations needed to reduce the description of the system only in terms of nuclear degrees of freedom are discussed. And the general language of the elements of vibrational strong coupling is established.

In chapter 3, an analysis of the theory by Galego and coworkers is presented using the

language of polariton modes, at the level of transition state theory, to illustrate why their formalism fails to include resonant and collective effects. The groundwork for dynamic considerations is laid out in this chapter.

Chapter 4 discusses the impact of VSC on Marcus rate theory of non-adiabatic charge transfer processes. It is argued that an entirely classical treatment is ineffective at incorporating the light-matter coupling effects. In contrast, the consideration of high-frequency modes results in a theory that successfully predicts rate modification because of collective coupling in near-resonant conditions.

In chapter 5, the generalized model of a collection of N dipoles with an arbitrary energy spectrum coupled to a single cavity mode is solved. Taking advantage of the permutational symmetry of the system, a group theoretical strategy is implemented to make the problem tractable. Symmetry considerations and observables are discussed.

Finally, in chapter 6, this work presents a perspective on the accomplished work and the future directions this research line might take.

Chapter 1, in part is currently being prepared for submission for publication of the material. "Thermally-activated vibro-polaritonic chemistry: theoretical perspectives." Campos-Gonzalez-Angulo, Jorge A.; Du, Matthew; Yuen-Zhou, Joel. The dissertation author was the primary investigator and author of this material.

Chapter 2

Theoretical background

This chapter lays-off the theoretical foundations of vibrational strong coupling, and introduces the language and notation that will be found in subsequent chapters. First, Cavity Quantum Electrodynamics (CQED) is used to describe confinement of electromagnetic (EM) fields and explain cavity resonances and photon leakage. Then, the description of the molecular degrees of freedom is simplified by framing vibrations in terms of nuclear motion. Next, the interaction of the confined modes with the molecular vibrations are discussed, exploring the accuracy of theoretical models for several ranges of coupling intensity, and reviewing the consequences of having a numerous ensemble of dipoles. Finally, some intuitions are developed with regards to possible consequences that vibrational strong-coupling might have on chemical reactivity.

2.1   Fundamentals of microcavities

Enhancement of light-matter interaction is achieved through confinement of the EM field, i.e., permanence of EM energy stored in a finite region of space. In practice, this is accomplished with optical cavities. While several kinds of these devices are discussed in the literature (e.g., plasmonic resonators, photonic crystal microcavities, and whispering gallery modes microcavities), this work focuses on the symmetric and planar Fabry-Perot resonator, which consists of a pair
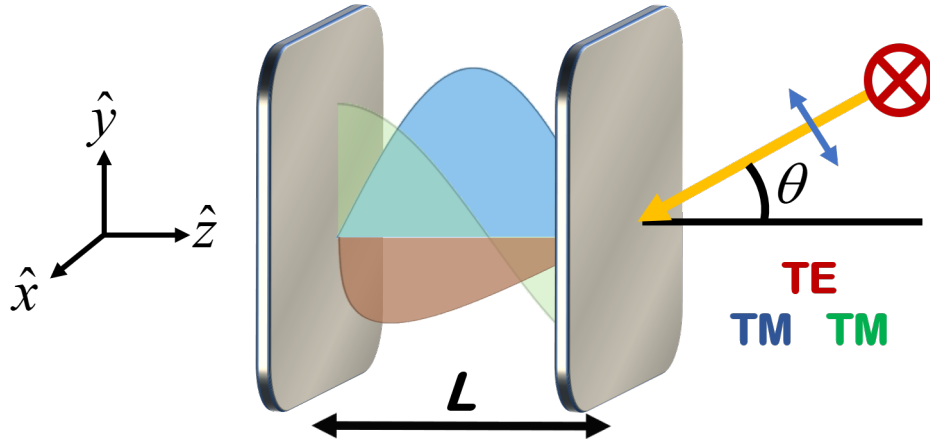
Figure 2.1: Cavity modes in cartesian space.

of parallel reflective surfaces, each of area $\mathcal{A}$, separated by a gap of length L, which is much smaller than $\sqrt{\mathcal{A}}$, and filled with a dielectric material of refractive index n. In the most convenient coordinate system, the mirrors are parallel to the xy plane, and therefore perpendicular to the z direction, which defines the confinement axis (fig. 2.1).

The following discussion follows the treatment found in [103–105].

In general, the electric and magnetic fields, **E** and **B** respectively, are functions of position, **r**, and time, t, that can be written terms of a vector potential, **A**, and a scalar potential, ϕ, as

$$\mathbf{E}(\mathbf{r}, t) = -\frac{\partial}{\partial t}\mathbf{A}(\mathbf{r}, t) - \boldsymbol{\nabla}\phi(\mathbf{r}, t), \tag{2.1a}$$

and

$$\mathbf{B}(\mathbf{r}, t) = \boldsymbol{\nabla} \times \mathbf{A}(\mathbf{r}, t). \tag{2.1b}$$

In turn, within the space between mirrors, and in absence of any other electrical charges, the potentials satisfy the Maxwell's equations in a dielectric medium:

$$\boldsymbol{\nabla} \cdot \frac{\partial}{\partial t}\mathbf{A}(\mathbf{r}, t) + \nabla^2\phi(\mathbf{r}, t) = 0 \tag{2.2a}$$

17

and

$$\frac{n^2}{c^2}\left[\frac{\partial^2}{\partial t^2}\mathbf{A}(\mathbf{r},t) + \boldsymbol{\nabla}\frac{\partial}{\partial t}\phi(\mathbf{r},t)\right] + \boldsymbol{\nabla}\times[\boldsymbol{\nabla}\times\mathbf{A}(\mathbf{r},t)] = 0, \tag{2.2b}$$

where c is the speed of light in vacuum. In the Coulomb gauge ($\boldsymbol{\nabla}\cdot\mathbf{A} = 0$), eq. (2.2) simplifies to

$$\nabla^2\phi(\mathbf{r},t) = 0 \tag{2.3a}$$

and

$$\frac{n^2}{c^2}\left[\frac{\partial^2}{\partial t^2}\mathbf{A}(\mathbf{r},t) + \boldsymbol{\nabla}\frac{\partial}{\partial t}\phi(\mathbf{r},t)\right] - \nabla^2\mathbf{A}(\mathbf{r},t) = 0. \tag{2.3b}$$

In this gauge, it is possible to identify a transverse component of the electric field, $\mathbf{E}_\perp = -\partial\mathbf{A}/\partial t$, and a longitudinal one, $\mathbf{E}_\parallel = -\boldsymbol{\nabla}\phi$. This section focuses on the former.

The boundary conditions imposed by the microcavity entail that this arrangement supports a set of standing EM waves with wave vectors

$$\mathbf{k} = \mathbf{k}_{xy} + \frac{m\pi}{L}\hat{\mathbf{z}} \qquad m \in \{0\}\cup\mathbb{Z}^+, \tag{2.4}$$

where $\mathbf{k}_{xy}$ is the wave vector component lying on the plane parallel to the plates. These wave vectors define the frequencies

$$\omega_{\mathbf{k}} = \omega_{\mathbf{k}_{xy},m} = \frac{c}{n}\sqrt{\left|\mathbf{k}_{xy}\right|^2 + \left(\frac{m\pi}{L}\right)^2}. \tag{2.5}$$

To be specific, the quantized vector potential in the space between mirrors has the form

$$\hat{\mathbf{A}}(\mathbf{r},t) = \sum_{\mathbf{k}}\sum_{\sigma\in\{s,p\}}\left[\mathbf{A}_{\mathbf{k},\sigma}(\mathbf{r})\hat{a}_{\mathbf{k},\sigma}\mathrm{e}^{-i\omega_{\mathbf{k}}t} + \mathbf{A}^*_{\mathbf{k},\sigma}(\mathbf{r})\hat{a}^\dagger_{\mathbf{k},\sigma}\mathrm{e}^{i\omega_{\mathbf{k}}t}\right], \tag{2.6}$$

where

$$\mathbf{A}_{\mathbf{k},\sigma}(\mathbf{r}) = i\sqrt{\frac{\hbar}{2\omega_{\mathbf{k}}\epsilon_0 \mathcal{V}_{\mathbf{k},\sigma}}}\,\mathbf{f}_{\mathbf{k},\sigma}(\mathbf{r}), \tag{2.7}$$

$\hbar$ is the reduced Planck's constant, and ϵ_0 is the vacuum permittivity. The mode volume is

$$\mathcal{V}_{\mathbf{k},\sigma} = \frac{\int_{AL} u_{\mathbf{k},\sigma}(\mathbf{r})\mathrm{d}^3 r}{\max_{\mathbf{r}}\left[u_{\mathbf{k},\sigma}(\mathbf{r})\right]} \approx AL, \tag{2.8}$$

where

$$u_{\mathbf{k},\sigma}(\mathbf{r}) = \epsilon_0\left(\epsilon_r(\mathbf{r})\left|\mathbf{E}_{\mathbf{k},\sigma}(\mathbf{r})\right|^2 + c^2\left|\mathbf{B}_{\mathbf{k},\sigma}(\mathbf{r})\right|^2\right) \tag{2.9}$$

is the energy density of the mode, $\epsilon_r(\mathbf{r})$ is the relative permittivity, and the quantities $\mathbf{E}_{\mathbf{k},\sigma}(\mathbf{r})$ and $\mathbf{B}_{\mathbf{k},\sigma}(\mathbf{r})$ are the spatial mode components of the transverse electric and magnetic fields, respectively. The index σ labels polarizations; for the current setting, $\sigma = s$ indicates transverse electric (TE) polarization, which is perpendicular (*senkrecht* in German) to the plates, and $\sigma = p$ identifies the transverse magnetic (TM) polarization, which is parallel to the mirrors. The operators $\hat{a}_{\mathbf{k},\sigma}$ and $\hat{a}_{\mathbf{k},\sigma}^{\dagger}$ annihilate and create, respectively, excitations in the electromagnetic modes, and fulfill the bosonic commutation relations

$$\left[\hat{a}_{\mathbf{k},\sigma}, \hat{a}_{\mathbf{k}',\sigma'}\right] = \left[\hat{a}_{\mathbf{k}^{\dagger},\sigma}, \hat{a}_{\mathbf{k}',\sigma'}^{\dagger}\right] = 0, \tag{2.10a}$$

and

$$\left[\hat{a}_{\mathbf{k},\sigma}, \hat{a}_{\mathbf{k}',\sigma'}^{\dagger}\right] = \delta_{\mathbf{k}_{xy},\mathbf{k}_{xy}'}^2\,\delta_{m,m'}\delta_{\sigma,\sigma'}. \tag{2.10b}$$

The orthogonal mode functions, $\mathbf{f}_{\mathbf{k},\sigma}(\mathbf{r})$, satisfy

$$\int_{\mathcal{V}_{\mathbf{k},\sigma}} \mathbf{f}_{\mathbf{k},\sigma}(\mathbf{r})\cdot\mathbf{f}_{\mathbf{k}',\sigma'}^*(\mathbf{r})\mathrm{d}^3 r = \mathcal{V}_{\mathbf{k},\sigma}\delta_{\mathbf{k}_{xy},\mathbf{k}_{xy}'}^2\,\delta_{m,m'}\delta_{\sigma,\sigma'}, \tag{2.11}$$

19

and, when the mirrors are perfect, they are given by

$$\mathbf{f}_{\mathbf{k},s}(\mathbf{r}) = \sqrt{2} e^{i\mathbf{k}_{xy} \cdot \mathbf{r}} \sin(k_z z) \hat{\mathbf{k}}_{xy} \times \hat{\mathbf{z}}, \tag{2.12}$$

and

$$\mathbf{f}_{\mathbf{k},p}(\mathbf{r}) = \frac{\sqrt{2} e^{i\mathbf{k}_{xy} \cdot \mathbf{r}}}{|\mathbf{k}|} \left(k_z \sin(k_z z) \hat{\mathbf{k}}_{xy} + i |\mathbf{k}_{\mathbf{xy}}| \cos(k_z z) \hat{\mathbf{z}} \right), \tag{2.13}$$

where $k_z = \mathbf{k} \cdot \hat{\mathbf{z}}$.

The form of the electric field afforded by the vector potential in eq. (2.6), and the mode functions in eq. (2.12), implies that the resonator experiences a strong interaction, i.e., is resonant, with an electromagnetic field only if its frequency is given by eq. (2.5). The electromagnetic energy inside the cavity is described by the Hamiltonian

$$\begin{aligned}
\hat{H}_{\text{cav}} &= \frac{\epsilon_0}{2} \int_{\mathcal{A}L} \left(\left| \hat{\mathbf{E}}_\perp \right|^2 + c^2 \left| \hat{\mathbf{B}} \right|^2 \right) \mathrm{d}^3 r \\
&= \sum_{\mathbf{k}} \sum_{\sigma \in \{s,p\}} \hbar \omega_{\mathbf{k}} \left(\hat{a}^\dagger_{\mathbf{k},\sigma} \hat{a}_{\mathbf{k},\sigma} + \frac{1}{2} \right).
\end{aligned} \tag{2.14}$$

Realistic resonators experience losses due to energy leakage through imperfect mirrors; under such consideration, the frequency-dependent intensity is

$$I(\omega) = \frac{I_{\text{max}}}{1 + \left(\frac{2\mathcal{F}}{\pi} \right)^2 \sin^2 \left(\frac{\omega m \pi}{\omega_{\text{FSR}}} \right)}, \tag{2.15}$$

where $I_{\text{max}} = (nc/\mathcal{A}L\mu_r)\hbar\omega_{\text{FSR}}$ is the intensity at resonance, and $\mu_r \approx 1$ is the relative magnetic permeability of the material in the gap. The frequency $\omega_{\text{FSR}} = \omega_{\mathbf{0},1}/\cos\theta$, where $\theta = \arccos(k_z/|\mathbf{k}|)$ is the incident angle, is known as free spectral range (FSR); it is related to the time it takes for the light to make a round trip between the mirrors, and corresponds to the distance in frequency between maxima in the absorption spectrum of the resonator. The lossy

nature of the cavity is characterized by its finesse:

$$\mathcal{F} = \frac{\pi \sqrt{r}}{1 - r}, \tag{2.16}$$

where r is the Fresnel reflection coefficient of the reflective surfaces. The full width at half maximum (FWHM) of $I(\omega)$ is given by

$$\kappa = \frac{\omega_{\mathrm{FSR}}}{\mathcal{F}}, \tag{2.17}$$

and corresponds to the cavity decay rate, i.e., the rate at which energy leaks-out of the resonator through the mirrors.

2.2 Normal modes of vibration

This section deals with the derivation of the vibrational degrees of freedom of a molecule from the general form of the coulombic interaction among nuclei and electrons [106, 107].

The energy of a molecule comprising n_n nuclei and n_e electrons is defined by the Hamiltonian

$$\hat{H}_{\mathrm{mol}}(\underline{\mathbf{R}}, \underline{\mathbf{r}}) = \hat{T}_n + \hat{V}_{nn}(\underline{\mathbf{R}}) + \hat{T}_e + \hat{V}_{ee}(\underline{\mathbf{r}}) + \hat{V}_{ne}(\underline{\mathbf{R}}, \underline{\mathbf{r}}), \tag{2.18}$$

where $\underline{\mathbf{R}}$ and $\underline{\mathbf{r}}$ are the arrays of all nuclear and electronic positions, respectively; to be specific, $\left[\underline{\mathbf{R}}\right]_{i,\alpha}$ denotes the Cartesian component $\alpha \in \{x, y, z\}$ of the position of the ith nucleus. The terms in eq. (2.18) can be split into nuclear and electronic kinetic energy operators:

$$\hat{T}_n = \frac{1}{2} \sum_{i=1}^{n_n} \frac{\hat{\mathbf{P}}_i^2}{M_i}, \tag{2.19a}$$

and

$$\hat{T}_e = \frac{1}{2} \sum_{j=1}^{n_e} \frac{\hat{\mathbf{p}}_j^2}{m_e}, \tag{2.19b}$$

where $\hat{\mathbf{P}}_a = -i\hbar \boldsymbol{\nabla}_{\mathbf{R}_a}$ and $\hat{\mathbf{p}}_a = -i\hbar \boldsymbol{\nabla}_{\mathbf{r}_a}$ are canonical momenta; and potential energy operators describing the electrostatic interactions among charges:

$$\hat{V}_{nn}(\underline{\mathbf{R}}) = \frac{e^2}{4\pi\epsilon_0} \sum_{i=1}^{n_n-1} \sum_{i'=i+1}^{n_n} \frac{Z_i Z_i'}{\left|\mathbf{R}_i - \mathbf{R}_i'\right|}, \tag{2.19c}$$

$$\hat{V}_{ee}(\underline{\mathbf{r}}) = \frac{e^2}{4\pi\epsilon_0} \sum_{j=1}^{n_e-1} \sum_{j'=j+1}^{n_e} \frac{1}{\left|\mathbf{r}_j - \mathbf{r}_j'\right|}, \tag{2.19d}$$

and

$$\hat{V}_{ne}(\underline{\mathbf{R}}, \underline{\mathbf{r}}) = - \frac{e^2}{4\pi\epsilon_0} \sum_{i=1}^{n_n} \sum_{j=1}^{n_e} \frac{Z_i}{\left|\mathbf{R}_i - \mathbf{r}_j\right|}, \tag{2.19e}$$

where e and m_e are, respectively, the electronic charge and mass, are the potential energy operators due to the electrostatic interactions among charges.

For the purposes of this work, it is useful to explore the dynamics of the nuclei in a timescale well separated from that of the electronic motion. With this consideration, the complexity of the problem can be significantly reduced with the so-called Born-Oppenheimer approximation in which the electronic Schrödinger equation

$$\left(\hat{T}_e + \hat{V}_{ee} + \langle \underline{\mathbf{R}} | \hat{V}_{ne} | \underline{\mathbf{R}} \rangle \right) |\chi_\varphi\rangle = \hat{\mathcal{E}}_\varphi |\chi_\varphi\rangle, \tag{2.20}$$

(where the arguments have been dropped for the sake of clarity) is solved treating the nuclear coordinates as parameters. The quantity $\hat{\mathcal{E}}_\varphi(\underline{\mathbf{R}})$ is the $\underline{\mathbf{R}}$ dependent energy of the ϕth electronic eigenstate, $|\chi_\varphi(\underline{\mathbf{R}})\rangle$; however, although an eigenvalue in the electronic Hilbert subspace, it is also

an operator in the nuclear subspace. Hence, the nuclear degrees of freedom are described by a set of simplified Hamiltonians of the form

$$\hat{H}_{\text{BO}}^{(\varphi)}(\underline{\mathbf{R}}) = \hat{T}_n + \hat{V}_{nn}(\underline{\mathbf{R}}) + \hat{\mathcal{E}}_\varphi(\underline{\mathbf{R}}). \tag{2.21}$$

Presumably, a bonding electronic state has a global minimum at the equilibrium nuclear configuration $\underline{\mathbf{R}}_{\text{eq}}^{(\varphi)}$. The Born-Oppenheimer nuclear potential, $\hat{V}_{\text{BO}}^{(\varphi)}(\underline{\mathbf{R}}) = \hat{V}_{nn}(\underline{\mathbf{R}}) + \hat{\mathcal{E}}_\varphi(\underline{\mathbf{R}})$, can be expanded around the nuclear configuration as

$$\hat{V}_{\text{BO}}^{(\varphi)}(\underline{\mathbf{R}}) = \hat{V}_{\text{BO}}^{(\varphi)}(\underline{\mathbf{R}}_{\text{eq}}^{(\varphi)}) + \frac{1}{2}\left(\hat{\underline{\mathbf{R}}} - \underline{\mathbf{R}}_{\text{eq}}^{(\varphi)}\right)^T \mathbf{H}_{\text{BO}}^{(\varphi)}(\underline{\mathbf{R}}_{\text{eq}}^{(\varphi)})\left(\hat{\underline{\mathbf{R}}} - \underline{\mathbf{R}}_{\text{eq}}^{(\varphi)}\right) + \mathcal{O}\left(\underline{\mathbf{R}}^3\right), \tag{2.22}$$

where $\mathbf{H}_{\text{BO}}^{(\varphi)}(\underline{\mathbf{R}})$ is the Hessian of $V_{\text{BO}}^{(\varphi)}(\underline{\mathbf{R}})$, i.e., the matrix with elements given by

$$\left[\mathbf{H}_{\text{BO}}^{(\varphi)}(\underline{\mathbf{R}})\right]_{i,\alpha;j,\beta} = \left.\frac{\partial^2 V_{\text{BO}}^{(\varphi)}(\underline{\mathbf{R}}')}{\partial R'_{i,\alpha}\partial R'_{j,\beta}}\right|_{\underline{\mathbf{R}}}. \tag{2.23}$$

In the neighborhood of the equilibrium configuration, the Hamiltonian becomes

$$\hat{H}_{\text{BO}}^{(\varphi)}(\underline{\mathbf{R}} \approx \underline{\mathbf{R}}_{\text{eq}}^{(\varphi)}) = \frac{1}{2}\hat{\underline{\mathbf{P}}}^T \mathbf{M}^{-1}\hat{\underline{\mathbf{P}}} + \hat{V}_{\text{BO}}^{(\varphi)}(\underline{\mathbf{R}} \approx \underline{\mathbf{R}}_{\text{eq}}^{(\varphi)}), \tag{2.24}$$

where $\underline{\mathbf{P}}$ is the vector of all nuclear momenta, and $\mathbf{M}$ is the diagonal matrix of nuclear masses. Defining $\hat{\underline{\tilde{\mathbf{P}}}} = \mathbf{M}^{-1/2}\hat{\underline{\mathbf{P}}}$ and $\underline{\tilde{\mathbf{R}}} = \mathbf{M}^{1/2}\left(\hat{\underline{\mathbf{R}}} - \underline{\mathbf{R}}_{\text{eq}}^{(\varphi)}\right)$ as the mass-scaled momenta and position, and setting $\hat{V}_{\text{BO}}^{(\varphi)}(\underline{\mathbf{R}}_{\text{eq}}^{(\varphi)}) = 0$, eq. (2.24) can be recast as

$$\hat{H}_{\text{BO}}^{(\varphi)}(\underline{\mathbf{R}} \approx \underline{\mathbf{R}}_{\text{eq}}^{(\varphi)}) = \frac{1}{2}\left(\underline{\tilde{\mathbf{P}}}^T\underline{\tilde{\mathbf{P}}} + \underline{\tilde{\mathbf{R}}}^T \mathbf{V}_{\text{BO}}^{(\varphi)}\underline{\tilde{\mathbf{R}}}\right) \tag{2.25}$$

where $\mathbf{V}_{\text{BO}}^{(\varphi)} = \mathbf{M}^{-1/2}\mathbf{H}_{\text{BO}}^{(\varphi)}(\underline{\mathbf{R}}_{\text{eq}}^{(\varphi)})\mathbf{M}^{-1/2}$. Upon diagonalization of the latter, the Hamiltonian

becomes

$$\hat{H}_{\text{BO}}^{(\varphi)}(\underline{\mathbf{R}} \approx \underline{\mathbf{R}}_{\text{eq}}^{(\varphi)}) = \frac{1}{2}\left(\hat{\underline{\mathbf{P}}}_{\varphi}^{T}\hat{\underline{\mathbf{P}}}_{\varphi} + \hat{\underline{\mathbf{R}}}_{\varphi}^{T}\mathbf{W}_{\varphi}\hat{\underline{\mathbf{R}}}_{\varphi}\right), \tag{2.26}$$

where $\mathbf{W}_{\varphi} = \mathbf{S}_{\varphi}^{-1}\mathbf{V}_{\text{BO}}^{(\varphi)}\mathbf{S}_{\varphi}$ is a diagonal matrix, and $\mathbf{S}_{\varphi}$ the unitary basis transformation whose columns are eigenvenctors of $\mathbf{V}_{\text{BO}}^{(\varphi)}$. The new momenta and positions, $\hat{\underline{\mathbf{P}}}_{\varphi} = \mathbf{S}_{\varphi}^{-1}\tilde{\underline{\mathbf{P}}}$ and $\hat{\underline{\mathbf{R}}}_{\varphi} = \mathbf{S}_{\varphi}^{-1}\tilde{\underline{\mathbf{R}}}$ respectively, define the molecular normal modes, which are mutually independent degrees freedom that correspond to oscillations with frequencies, $\omega_{\varphi,\xi}$, given by the main diagonal of $\mathbf{W}_{\varphi}^{1/2}$. Three out of the $3n_n$ eigenvalues of $\mathbf{V}_{\text{BO}}^{(\varphi)}$ are non-positive, thus corresponding to translations. Depending on whether the molecule is linear in its equilibrium configuration, two or three of the normal modes are isometric motions, i.e., rotations, and the remaining n_{vib} correspond to vibrations.

Let $\hat{p}_{\varphi,\xi}$ and $\hat{q}_{\varphi,\xi}$ be the ξth element of $\hat{\underline{\mathbf{P}}}_{\varphi}$ and $\hat{\underline{\mathbf{R}}}_{\varphi}$, respectively, it is possible to define vibrational Hamiltonians

$$\hat{H}_{\text{vib}}^{(\varphi,\xi)} = \frac{1}{2}\left(\hat{p}_{\varphi,\xi}^2 + \omega_{\varphi,\xi}^2\hat{q}_{\varphi,\xi}^2\right) = \hbar\omega_{\varphi,\xi}\left(\hat{b}_{\varphi,\xi}^{\dagger}\hat{b}_{\varphi,\xi} + \frac{1}{2}\right), \tag{2.27}$$

such that

$$\hat{H}_{\text{BO}}^{(\varphi)}(\underline{\mathbf{R}} \approx \underline{\mathbf{R}}_{\text{eq}}^{(\varphi)}) = \sum_{\xi=1}^{n_{\text{vib}}}\hat{H}_{\text{vib}}^{(\varphi,\xi)} + \hat{H}_{\text{rot}} + \hat{H}_{\text{trans}}, \tag{2.28}$$

where $\hat{b}_{\varphi,\xi} = \left(\omega_{\varphi,\xi}\hat{q}_{\varphi,\xi} - i\hat{p}_{\varphi,\xi}\right)/\sqrt{2\hbar\omega_{\varphi,\xi}}$ is a harmonic annihilation operator fulfilling

$$\left[\hat{b}_{\varphi,\xi}, \hat{b}_{\varphi,\xi'}\right] = \left[\hat{b}_{\varphi,\xi}^{\dagger}, \hat{b}_{\varphi,\xi'}^{\dagger}\right] = 0 \tag{2.29}$$

and

$$\left[\hat{b}_{\varphi,\xi}, \hat{b}_{\varphi,\xi'}^{\dagger}\right] = \delta_{\xi,\xi'}. \tag{2.30}$$

The Hamiltonians containing the rotational and translational degrees of freedom, $\hat{H}_{\text{rot}}$ and $\hat{H}_{\text{trans}}$, respectively, are of little interest to the present discussion.

2.3 Molecules in cavities

2.3.1 The Cavity Born-Oppenheimer approximation

In the prescence of the nuclear and electronic charges, eq. (2.3a) turns into the Poison's equation $\nabla^2 \phi(\mathbf{r}) = -\rho(\underline{\mathbf{R}}, \underline{\mathbf{r}})/\epsilon_0$, where

$$\rho(\underline{\mathbf{R}}, \underline{\mathbf{r}}) = e \left(\sum_{j=1}^{n_e} \delta(\mathbf{r} - \mathbf{r}_j) - \sum_{i=1}^{n_n} Z_i \delta(\mathbf{R} - \mathbf{R}_i) \right), \tag{2.31}$$

is the charge density; therefore,

$$\int_{AL} \rho(\underline{\mathbf{R}}, \underline{\mathbf{r}}) \phi(\mathbf{r}) \mathrm{d}^3 r = V_{nn}(\underline{\mathbf{R}}) + V_{ee}(\underline{\mathbf{r}}) + V_{ne}(\underline{\mathbf{R}}, \underline{\mathbf{r}}). \tag{2.32}$$

As a consequence, when a molecule is subjected to the EM field inside the cavity, the Hamiltonian of the system is

$$\hat{H}_{\text{mol-cav}}^C = \hat{H}_{\text{cav}} + \hat{T}_{n\text{cav}} + \hat{V}_{nn}(\underline{\mathbf{R}}) + \hat{T}_{e\text{cav}} + \hat{V}_{ee}(\underline{\mathbf{r}}) + \hat{V}_{ne}(\underline{\mathbf{R}}, \underline{\mathbf{r}}), \tag{2.33}$$

where the kinetic energy operators have the form

$$\hat{T}_{n\text{cav}} = \frac{1}{2} \sum_{i=1}^{n_n} \frac{\left(\hat{\mathbf{P}}_i - e Z_i \hat{\mathbf{A}}(\mathbf{R}_i) \right)^2}{M_i}, \tag{2.34}$$

and

$$\hat{T}_{e\text{cav}} = \frac{1}{2m_e} \sum_{j=1}^{n_e} \left(\hat{\mathbf{p}}_j + e \hat{\mathbf{A}}(\mathbf{r}_j) \right)^2. \tag{2.35}$$

Let's introduce the Power-Zienau-Wooley (PZW) transformation:

$$\hat{U}_{\mathrm{PZW}} = \exp\left(-\frac{i}{\hbar}\int_{\mathcal{AL}}\hat{\mathbf{P}}(\mathbf{r})\cdot\hat{\mathbf{A}}(\mathbf{r})\mathrm{d}^3 r\right),\tag{2.36}$$

where

$$\hat{\mathbf{P}}(\mathbf{r}) = e\left(\sum_{i=1}^{n_n} Z_i\mathbf{R}_i\int_0^1 \delta^3(\mathbf{r}-s\mathbf{R}_i)\mathrm{d}s - \sum_{j=1}^{n_e}\mathbf{r}_j\int_0^1 \delta^3(\mathbf{r}-s\mathbf{r}_j)\mathrm{d}s\right)\tag{2.37}$$

(not to be confused with nuclear momentum) is the polarization vector. This gauge transformation takes an operator from the Coulomb gauge to the dipole, or length, gauge. The transformed Hamiltonian has the form

$$
\begin{aligned}
\hat{H}^D_{\mathrm{mol-cav}} &= \hat{U}^\dagger_{\mathrm{PZW}}\hat{H}^C_{\mathrm{mol-cav}}\hat{U}_{\mathrm{PZW}}\\
&= \hat{H}_{\mathrm{cav}} + \hat{H}_{\mathrm{mol}}(\underline{\mathbf{R}},\underline{\mathbf{r}}) + \hat{V}_{\mathrm{int}}[\hat{\boldsymbol{\mu}}(\underline{\mathbf{R}},\underline{\mathbf{r}})],
\end{aligned}\tag{2.38}
$$

where

$$\hat{V}_{\mathrm{int}}[\hat{\boldsymbol{\mu}}(\underline{\mathbf{R}},\underline{\mathbf{r}})] = -\hat{\boldsymbol{\mu}}(\underline{\mathbf{R}},\underline{\mathbf{r}})\cdot\hat{\mathbf{E}}_\perp(\mathbf{R}_0) + \frac{1}{\hbar}\sum_{\mathbf{k}}\sum_{\sigma\in\{s,p\}}\omega_{\mathbf{k}}\left[\hat{\boldsymbol{\mu}}(\underline{\mathbf{R}},\underline{\mathbf{r}})\cdot\mathbf{A}_{\mathbf{k},\sigma}(\mathbf{R}_0)\right]^2,\tag{2.39}$$

is the potential energy operator describing the interaction,

$$\hat{\boldsymbol{\mu}}(\underline{\mathbf{R}},\underline{\mathbf{r}}) = e\left(\sum_{i=1}^{n_n} Z_i\hat{\mathbf{R}}_i - \sum_{j=1}^{n_e}\hat{\mathbf{r}}_j\right)\tag{2.40}$$

is the dipole moment operator, and

$$\mathbf{R}_0 = \frac{\sum_{i=1}^{n_n} M_i\mathbf{R}_i}{\sum_{i=1}^{n_n} M_i}\tag{2.41}$$

is the center of mass of the molecule, typically in an equilibrium configuration. Writing eq. (2.38) requires the invocation of the long-wavelength approximation, which assumes that the

electromagnetic field remains spatially constant at the length scales of the motion of the charges. This assumption is valid for cavity resonances in the infrared and molecular vibrations, which are the main focus of the present work.

The electronic degrees of freedom can be removed from $\hat{H}^D_{\text{mol−cav}}$ through the same procedure as in section 2.2, yielding the Cavity Born-Oppenheimer (CBO) Hamiltonian,

$$\hat{H}^{(\varphi)}_{\text{CBO}}(\underline{\mathbf{R}}) = \hat{H}^{(\varphi)}_{\text{BO}} + \hat{H}_{\text{cav}} + \hat{V}_{\text{int}}[\hat{\boldsymbol{\mu}}_{\varphi}(\underline{\mathbf{R}})], \tag{2.42}$$

with

$$\hat{\boldsymbol{\mu}}_{\varphi}(\underline{\mathbf{R}}) = \hat{\boldsymbol{\mu}}^{(\varphi)}_0(\underline{\mathbf{R}}) + \alpha_{\varphi}(\underline{\mathbf{R}})\hat{\mathbf{E}}_{\perp}(\mathbf{R}^{(\varphi)}_0) + \mathcal{O}(\hat{\mathbf{E}}^2), \tag{2.43}$$

where

$$\hat{\boldsymbol{\mu}}^{(\varphi)}_0(\underline{\mathbf{R}}) = \langle \chi_{\varphi}|\hat{\boldsymbol{\mu}}(\underline{\mathbf{R}},\underline{\mathbf{r}})|\chi_{\varphi}\rangle, \tag{2.44a}$$

and

$$\alpha_{\varphi}(\underline{\mathbf{R}}) = 2\sum_{\varphi'\neq\varphi}\frac{\left|\langle\underline{\mathbf{R}}|\langle\chi_{\varphi'}|\hat{\boldsymbol{\mu}}(\underline{\mathbf{R}},\underline{\mathbf{r}})|\chi_{\varphi}\rangle|\underline{\mathbf{R}}\rangle\right|^2}{V^{(\varphi')}_{\text{BO}}(\underline{\mathbf{R}}) - V^{(\varphi)}_{\text{BO}}(\underline{\mathbf{R}})} \tag{2.44b}$$

is the static polarizability of the molecule.

The series expansion of the dipole moment operator,

$$\hat{\boldsymbol{\mu}}^{(\varphi)}_0(\underline{\mathbf{R}}) = \boldsymbol{\mu}^{(\varphi)}_0(\underline{\mathbf{R}}_{\text{eq}}) + \sum_{\xi=1}^{n_{\text{vib}}}\hat{\boldsymbol{\mu}}'_{\varphi,\xi}\hat{q}_{\varphi,\xi} + \mathcal{O}(\hat{q}^2), \tag{2.45}$$

where

$$\hat{\boldsymbol{\mu}}'_{\varphi,\xi} = \left.\frac{\partial\hat{\boldsymbol{\mu}}^{(\varphi)}_0}{\partial q_{\varphi,\xi}}\right|_{\underline{\mathbf{R}}_{\text{eq}}}, \tag{2.46}$$

helps to distribute the dipole moment among the normal modes.

27

The equilibrium configuration can be chosen to define a phase such that the mode functions are entirely real and the electric field adopts the form

$$\hat{\mathbf{E}}(\mathbf{R}_0^{(\varphi)}) = \sum_{\mathbf{k}} \sum_{\sigma \in \{s,p\}} \sqrt{\frac{\hbar \omega_{\mathbf{k}}}{2\epsilon_0 \mathcal{V}_{\mathbf{k},\sigma}}} \mathbf{f}_{\mathbf{k},\sigma}(\mathbf{R}_0^{(\varphi)}) \left(\hat{a}_{\mathbf{k},\sigma} + \hat{a}_{\mathbf{k},\sigma}^{\dagger} \right). \tag{2.47}$$

This fact allows to define the photon coordinates

$$\hat{q}_{\mathbf{k},\sigma} = \sqrt{\frac{\hbar}{2\omega_{\mathbf{k}}}} \left(\hat{a}_{\mathbf{k},\sigma}^{\dagger} + \hat{a}_{\mathbf{k},\sigma} \right), \tag{2.48a}$$

and the photon momenta

$$\hat{p}_{\mathbf{k},\sigma} = \sqrt{\frac{\hbar \omega_{\mathbf{k}}}{2}} \left(\hat{a}_{\mathbf{k},\sigma}^{\dagger} - \hat{a}_{\mathbf{k},\sigma} \right), \tag{2.48b}$$

with which the cavity Hamiltonian becomes

$$\hat{H}_{\text{cav}} = \frac{1}{2} \sum_{\mathbf{k}} \sum_{\sigma \in \{s,p\}} \left(\hat{p}_{\mathbf{k},\sigma}^2 + \omega_{\mathbf{k}}^2 \hat{q}_{\mathbf{k},\sigma}^2 \right), \tag{2.49}$$

and the vibrational contribution from the vibrational normal modes to the interaction potential is

$$\hat{V}_{\text{int-vib}} = -\sum_{\mathbf{k}} \sum_{\sigma \in \{s,p\}} \left[\hat{V}_{\text{int-vib}}^{(\varphi;\mathbf{k},\sigma;1)} + \hat{V}_{\text{int-vib}}^{(\varphi;\mathbf{k},\sigma;2)} + \mathcal{O}\left(\hat{q}^3 \right) \right], \tag{2.50}$$

where

$$\hat{V}_{\text{int-vib}}^{(\varphi;\mathbf{k},\sigma;1)} = \frac{\omega_{\mathbf{k}} \hat{q}_{\mathbf{k},\sigma}}{\sqrt{\epsilon_0 \mathcal{V}_{\mathbf{k},\sigma}}} \left[\left(\boldsymbol{\mu}_0^{(\varphi)}(\underline{\mathbf{R}}_{\text{eq}}^{(\varphi)}) + \sum_{\xi=1}^{n_{\text{vib}}} \boldsymbol{\mu}_{\varphi,\xi}' \hat{q}_{\varphi,\xi} \right) \cdot \mathbf{f}_{\mathbf{k},\sigma}(\mathbf{R}_0^{(\varphi)}) + \alpha_{\varphi}(\underline{\mathbf{R}}_{\text{eq}}^{(\varphi)}) \frac{\omega_{\mathbf{k}} \hat{q}_{\mathbf{k},\sigma}}{\sqrt{\epsilon_0 \mathcal{V}_{\mathbf{k},\sigma}}} \right], \quad (2.51a)$$

and

$$
\hat{V}_{\text{int-vib}}^{(\varphi;\mathbf{k},\sigma;2)} = \frac{1}{2\epsilon_0 \mathcal{V}_{\mathbf{k},\sigma}} \left[\left(\boldsymbol{\mu}_0^{(\varphi)}(\underline{\mathbf{R}}_{\text{eq}}^{(\varphi)}) + \sum_{\xi=1}^{n_{\text{vib}}} \boldsymbol{\mu}'_{\varphi,\xi} \hat{q}_{\varphi,\xi} \right) \cdot \mathbf{f}_{\mathbf{k},\sigma}(\mathbf{R}_0^{(\varphi)}) \right]^2 . \tag{2.51b}
$$

From the structure of eqs. (2.49) and (2.51) it is possible to infer that the photon modes can be treated as additional vibrational modes coupled to the normal modes of the bare molecule. The BO approximation relies on the fact that the timescales of electronic dynamics are considerably distinct to those of nuclear dynamics; this consideration rises questions about the timescales of photon dynamics which are reflected on the values of $\omega_{\mathbf{k}}$. Since all the EM modes are independent, for the CBO approximation to hold, the sum over wave vectors $\mathbf{k}$ is constrained to those frequencies for which $\omega_{\mathbf{k}} \approx \omega_{\varphi,\xi}$, i.e., infrared frequencies.

To gain some insight as to what the consequences of VSC are on the PES, let's consider the simple case of a single vibrational mode in the electronic ground-state, $\varphi = 0$, coupled to a single photon mode. In this scenario, the potential energy function takes the form

$$
\begin{aligned}
V(q_{\mathbf{k}}, q_{\xi}) = & \left(1 - \frac{2\alpha_0}{\epsilon_0 \mathcal{V}_{\mathbf{k}}} \right) \frac{\omega_{\mathbf{k}}^2 q_{\mathbf{k}}^2}{2} + \left(1 - \frac{4 g_{\mathbf{k};\xi}^2}{\omega_{\mathbf{k}} \omega_1} \right) \frac{\omega_{\xi}^2 q_{\xi}^2}{2} - \frac{2 g_{\mathbf{k};\xi}}{\sqrt{\omega_{\xi} \omega_{\mathbf{k}}}} \omega_{\mathbf{k}} \omega_{\xi} q_{\mathbf{k}} q_{\xi} \\
& - \frac{\mu_0}{\sqrt{\epsilon_0 \mathcal{V}_{\mathbf{k}}}} \left(\omega_{\mathbf{k}} q_{\mathbf{k}} + \frac{2 g_{\mathbf{k};\xi}}{\sqrt{\omega_{\xi} \omega_{\mathbf{k}}}} \omega_{\xi} q_{\xi} \right) - \frac{\mu_0^2}{2 \epsilon_0 \mathcal{V}_{\mathbf{k}}},
\end{aligned}
\tag{2.52}
$$

where $\mu_0 = \boldsymbol{\mu}_0^{(0)}(\underline{\mathbf{R}}_{\text{eq}}^{(0)}) \cdot \mathbf{f}_{\mathbf{k}}(\mathbf{R}_0^{(0)})$ is the component of the molecular permanent dipole moment along the polarization vector, and $g_{\mathbf{k};\xi} = \boldsymbol{\mu}'_{\xi} \cdot \mathbf{f}_{\mathbf{k}}(\mathbf{R}_0^{(0)}) \sqrt{\omega_{\mathbf{k}}/4\omega_{\xi} \epsilon_0 \mathcal{V}_{\mathbf{k}}}$ is a coupling constant. From this expression it can be concluded the following (fig. 2.2):

- The polarizability effectively squeezes the photon mode.

- The molecular transition dipole moment squared effectively squeezes the vibrational mode.

- The strength of the bi-linear coupling increases with the vibrational transition dipole moment, and decreases with the quantization volume.
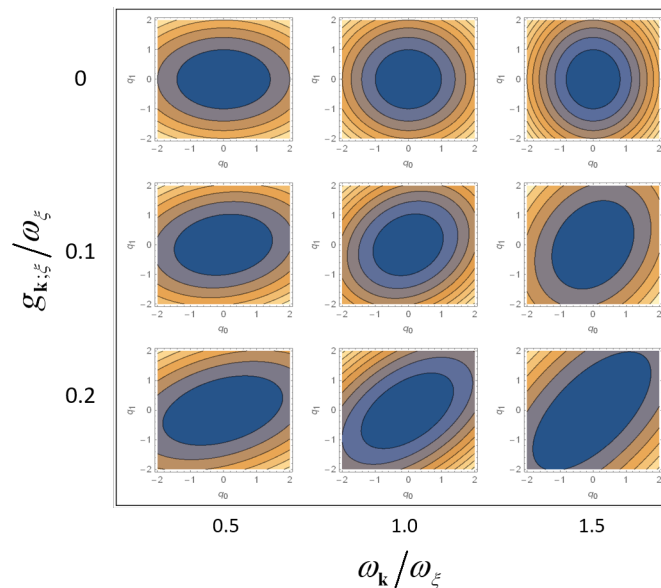
Figure 2.2: Contour plot around the minimum of the PES for a single vibrational mode coupled to a single EM mode. The used parameters are for carbon monoxide [108]: $\omega_\xi = 2196\,\mathrm{cm}^{-1}$, $\mu_0 = 0.112\,\mathrm{D}$, $\mu'_\xi = -94.32\,\mathrm{cm}^{3/2}\,\mathrm{s}^{-1}$, and $\alpha_0 = 1.95\,\mathrm{\mathring{A}}^3$.

- Light matter coupling results in a rotation of the potential energy surface, which redefines the normal modes.

- The molecular permanent dipole moment shifts the effective minima of both modes, as well as the overall value of the potential energy.

The new normal modes are a mixture of photon and molecular vibration and are called *polariton modes*, with the highest frequency belonging to the *upper polariton*, UP, while the smallest frequency belongs to the *lower polariton*, LP.

The features regarding displacement of minima and squeezing are relevant in the semiclassical analysis of adiabatic reactions as shown in [83] and chapter 3.

2.3.2 Regimes of coupling intensity

This section illustrates the relevance and gives some insight into the physical meaning of the various terms contributing to the Hamiltonian. Let's consider the simple case of a single
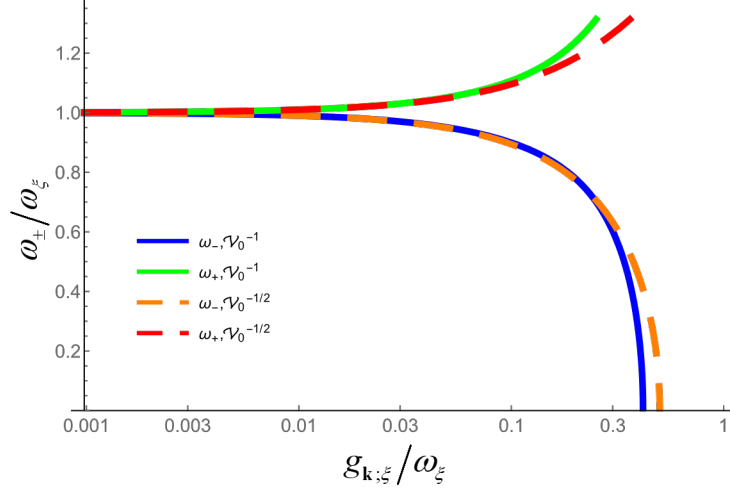
Figure 2.3: Frequencies of LP and UP as a function of the coupling constant between the vibration of CO [108] and a resonant cavity. The calculation compares leading terms proportional to $1/\mathcal{V}_\mathbf{k}$ and to $1/\sqrt{\mathcal{V}_\mathbf{k}}$.

vibrational mode in the electronic ground-state coupled to a single EM mode with TE polarization. The permanent dipole shifts the equilibrium configuration but has no impact on the frequencies; therefore the terms in the Hamiltonian that depend on it will b excluded from the remaining of this discussion.

Figure 2.3 compares the frequencies of the UP, ω_+, and LP, ω_-, calculated with and without the terms proportional to $1/\mathcal{V}_\mathbf{k}$, i.e., the contributions from the polarizability and the coupling constant squared. It becomes clear that these terms can be neglected for small values of $g_{\mathbf{k};\xi}/\omega_\xi$. The regime in which the coupling is large enough for this terms to be relevant is known as the *deep strong coupling* regime. In particular, the term proportional to $\hbar^2 g_{\mathbf{k};\xi}^2$ is commonly known as the A^2 term, and the relevance of its presence for the situations explored in this work is still under debate [95].

After removing the deep-strong-coupling terms, the Hamiltonian of the system, in terms of creation and annihilation operator, reads

$$\hat{H}_{\mathbf{k};\xi} = \hbar\omega_\mathbf{k}\left(\hat{a}_\mathbf{k}^\dagger \hat{a}_\mathbf{k} + \frac{1}{2}\right) + \hbar\omega_\xi\left(\hat{b}_\xi^\dagger \hat{b}_\xi + \frac{1}{2}\right) - \hbar g_{\mathbf{k};\xi}\left(\hat{a}_\mathbf{k}^\dagger + \hat{a}_\mathbf{k}\right)\left(\hat{b}_\xi^\dagger + \hat{b}_\xi\right), \qquad (2.53)$$

31

which is reminiscent of the Rabi Hamiltonian [8, 9]. The frequencies of the polariton modes derived from this model are

$$\omega_\pm = \left[\frac{1}{2}\left(\omega_\mathbf{k}^2 + \omega_\xi^2 \pm \sqrt{\left(\omega_\mathbf{k}^2 - \omega_\xi^2\right)^2 + 4g_{\mathbf{k};\xi}^2 \omega_\mathbf{k}\omega_\xi}\right)\right]^{1/2}. \tag{2.54}$$

The Hamiltonian in eq. (2.53), includes the so-called non-energy-conserving terms: $\hat{a}_\mathbf{k}^\dagger \hat{b}_\xi^\dagger$ and $\hat{a}_\mathbf{k}\hat{b}_\xi$, which correspond to high-frequency oscillations in the Heisenberg interaction picture. It is customary to apply the rotating wave approximation (RWA) in which these terms, also called counter-rotating, are neglected to give rise to the Hamiltonian

$$\hat{H}_{\text{RWA}} = \hbar\omega_\mathbf{k}\left(\hat{a}_\mathbf{k}^\dagger\hat{a}_\mathbf{k} + \frac{1}{2}\right) + \hbar\omega_\xi\left(\hat{b}_\xi^\dagger\hat{b}_\xi + \frac{1}{2}\right) - \hbar g_{\mathbf{k};\xi}\left(\hat{a}_\mathbf{k}^\dagger\hat{b}_\xi + \hat{b}_\xi^\dagger\hat{a}_\mathbf{k}\right), \tag{2.55}$$

which is now similar to the Jaynes-Cummings (JC) model [109]. The new polaritonic frequencies are

$$\omega_\pm = \frac{\omega_\mathbf{k} + \omega_\xi \pm \Omega}{2}, \tag{2.56}$$

where

$$\Omega = \sqrt{\Delta^2 + 4g_{\mathbf{k};\xi}^2} \tag{2.57}$$

is the Rabi frequency, with detuning $\Delta = \omega_\mathbf{k} - \omega_\xi$, which corresponds to the frequency of oscillations of the probability of measuring the system in either a photonic or a molecular state. Figure 2.4 illustrates the polaritonic frequencies obtained from the Rabi-like and the JC-like Hamiltonians. The values of the corresponding frequencies diverge as $g_{\mathbf{k};\xi}/2\omega_\xi$; however, for $g_{\mathbf{k};\xi} < \omega_\xi/10$, the gains due to the simplification afforded by the RWA outweigh the error it introduces. Typically, when a system is coupled so strongly that the RWA is bad, it is said to be in the *ultra-strong* coupling regime.

When the light-matter coupling is small, it becomes necessary to acknowledge the dissipation mechanisms. The EM mode is subject to cavity leakage, while intermolecular
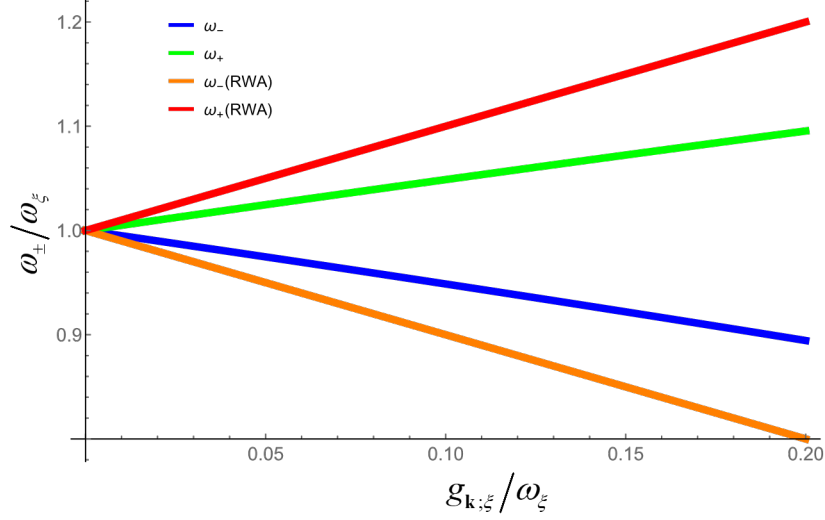
Figure 2.4: Frequencies of LP and UP as a function of the coupling constant for a Hamiltonian with counter-rotating terms and one under the RWA. The resonance condition, $\omega_{\mathbf{k}} = \omega_\xi$ is considered

interactions give rise to vibrational broadening. To include these dissipative channels the Hamiltonian of the system adopts the form

$$\hat{H}_{\text{RWA}-\text{dis}} = \hbar(\omega_{\mathbf{k}} + i\kappa)\left(\hat{a}_{\mathbf{k}}^\dagger \hat{a}_{\mathbf{k}} + \frac{1}{2}\right) + \hbar(\omega_\xi + i\gamma)\left(\hat{b}_\xi^\dagger \hat{b}_\xi + \frac{1}{2}\right) - \hbar g_{\mathbf{k};\xi}\left(\hat{a}_{\mathbf{k}}^\dagger \hat{b}_\xi + \hat{b}_\xi^\dagger \hat{a}_{\mathbf{k}}\right), \quad (2.58)$$

where γ is the vibrational linewidth. Figure 2.5 shows the absorption signal as a function of coupling. Three regimes can be identified:

- Weak coupling: $g_{\mathbf{k};\xi} < |\kappa - \gamma|/2$

  The Rabi frequency is imaginary and, therefore, the polariton modes are degenerate.

- Intermediate coupling: $|\kappa - \gamma|/2 < g_{\mathbf{k};\xi} < \sqrt{(\kappa^2 + \gamma^2)/2}$

  The polariton modes are non-degenerate, strictly speaking, but the signals overlap so that there is a single maximum. Dissipation overcomes the coupling.

- Strong coupling: $\sqrt{(\kappa^2 + \gamma^2)/2} < g_{\mathbf{k};\xi}$
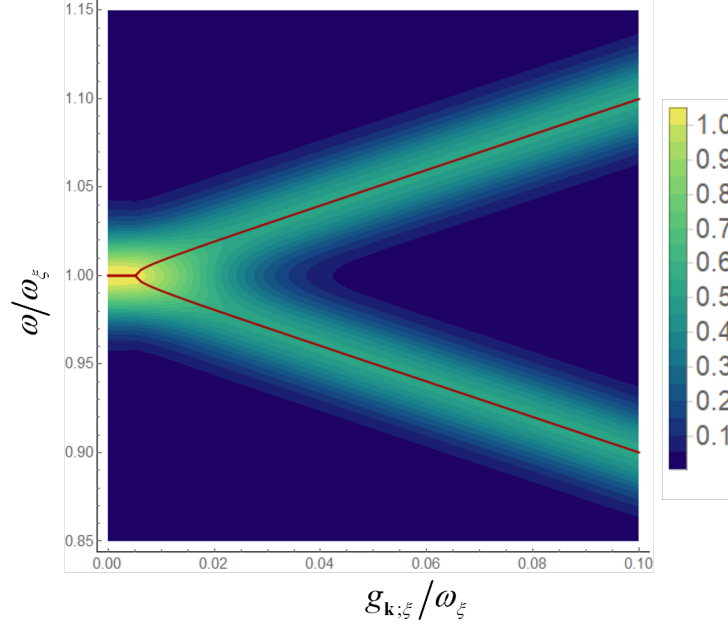
Figure 2.5: Absorption signal of the polariton modes as a function of the intensity of light-matter coupling. The signal intensity goes from blue to yellow. In red it is shown the frequencies of UP and LP.

Each polariton mode produces a well-defined absorption signal, i.e., the modes are robust to dissipation.

In the strong-coupling regime, the difference between maxima corresponds to the Rabi frequency, because of that, this quantity is also known referred to as Rabi splitting.

2.3.3   Many molecules inside the cavity

The Hamiltonian for a collection of N molecules in their electronic ground-state inside a cavity is

$$\hat{H} = \sum_{\mathbf{k}_{xy}} \sum_{m>0} \sum_{\sigma \in \{s,p\}} \hat{H}_{\text{cav}}^{(\mathbf{k}_{xy},m,\sigma)} + \sum_{i=1}^{N} \sum_{\xi=1}^{n_{\text{vib}}} \hat{H}_{\text{vib}}^{(i,\xi)} + \sum_{\mathbf{k}_{xy}} \sum_{m>0} \sum_{\sigma \in \{s,p\}} \sum_{i=1}^{N} \sum_{\xi=1}^{n_{\text{vib}}} \hat{H}_{\text{int}}^{(\mathbf{k}_{xy},m,\sigma;i,\xi)}. \quad (2.59)$$

For a cavity with thickness in the range of typical vibrational wavelengths for organic molecules, a reasonable assumption is that the only cavity modes that witness the presence of

34
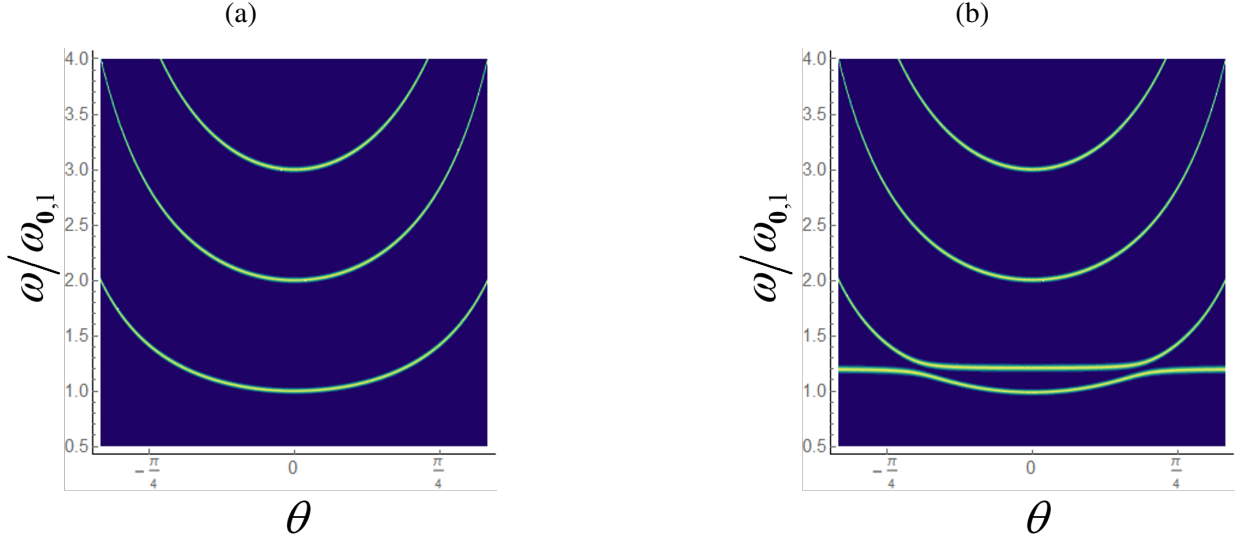
Figure 2.6: Cavity angular dispersion spanning modes $1 \leq m \leq 3$. (a) Empty cavity. (b) Cavity including a sample with a vibrational mode with frequency $\omega_\xi = 1.2\omega_{0,1}$ and coupling constant $g = 0.07\omega_{0,1}$.

the molecules are those with $m = 1$ (fig. 2.6). In the same fashion, the independence among normal modes imply that only those near resonant with the cavity would contribute significantly to the coupling. With these considerations in mind, the notation can be simplified by making $(\mathbf{k}_{xy}, 1, \sigma) \to (\mathbf{k}, \sigma)$ and $(i, \xi) \to (i)$, and the components of eq. (2.59) become

$$\hat{H}_{\mathrm{cav}}^{(\mathbf{k},\sigma)} = \hbar\omega_{\mathbf{k}}\left(\hat{a}_{\mathbf{k},\sigma}^\dagger \hat{a}_{\mathbf{k},\sigma} + \frac{1}{2}\right), \tag{2.60a}$$

$$\hat{H}_{\mathrm{vib}}^{(i)} = \hbar\omega_\xi\left(\hat{b}_i^\dagger \hat{b}_i + \frac{1}{2}\right), \tag{2.60b}$$

and

$$\hat{H}_{\mathrm{int}}^{(\mathbf{k},\sigma;i)} = -\hbar g_{\mathbf{k},\sigma;i}\left(\hat{a}_{\mathbf{k},\sigma}^\dagger + \hat{a}_{\mathbf{k},\sigma}\right)\left(\hat{b}_i^\dagger + \hat{b}_i\right). \tag{2.60c}$$

where the self-interacting (quadratic) terms have been neglected.

If the sample inside the cavity is approximated as a regular grid of cells with volume $\mathcal{A}L/N$, the molecular operators can be written as position dependent $\hat{b}_i \to \hat{b}_{\mathbf{r},z}$, where $\mathbf{r}$ is the

position of the molecule in the plane parallel to the plates, and z is its position along the cavity axis. The total number of values of $\mathbf{r}$ is $N_\perp$ and that of z is N_z, such that $N_\perp N_z = N$. For fixed wave-vector and polarization, it is possible to define a collective mode whose operators are of the form

$$\hat{b}_{\mathbf{k},\sigma;z,0} = \frac{1}{\sqrt{N_\perp} g_{\mathbf{k},\sigma;z}} \sum_{\mathbf{r}} g_{\mathbf{k},\sigma;\mathbf{r},z} \hat{b}_{\mathbf{r},z}, \tag{2.61}$$

such that the interaction Hamiltonian becomes

$$\hat{H}_{\text{int}}^{(\mathbf{k},\sigma)} = -\sqrt{N_\perp} \sum_{z} \hbar g_{\mathbf{k},\sigma;z} \left(\hat{a}_{\mathbf{k},\sigma}^\dagger + \hat{a}_{\mathbf{k},\sigma} \right) \left(\hat{b}_{\mathbf{k},\sigma;z}^\dagger + \hat{b}_{\mathbf{k},\sigma;z} \right), \tag{2.62}$$

where

$$g_{\mathbf{k},\sigma;z} = \sqrt{\sum_{\mathbf{r}} \left| g_{\mathbf{k},\sigma;\mathbf{r},z} \right|^2}. \tag{2.63}$$

In turn, the vibrational Hamiltonian is rewritten as

$$\hat{H}_{\text{vib}}^{(\mathbf{k},\sigma)} = \hbar \omega_\xi \sum_{z} \sum_{\zeta=0}^{N_\perp - 1} \left(\hat{b}_{\mathbf{k},\sigma;z,\zeta}^\dagger \hat{b}_{\mathbf{k},\sigma;z,\zeta} + \frac{1}{2} \right), \tag{2.64}$$

where the operators related to the collective modes are of the form

$$\hat{b}_{\mathbf{k},\sigma;z,\zeta} = \sum_{\mathbf{r}} c_{\zeta,\mathbf{r}} \hat{b}_{\mathbf{k},\sigma;\mathbf{r},z}, \tag{2.65}$$

where the coefficients in the linear combination fulfill

$$\sum_{\mathbf{r}} c_{\zeta,\mathbf{r}}^* c_{\zeta',\mathbf{r}} = \delta_{\zeta,\zeta'}, \tag{2.66a}$$

which implies

$$\sum_{\mathbf{r}} c_{\zeta,\mathbf{r}}^* g_{\mathbf{k},\sigma;\mathbf{r},z} = g_{\mathbf{k},\sigma;z} \delta_{\zeta,0}. \tag{2.66b}$$

All the modes with $\zeta > 0$ do not take part in the light-matter interaction, and are therefore dark.

The previous treatment implies that the number of $\mathbf{k}_{xy}$ modes is $N_\perp$, and it has been argued that the ratio $N/N_\perp = N_z$ in infrared microcavities has an order of magnitude between 10^7 and 10^{12} [81, 82]. In any case, since the number of molecules vastly outnumber that of photon modes, it is safe to assume that the physics of the system can be captured with a coarse-grained scheme of a single photon mode and N_z molecules.

With some simplifications to the notation, such model is described by the Hamiltonian

$$\hat{H} = \hbar\omega_0\left(\hat{a}_0^\dagger\hat{a}_0 + \frac{1}{2}\right) + \hbar\omega_1\sum_{i=1}^{N}\left(\hat{a}_i^\dagger\hat{a}_i + \frac{1}{2}\right) - \hbar g\left(\hat{a}_0^\dagger + \hat{a}_0\right)\sum_{i=1}^{N}\left(\hat{a}_i^\dagger + \hat{a}_i\right), \qquad (2.67)$$

which is reminiscent of the Dicke model [110], or the Tavis-Cummings model if the RWA is considered [111]. In eq. (2.67), ω_0 is the frequency of the EM mode, and ω_1 that of the vibrational modes. The operators $\hat{a}_0$ and $\hat{a}_0^\dagger$ represent the photon mode, while $\hat{a}_i$ and $\hat{a}_i^\dagger$ represent the ith molecule. The coupling constant $g = \langle 1|e\hat{x}|0\rangle\sqrt{\omega_0 N_\perp/2\hbar\varepsilon_0\mathcal{A}L}$, is written under the assumption that the molecular dipoles are isotropically oriented and all of them experience the same coupling to the cavity.

Since the vibrations are all degenerate, the Hamiltonian can be recast as

$$\begin{aligned}\hat{H} =&\hbar\omega_0\left(\hat{a}_0^\dagger\hat{a}_0 + \frac{1}{2}\right) + \hbar\omega_1\left(\hat{a}_B^\dagger\hat{a}_B + \frac{1}{2}\right) - \sqrt{N}\hbar g\left(\hat{a}_0^\dagger + \hat{a}_0\right)\left(\hat{a}_B^\dagger + \hat{a}_B\right) \\ &+ \hbar\omega_1\sum_{k=1}^{N-1}\left(\hat{a}_{D(k)}^\dagger\hat{a}_{D(k)} + \frac{1}{2}\right),\end{aligned} \qquad (2.68)$$

where

$$\hat{a}_B = \frac{1}{\sqrt{N}}\sum_{i=1}^{N}\hat{a}_i \qquad (2.69)$$

defines a *bright mode* that is the only one experiencing coupling to the EM mode, and

$$\hat{a}_{D(k)} = \sum_{i=1}^{N} c_{k,i} \hat{a}_i, \tag{2.70a}$$

$$\sum_{i=1}^{N} c_{k,i} = 0, \tag{2.70b}$$

$$\sum_{i=1}^{N} c_{k,i}^* c_{k',i} = \delta_{k,k'}, \tag{2.70c}$$

define a set of *dark modes* that do not take part in the light-matter interaction.

It is now possible to write the Hamiltonian in terms of the polariton modes:

$$\hat{H} = \frac{1}{2}\left(\hat{p}_+^2 + \omega_+^2 \hat{q}_+^2\right) + \frac{1}{2}\left(\hat{p}_-^2 + \omega_-^2 \hat{q}_-^2\right) + \frac{1}{2}\sum_{k=1}^{N-1}\left(\hat{p}_{D(k)}^2 + \omega_1^2 \hat{q}_{D(k)}^2\right), \tag{2.71}$$

if the counter-rotating terms are take into account, or

$$\hat{H} = \hbar\omega_+\left(\hat{a}_+^\dagger \hat{a}_+ + \frac{1}{2}\right) + \hbar\omega_-\left(\hat{a}_-^\dagger \hat{a}_- + \frac{1}{2}\right) + \hbar\omega_1 \sum_{k=1}^{N-1}\left(\hat{a}_{D(k)}^\dagger \hat{a}_{D(k)} + \frac{1}{2}\right), \tag{2.72}$$

under the RWA. In both cases, the polaritonic modes can be defined through

$$\begin{pmatrix} \hat{a}_+ \\ \hat{a}_- \end{pmatrix} = \begin{pmatrix} \cos\theta_N & \sin\theta_N \\ -\sin\theta_N & \cos\theta_N \end{pmatrix} \begin{pmatrix} \hat{a}_0 \\ \hat{a}_B \end{pmatrix} \tag{2.73}$$

where θ_N is the mixing angle fulfilling

$$\tan(2\theta_N) = \begin{cases} \frac{2g\sqrt{N\omega_0\omega_1}}{\omega_0^2 - \omega_1^2} & \text{Dicke-like} \\ \frac{2g\sqrt{N}}{\omega_0 - \omega_1} & \text{TC-like} \end{cases}. \tag{2.74}$$

A remarkable feature of the many-body Hamiltonians is that the intensity of the light-matter interaction experiences an enhancement by a factor of $\sqrt{N}$. It is thanks to this collective effect

that an ensemble of organic molecules can achieve the strong-coupling regime and exhibit the well-known optical features of polaritonic systems. On the other hand, it must be taken into account that, for every two polaritonic modes formed, there are $N - 1$ dark modes that are, in principle, indistinguishable from bare molecular modes in all regards except for localization.

2.4 Notions of cavity-modified chemical kinetics

This section explores the simplest approaches to develop some intuition as to how VSC might modify chemical reactivity.

First, let's consider the partition function for a collection of N degenerate harmonic oscillators with frequency ω_1, plus an additional one with frequency ω_0:

$$Z_{\text{bare}} = \text{csch}\left(\frac{\hbar\omega_0}{2k_{\text{B}}T}\right)\text{csch}^N\left(\frac{\hbar\omega_1}{2k_{\text{B}}T}\right), \tag{2.75}$$

where k_{B} is the Boltzmann's constant, and T is the temperature. This partition function corresponds to the ensemble of uncoupled molecules and the cavity mode. On the other hand, when strong-coupling is introduced, the partition function is

$$Z_{\text{VSC}} = \text{csch}\left(\frac{\hbar\omega_+}{2k_{\text{B}}T}\right)\text{csch}\left(\frac{\hbar\omega_-}{2k_{\text{B}}T}\right)\text{csch}^{N-1}\left(\frac{\hbar\omega_1}{2k_{\text{B}}T}\right). \tag{2.76}$$

At room temperature, and for typical vibrational frequencies, $Z_{\text{bare}}/Z_{\text{VSC}} \approx 1$. Moreover, a chemical transformation occurs, presumably, one molecule at a time, which means that the true comparison is between a polaritonic ensemble with N coupled molecules and one with $N - 1$. Thus, the partition functions are, for all practical purposes, identical.

Lastly, consider now a chemical reaction described by the Lindemann-Hinshelwood mechanism:

$$R \underset{k_{-1}}{\overset{k_1}{\rightleftharpoons}} R^* \overset{k_2}{\longrightarrow} P. \tag{2.77}$$

Here, a reactant R acquires an excess of energy, thus transforming into a n intermediate "hot" species R^* before relaxing into the final product P. The differential rate expressions for the concentration of each species are

$$\frac{d[R]}{dt} = k_{-1}[R^*](t) - k_1[R](t),$$ (2.78a)

$$\frac{d[R^*]}{dt} = k_1[R](t) - (k_{-1} + k_2)[R^*](t),$$ (2.78b)

and

$$\frac{d[P]}{dt} = k_2[R^*](t).$$ (2.78c)

Applying the steady state approximation to the activated state yields

$$[R^*](t) = \frac{k_1[R](t)}{k_{-1} + k_2},$$ (2.79)

with which the production rate law can be written as

$$\frac{d[P]}{dt} = \frac{k_1 k_2}{k_{-1} + k_2}[R](t).$$ (2.80)

Therefore, a bare rate constant can be defined as

$$k_{\text{bare}} = \frac{k_1 k_2}{k_{-1} + k_2}.$$ (2.81)

A possibile scenario inside the cavity is that the activated state corresponds to a manifold with polaritonic character, i.e., the mechanisms includes the additional channels:

$$R \underset{k_{-\text{UP}}}{\overset{k_{+\text{UP}}}{\rightleftarrows}} R^*_{\text{UP}} \overset{k_{2\text{UP}}}{\longrightarrow} P,$$ (2.82a)

and

$$R \underset{k_{-LP}}{\overset{k_{+LP}}{\rightleftharpoons}} R^*_{LP} \xrightarrow{k_{2UP}} P. \tag{2.82b}$$
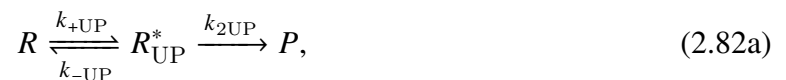
The rates can be assumed to be formulated according to Fermi's Golden Rule (FGR):

$$k_{i \to f} \propto \left| \langle i | \hat{V}_{rxn} | f \rangle \right|^2 \rho_f, \tag{2.83}$$

where i and f denote the initial and final states, respectively, $\hat{V}_{rxn}$ is a transition inducing potential representing the chemical transformation, and ρ_f is the density of final states. In this situation then $k_{-UP} \approx k_{-LP} \approx k_{-1}$, $k_{2UP} \approx k_{2LP} \approx k_2$, but $k_1 \approx N k_{+UP} \approx N k_{+LP}$. With these considerations, the rate constant becomes

$$k_{VSC} = \frac{(k_1 + k_{+UP} + k_{LP})k_2}{k_{-1} + k_2}. \tag{2.84}$$

However, by virtue of the of the proportions between the elementary-step rate constants, k_{VSC} is effectively k_{bare}.

A final consideration is the fact that the equilibrium between the reactant and the activated state could be affected by cavity leakage. This relaxation channel contributes to the back reaction $R^* \to R$. Nonetheless, in the timescale of photon leakage is much shorter than that of substitution reactions. This fact implies that the equilibrium between the reactant and the activated state is impervious to the new relaxation channel. Therefore, the upgraded rate constant is now

$$k_{VSC} = \frac{k_1 + K\kappa}{k_{-1} + \kappa + k_2} k_2. \tag{2.85}$$

Since κ is expected to be much larger than any other rate constant, then

$$k_{VSC} \approx K k_2. \tag{2.86}$$

41

If relaxation to the product is much slower than back to the reactant, the rate constants inside and outside of the cavity are the same. On the other hand, for $k_2 \gg k_{-1}$, $k_{\text{bare}} \approx k_1$, which can be much smaller than k_{VSC}. By introducing an additional relaxation channel, light-matter coupling resulted in shifting the slowest step in the mechanism.

Although intuitive, this analysis is mostly phenomenological and is not grounded in in a solid basis of first principles. The following chapters of this work explore in-depth some theoretical approaches intended to formally explain the presence, or lack thereof, of VSC effects on the observed chemical rates.

Chapter 3

Effects of vibrational strong coupling on adiabatic reactions

3.1   Introduction

Multiple experimental results show that reactions taking place inside of optical microcavities proceed with different kinetics than outside of them [56, 71, 74, 75, 77, 78]. Rate modification seems to require that the confined electromagnetic mode couples to one of the varieties of molecular vibrational modes present in the reactive medium [74]. For reactions in solution, where molecules are isotropically distributed, this coupling is maximized under resonant conditions, *i.e.*, when the cavity is tuned to a vibrational frequency in the molecules. Also, the effect on the kinetics has been observed to increase as the collective coupling intensifies, as a consequence of the large number of molecules present in a sample [41, 71].

These observations are reminiscent of the description of light-matter coupling in terms of hybrid states known as polaritons [37–40, 42, 112], which successfully explains the optical properties of these systems [55, 58, 67, 113, 114]. Recently, it has been suggested that a class of nonadiabatic charge transfer reactions would experience a catalytic effect from resonant collective

43

coupling between high-frequency modes and infrared cavity modes; the mechanism relies on the formation of vibrational polaritons which feature reduced activation energies compared to the bare molecules [96, 115].

However, a large class of reactions fall in the adiabatic regime, where the potential energy surfaces of the electronic ground and excited states are well-separated. These reactions should be accurately described by a transition state theory (TST) [116–118] that accounts for vibrational strong coupling (VSC). Feist and coworkers have in fact developed a theoretical framework with the essential ingredients to capture the action of a confined electromagnetic field on chemical processes such as nucleophylic substitution [83, 84]. Within this framework, they find that the presence of a cavity mode modifies the reactive potential energy surface, thus predicting conditions for increase and decrease of reaction rates. However, according to their results, resonance is not essential for this modification to take place. Furthermore, the effect depends on the intensity of the single-molecule coupling, and cooperativity can only occur under conditions such as the anisotropic alignment of the permanent dipoles, an unlikely condition for the aforementioned reported experiments [102]. Remarkably, Feist's formalism excludes the language of polaritons. In fact, they concede that polaritonic degrees of freedom appear inconsequentially in the form of normal modes near the equilibrium configurations of the system, and that the effects are of the Casimir-Polder type [83]. In the present work, we restate their formalism bringing the polaritonic modes into the limelight; we take advantage of the polaritonic framework to expand the formalism and obtain simple and physically intuitive analytical TST expressions that describe the modified collisional prefactors and activation energies in terms of light and matter parameters. Our results are in line with the predictions of [83, 84], highlighting that further work must be carried out to understand the difference between experiment and theory in the context of thermally-activated reactions under VSC. A similar discussion to the present one can be found in [85].

3.2 Theory

According to TST, the rate constant at temperature T is defined as [119–123]

$$k_{\text{TST}} = \frac{k_B T}{2\pi\hbar} \frac{Z_{\ddagger}}{Z_{\text{eq}}} e^{-\frac{E_a}{k_B T}}, \tag{3.1}$$

where k_B and $\hbar$ are the Boltzmann and reduced Planck constants, respectively. $Z_{\ddagger}$ is the partition function of the transition state (TS) without the contribution of the reactive mode, and Z_{eq} is the total partition function of the reactant state. $E_a = V_{\ddagger} + \frac{1}{2} \sum_i \hbar\omega_{i,\ddagger} - V_{\text{eq}} - \frac{1}{2} \sum_j \hbar\omega_{j,\text{eq}}$ is the activation energy, where the frequency $\omega_{i,r}$ corresponds to the square root of the i-th positive eigenvalue of the Hessian of the potential energy surface evaluated at the state r. We will determine how the rate constant changes for a thermally-activated process in which the reactant is a heteronuclear diatomic molecule, when it takes place inside an optical microcavity. While the following analysis can be straightforwardly generalized for a multimode system, we will treat only the simplest case for the sake of conceptual clarity. Such a system with N identical reactant molecules can be described by the Hamiltonian [52, 83]

$$\hat{H} = \hat{H}_{\text{EM}} + \sum_{i=1}^{N} \left(\hat{H}_{\text{mol}}^{(i)} + \hat{V}_{\text{int}}^{(i)} \right), \tag{3.2}$$

where $\hat{H}_{\text{EM}} = \hbar\omega_0 \left(\hat{a}_0^{\dagger}\hat{a}_0 + \frac{1}{2} \right)$ characterizes a confined electromagnetic field of frequency ω_0, and creation and annihilation operators $\hat{a}_0^{\dagger}$ and $\hat{a}_0$, respectively. $\hat{H}_{\text{mol}}^{(i)} = \hat{T}_{\text{nuc}}^{(i)} + \hat{V}_{\text{nuc}}^{(i)} + \hat{T}_{\text{elec}}^{(i)} + \hat{V}_{\text{elec}}^{(i)} + \hat{V}_{\text{nuc-elec}}^{(i)}$ is the Hamiltonian of the i-th molecule containing the kinetic, $\hat{T}$, and potential, $\hat{V}$, energies of the nuclear and electronic degrees of freedom, as well as their Coulomb interaction. The coupling between light and matter is given by $\hat{V}_{\text{int}}^{(i)} = g\omega_0\hat{q}_0\boldsymbol{\epsilon}\cdot\hat{\mu}_i$, where $\hat{q}_0 = \sqrt{\frac{\hbar}{2\omega_0}} \left(\hat{a}_0^{\dagger} + \hat{a}_0 \right)$, and $g = -(\mathcal{V}\varepsilon_0)^{-1/2}$ is the coupling constant, with $\mathcal{V}$ the mode volume and ε_0 the vacuum permittivity; $\boldsymbol{\epsilon}$ is the polarization vector of the cavity field, and $\hat{\mu}_i$ is the molecular vibrational electric dipole moment. In the (cavity) Born-Oppenheimer approximation [51, 112], the ground state potential
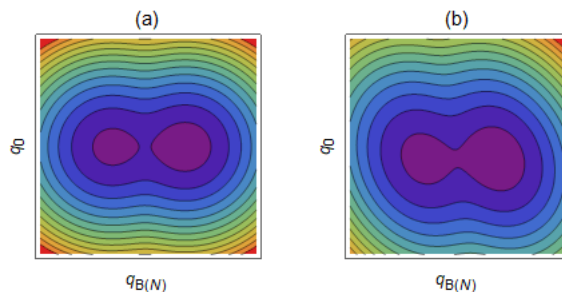
Figure 3.1: Effect of VSC on a reactive potential energy surface. a) Asymmetric double well potential uncoupled to an orthogonal harmonic cavity mode. b) Same as in (a) but with non-zero light-matter coupling. The distortion of the wells reveals the redefinition of normal modes from cavity and molecule to upper and lower polaritons.

energy for the electronic Schrödinger equation with Hamiltonian $\hat{H}_{\text{elec}} = \hat{H} - \sum_{i=1}^{N} \hat{T}_{\text{nuc}}$, can be parameterized in terms of the nuclear coordinates, $\mathbf{R}$, and the photon coordinate q_0, which is an eigenvalue of the operator $\hat{q}_0$. Thus, the potential energy surface governing the nuclear degrees of freedom (Fig. 3.1) becomes

$$V(\mathbf{R}, q_0) = \sum_{i=1}^{N} V_{\text{nuc}}(\mathbf{R}_i) + \frac{\omega_0^2}{2} q_0^2 + \omega_0 g q_0 \boldsymbol{\epsilon} \cdot \sum_{i=1}^{N} \boldsymbol{\mu}(\mathbf{R}_i). \tag{3.3}$$

Equation 3 implicitly assumes that the excited potential energy surfaces are well separated in energy from the ground state. This is reasonable given that ω_0 is a frequency in the infrared region of the electromagnetic spectrum. In writing Eqs. (3.2) and (3.3) we have neglected the diamagnetic term arising from the Power-Zienau-Woolley transformation [7]. Its relevance for problems in the current context is explored in detail in Refs. [95, 102]. Nevertheless, since even in the ultrastrong regime, light-matter coupling *per molecule* is much smaller than the vibrational transition energies [50], the inclusion of such term should only account for slight modifications to the formalism that leave the findings unchanged.

In the neighborhood of the equilibrium configuration of the reactants, $\mathbf{R}_{\text{eq}}$, the potential is reasonably well described by a second order expansion while the dipole moment can be

approximated to first order:

$$V(\mathbf{R} \approx \mathbf{R}_{eq}, q_0) = \sum_{i=1}^{N} V_{nuc}(\mathbf{R}_{i,eq}) + \frac{\omega_{eq}^2}{2} \sum_{i=1}^{N} q_i^2 + \frac{\omega_0^2}{2} q_0^2 + \omega_0 g q_0 \sum_{i=1}^{N} \left(\mu_{i,eq} + \mu'_{i,eq} q_i \right), \quad (3.4)$$

where q_i is the mass-reduced bond elongation with respect to the equilibrium length of the i-th molecule, $\omega_{eq}^2 = \left. \frac{\partial^2 V_{nuc}^{(i)}}{\partial q_i^2} \right|_0$, $\mu_{i,eq} = \boldsymbol{\epsilon} \cdot \boldsymbol{\mu}(\mathbf{R}_{i,eq})$, and $\mu'_{i,eq} = \boldsymbol{\epsilon} \cdot \left. \frac{\partial \boldsymbol{\mu}(\mathbf{R}_i)}{\partial q_i} \right|_0$. We note that this expansion excludes the polarizability term present in the perturbative treatment by [83]; however, as we shall see, this omission does not affect the main conclusions.

Differentiation of Eq. (3.4) yields

$$\frac{\partial V}{\partial q_0} = \omega_0^2 q_0 + \omega_0 g \sum_{i=1}^{N} \left(\mu_{i,eq} + \mu'_{i,eq} q_i \right) \tag{3.5a}$$

$$\frac{\partial V}{\partial q_j} = \omega_{eq}^2 q_j + \omega_0 g q_0 \mu'_{j,eq} \quad 1 \le j \le N; \tag{3.5b}$$

therefore, at the new minimum, $\mathbf{R}_{eq}^{VSC}$, close to $\mathbf{R}_{eq}$, the coordinates fulfill

$$\begin{pmatrix} \omega_0^2 & \omega_0 g \sqrt{N \langle \mu'^2_{eq} \rangle_N} \\ \omega_0 g \sqrt{N \langle \mu'^2_{eq} \rangle_N} & \omega_{eq}^2 \end{pmatrix} \begin{pmatrix} q_0 \\ q_{B(N)} \end{pmatrix} = -\omega_0 g N \langle \mu_{eq} \rangle_N \begin{pmatrix} 1 \\ 0 \end{pmatrix}, \tag{3.6}$$

where $\langle x \rangle_N = \frac{1}{N} \sum_{i=1}^{N} x_i$, and the bright molecular mode is given by $q_{B(N)} = \sqrt{\frac{N}{\langle \mu'^2_{eq} \rangle_N}} \langle \mu'_{eq} q \rangle_N$.

The coefficient matrix in Eq. (3.6) corresponds to the Hopfield-Bogoliubov form of the Dicke model in the normal phase [124, 125]; therefore, its diagonalization gives rise to polariton modes, as shown in Fig. 3.1. To be specific, Eq. (3.6) can be rewritten as

$$\begin{pmatrix} \omega_{+(N)}^2 & 0 \\ 0 & \omega_{-(N)}^2 \end{pmatrix} \begin{pmatrix} q_{+(N)} \\ q_{-(N)} \end{pmatrix} = -\omega_0 g N \langle \mu_{eq} \rangle_N \begin{pmatrix} \cos \theta_N \\ \sin \theta_N \end{pmatrix}, \tag{3.7}$$

where $\omega_{\pm(N)}^2 = \frac{1}{2} \left[\omega_0^2 + \omega_{eq}^2 \pm \sqrt{4 \omega_0^2 g^2 N \langle \mu'^2_{eq} \rangle_N + \left(\omega_0^2 - \omega_{eq}^2 \right)^2} \right]$ is the frequency squared of the

upper(lower) polaritonic mode, $\begin{pmatrix} q_{+(N)} \\ q_{-(N)} \end{pmatrix} = \begin{pmatrix} \cos\theta_N & -\sin\theta_N \\ \sin\theta_N & \cos\theta_N \end{pmatrix} \begin{pmatrix} q_0 \\ q_{\mathrm{B}(N)} \end{pmatrix}$ are the polaritonic mode

coordinates, and $\theta_N = -\frac{1}{2}\arctan\frac{2\omega_0 g\sqrt{N\langle\mu_{\mathrm{eq}}'^2\rangle_N}}{\omega_0^2 - \omega_{\mathrm{eq}}^2}$ is the mixing angle.

Equation (3.4) can be recast using this new set of coordinates in the form

$$
V(\mathbf{R} \approx \mathbf{R}_{\mathrm{eq}}, q_0) = \sum_{i=1}^{N} V_{\mathrm{nuc}}(\mathbf{R}_{i,\mathrm{eq}}) + \frac{\omega_{\mathrm{eq}}^2}{2} \sum_{k=1}^{N-1} q_{\mathrm{D}(N)}^{(k)2} + \frac{\omega_{+(N)}^2}{2} q_{+(N)}^2 + \frac{\omega_{-(N)}^2}{2} q_{-(N)}^2
$$
$$
+ \omega_0 g N \langle\mu_{\mathrm{eq}}\rangle_N \left(\cos\theta_N q_{+(N)} + \sin\theta_N q_{-(N)}\right),
$$

(3.8)

where $q_{\mathrm{D}(N)}^{(k)} = \sum_{i=1}^{N} c_{ki} q_i$ are the dark vibrational modes, with the coefficients c_{ki} fulfilling $\sum_{i=1}^{N} \mu_{i,\mathrm{eq}}'^* c_{ki} = 0$ and $\sum_{i=1}^{N} c_{k'i}^* c_{ki} = \delta_{k'k}$. Evaluating the potential in Eq. (3.8) at $\mathbf{R}_{\mathrm{eq}}^{\mathrm{VSC}}$ yields

$$
V_{\mathrm{eq}}^{\mathrm{VSC}} = \sum_{i=1}^{N} V_{\mathrm{nuc}}(\mathbf{R}_{i,\mathrm{eq}}) - \left(\frac{\omega_0 \omega_{\mathrm{eq}}}{\omega_{+(N)}\omega_{-(N)}} g N \langle\mu_{\mathrm{eq}}\rangle_N\right)^2.
$$

(3.9)

We note that the modification to the potential is proportional to the ratio of the determinants of the Hessian without and with light-matter coupling, which acts as a measure of the redefinition of the normal modes. Additionally, the presence of the permanent dipole reveals the largely electrostatic nature of this effect.

Without loss of generality, let us assume that the molecule with label N undergoes a reaction. The potential energy surface in the neighborhood of the TS configuration, $\mathbf{R}_\ddagger$, is

$$
V(\mathbf{R} \approx \mathbf{R}_\ddagger, q_0) = \sum_{i=2}^{N} V_{\mathrm{nuc}}(\mathbf{R}_{i,\mathrm{eq}}) + V_{\mathrm{nuc}}(\mathbf{R}_{N,\ddagger}) + \frac{\omega_{\mathrm{eq}}^2}{2} \sum_{i=1}^{N-1} q_i^2 + \frac{\omega_0^2}{2} q_0^2 + \frac{\omega_\ddagger^2}{2} q_N^2
$$
$$
+ \omega_0 g q_0 \left[\sum_{i=1}^{N-1} \left(\mu_{i,\mathrm{eq}} + \mu_{i,\mathrm{eq}}' q_i\right) + \mu_\ddagger + \mu_\ddagger' q_N\right].
$$

(3.10)

Here, $\omega_\ddagger^2 = \left.\frac{\partial^2 V_{\mathrm{nuc}}^{(N)}}{\partial q_N^2}\right|_{q_\ddagger} < 0$ is the squared frequency of the unstable mode, $\mu_\ddagger = \boldsymbol{\epsilon} \cdot \boldsymbol{\mu}(\mathbf{R}_{N,\ddagger})$, and

$$\mu'_{\ddagger} = \boldsymbol{\epsilon} \cdot \left.\frac{\partial \mu(\mathbf{R}_N)}{\partial q_N}\right|_{q_{\ddagger}}.$$

Applying the previous treatment to the potential energy surface in the saddle point, $\mathbf{R}_{\ddagger}^{\text{VSC}}$, the coordinates fulfill

$$
\begin{pmatrix}
\omega_0^2 & \omega_0 g \sqrt{(N-1)\langle\mu_{\text{eq}}'^2\rangle_{N-1}} & \omega_0 g \mu'_{\ddagger} \\
\omega_0 g \sqrt{(N-1)\langle\mu_{\text{eq}}'^2\rangle_{N-1}} & \omega_{\text{eq}}^2 & 0 \\
\omega_0 g \mu'_{\ddagger} & 0 & \omega_{\ddagger}^2
\end{pmatrix}
\begin{pmatrix}
q_0 \\
q_{\text{B}(N-1)} \\
q_N
\end{pmatrix}
$$

$$
= -\omega_0 g \left[(N-1)\langle\mu_{\text{eq}}\rangle_{N-1} + \mu_{\ddagger}\right]
\begin{pmatrix}
1 \\
0 \\
0
\end{pmatrix}. \quad (3.11)
$$

For typical values of the transition dipole moments, the off-diagonal terms that depend on N remain significant since the number of molecules per cavity mode is estimated between 10^6 and 10^{10} [81, 82]. The term $g\omega_0\mu'_{\ddagger}$ is several orders of magnitude smaller, and we can neglect it to recover a polaritonic picture where

$$
\begin{pmatrix}
\omega_{+(N-1)}^2 & 0 & 0 \\
0 & \omega_{-(N-1)}^2 & 0 \\
0 & 0 & \omega_{\ddagger}^2
\end{pmatrix}
\begin{pmatrix}
q_{+(N-1)} \\
q_{-(N-1)} \\
q_N
\end{pmatrix}
\approx -\omega_0 g \left[(N-1)\langle\mu_{\text{eq}}\rangle_{N-1} + \mu_{\ddagger}\right]
\begin{pmatrix}
\cos\theta_{N-1} \\
\sin\theta_{N-1} \\
0
\end{pmatrix} \quad (3.12)
$$

at $\mathbf{R}_{\ddagger}^{\text{VSC}}$. Thus, the potential at the saddlepoint becomes

$$
V_{\ddagger}^{\text{VSC}} = \sum_{i=1}^{N-1} V_{\text{nuc}}(\mathbf{R}_{i,\text{eq}}) + V_{\text{nuc}}(\mathbf{R}_{N,\ddagger}) - \left(\frac{\omega_0 \omega_{\text{eq}}}{\omega_{+(N-1)}\omega_{-(N-1)}} g \left[(N-1)\langle\mu_{\text{eq}}\rangle_{N-1} + \mu_{\ddagger}\right]\right)^2. \quad (3.13)
$$

From Eqs. (3.4), (3.10) and (3.12), it follows that the step to the TS can be written as

$$
\text{UP}_N + \text{LP}_N + \sum_{k=1}^{N-1} D_N^{(k)} \longrightarrow \text{UP}_{N-1} + \text{LP}_{N-1} + \sum_{k'=1}^{N-2} D_{N-1}^{(k')} + R_N^{\ddagger} \quad (3.14)
$$

where $R_N^\ddagger$ represents the reactive molecule in the TS. Therefore, the rate constant should include the partition functions of the whole ensemble of molecules coupled to light; however, as we will see, since only one molecule undergoes the reaction, the ratio of partition functions simplifies to an intelligible expression in terms of the single molecule k_{TST}.

Outside of the cavity the rate constant takes the form

$$k_{\text{TST}} = \frac{k_B T}{\pi \hbar} \frac{Q_\ddagger}{Q_{\text{eq}}} \sinh\left(\frac{\hbar \omega_{\text{eq}}}{2 k_B T}\right) \exp\left(-\frac{V_{\text{nuc}}\left(\mathbf{R}_{N,\ddagger}\right) - V_{\text{nuc}}\left(\mathbf{R}_{N,\text{eq}}\right)}{k_B T}\right), \tag{3.15}$$

where the ratio $Q_\ddagger/Q_{\text{eq}}$ captures all the information from the translational and rotational degrees of freedom (for a 1D system comprised of the reactive mode only, $Q_\ddagger = Q_{\text{eq}}$). To characterize the effect of the cavity mode on the kinetics, we define

$$k_{\text{TST}}^{\text{VSC}} = \kappa_N k_{\text{TST}}, \tag{3.16}$$

where the ratio of rate constants is given by

$$\kappa_N = A_{\text{VSC}}(T) \exp\left(-\frac{\Delta V_{\text{VSC}} + \Delta E_0^{\text{VSC}}}{k_B T}\right), \tag{3.17a}$$

with prefactor

$$A_{\text{VSC}}(T) = \frac{\sinh\left(\hbar \omega_{+(N)}/2 k_B T\right) \sinh\left(\hbar \omega_{-(N)}/2 k_B T\right)}{\sinh\left(\hbar \omega_{+(N-1)}/2 k_B T\right) \sinh\left(\hbar \omega_{-(N-1)}/2 k_B T\right)}, \tag{3.17b}$$

cavity-induced potential energy difference

$$\Delta V_{\text{VSC}} = \omega_0^2 \omega_{\text{eq}}^2 g^2 \left[\left(\frac{N \langle \mu_{\text{eq}} \rangle_N}{\omega_{+(N)} \omega_{-(N)}}\right)^2 - \left(\frac{(N-1) \langle \mu_{\text{eq}} \rangle_{N-1} + \mu_\ddagger}{\omega_{+(N-1)} \omega_{-(N-1)}}\right)^2\right], \tag{3.17c}$$

and zero-point-energy difference

$$\Delta E_0^{\text{VSC}} = \frac{\hbar\omega_{+(N-1)} + \hbar\omega_{-(N-1)} - \hbar\omega_{+(N)} - \hbar\omega_{-(N)}}{2}. \tag{3.17d}$$

As stated before, $N \gg 1$. In this limit, $A_{\text{VSC}}(T) \approx 1$, $\Delta E_0^{\text{VSC}} \approx 0$, and the ratio of rate constants becomes

$$\kappa_N \approx \exp\left[\frac{\left(\omega_{\text{eq}} g \mu_\ddagger\right)^2}{\left(\omega_{\text{eq}}^2 - g^2 N \left\langle\mu_{\text{eq}}'^2\right\rangle\right) k_B T}\right], \tag{3.18}$$

where we have considered that, for typical reactions in liquid solution, the molecular dipoles are isotropically distributed; therefore, $\langle\mu_{\text{eq}}\rangle_N = 0$. Regarding collective effects, in Fig. 3.2, we show the ratio of rate constants as a function of the collective coupling and the permanent dipole moment of the TS. We can see that the variation of κ_N throughout the span of the weak and strong light-matter coupling regimes is negligible. Furthermore, even over a huge range of possible values of $\mu_\ddagger$, the ratio of rate constants remains too close to 1 to imply any observable change in the reaction rate. In contrast, note that in a sample with perfectly aligned dipoles, $\langle\mu_{\text{eq}}\rangle_N \neq 0$, leading to substantial collective $O(N)$ contributions to ΔV_{VSC} [see Eq. (3.17c)]. Furthermore, regardless of dipole alignment, it can be shown that ΔV_{VSC} is independent of ω_0, and is therefore unable to describe a resonant effect.

3.2.1   Single-molecule case

When there is a single molecule per cavity mode, the only surviving coupling in Eq. (3.11) is that between the TS and the photon. In this case, the saddlepoint condition can be recast in terms of the eigenmodes as

$$\begin{pmatrix} \omega_{-\ddagger}^2 & 0 \\ 0 & \omega_{+\ddagger}^2 \end{pmatrix}\begin{pmatrix} q_{+\ddagger} \\ q_{-\ddagger} \end{pmatrix} = -\omega_0 g \mu_\ddagger \begin{pmatrix} \cos\theta_\ddagger \\ \sin\theta_\ddagger \end{pmatrix}, \tag{3.19}$$
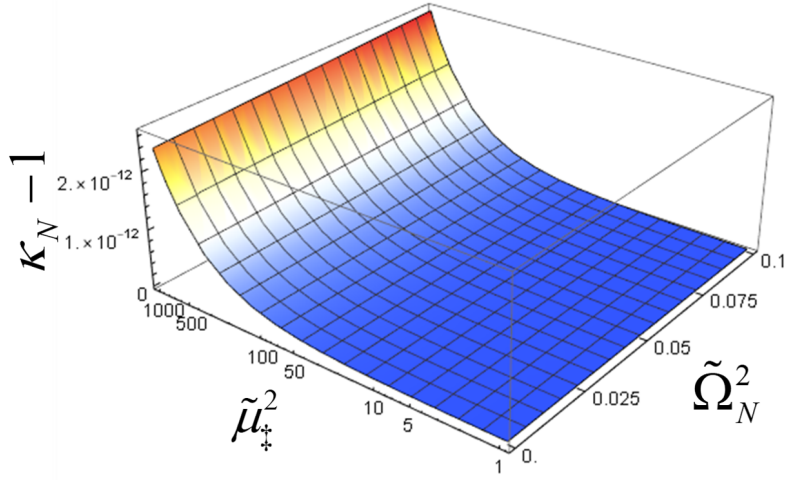
Figure 3.2: Ratio of rate constants as a function of the permanent dipole in the TS, and the collective light-matter coupling. $\tilde{\mu}_{\ddagger} = \mu_{\ddagger}/|\langle n+1| \hat{\mu}_{\text{eq}} |n\rangle|$ is the permanent dipole moment in the TS normalized with respect to the transition dipole moment in the equilibrium configuration, and $\tilde{\Omega}_N = g\sqrt{N \langle \mu_{\text{eq}}^2 \rangle}/\omega_{\text{eq}}$ is the light-matter coupling normalized with respect to the frequency in the same configuration. Over the span of the weak and strong coupling regimes, and a wide range of values of the TS dipole, the transmission coefficient remains close to 1. For this calculation, $\omega_{eq} = 2000 \text{ cm}^{-1}$, $N = 10^9$, and $k_BT = 208.5 \text{ cm}^{-1}$.

where $\omega_{-\ddagger}^2 < 0 < \omega_{+\ddagger}^2$. The potential energy evaluated at $\mathbf{R}_{\ddagger}^{\text{VSC}}$ is

$$V_{\ddagger}^{\text{VSC}} = V_{\text{nuc}}(\mathbf{R}_{\ddagger}) - \left(\frac{\omega_0 \omega_{\ddagger}}{\omega_{+\ddagger}\omega_{-\ddagger}} g\mu_{\ddagger} \right)^2, \tag{3.20}$$

which produces

$$A_{\text{VSC}} = \frac{\sinh\left(\hbar\omega_+/2k_BT\right)\sinh\left(\hbar\omega_-/2k_BT\right)}{\sinh\left(\hbar\omega_{+\ddagger}/2k_BT\right)\sinh\left(\hbar\omega_{\text{eq}}/2k_BT\right)}, \tag{3.21a}$$

$$\Delta V_{\text{VSC}} = g^2\omega_0^2 \left[\left(\frac{\omega_{\text{eq}}\mu_{\text{eq}}}{\omega_+\omega_-} \right)^2 - \left(\frac{\omega_{\ddagger}\mu_{\ddagger}}{\omega_{+\ddagger}\omega_{-\ddagger}} \right)^2 \right], \tag{3.21b}$$

$$\Delta E_0^{\text{VSC}} = \frac{\hbar\omega_{+\ddagger} - \hbar\omega_+ - \hbar\omega_- + \hbar\omega_{\text{eq}}}{2}. \tag{3.21c}$$

It is worth noting that, despite $A_{\text{VSC}}(T)$ and ΔE_0^{VSC} deviating from 1 and 0, respectively, in the single-molecule limit, the effect is still off-resonant, thus reinforcing the findings in [83]. In any

case, the mode volumes and transition dipole moments required to modify a reaction rate are unrealistic unless we consider nano- and picocavities.

3.3   Conclusions

From the previous analysis we reach the same conclusions of [83]: effects of resonance between the cavity and the vibrational modes cannot be captured in a description at the level of TST, and the isotropic distribution of the permanent dipole moments negates the possibility of cooperative light-matter coupling effects. These results contrast with the situation of thermally-activated nonadiabatic charge transfer reactions, where the role of collective light-matter resonance in isotropic media is more evident. While we agree that the role of the polaritonic picture in our present analysis is rather shallow, it undoubtedly simplifies and clarifies the theoretical analysis. In conclusion, our results restate that a TST that takes into account strong coupling of the reactive mode to a resonant optical cavity mode is still insufficient to explain the experimental results involving thermally-activated adiabatic reactions in Refs. [56, 71, 73, 75, 77, 78].

Chapter 3, in full, is adapted from the material as it appears in "Polaritonic normal modes in transition state theory". Campos-Gonzalez-Angulo, Jorge A.; Yuen-Zhou, Joel. The Journal of Chemical Physics, 152, 161101 (2020). The dissertation author was the primary investigator and author of this paper.

Chapter 4

Effects of vibrational strong coupling on non-adiabatic processes

4.1 Introduction

The strong interaction between excitations in a material medium and a resonant confined electromagnetic mode results in new states with light-matter hybrid character (polaritons) [10, 126]. Recent studies of molecular polaritons have revealed new phenomena and features that are appealing for applications in chemistry and materials science. These discoveries opened the doors to the emerging field of *polariton chemistry* [37–40, 46, 112, 127–129]. Of particular interest are recent observations of chemoselective suppression and enhancement of reactive pathways for molecules whose high-frequency vibrational modes are strongly coupled to infrared optical cavities [71, 74, 77, 78]. These effects of vibrational strong coupling (VSC) are noteworthy in that they occur in the absence of external photon pumping; implying that they involve thermally-activated (TA) processes, and potentially paving the road for a radically new synthetic chemistry strategy that involves injecting microfluidic solutions in suitable optical cavities (Fig. 4.1) to induce desired transformations. It is important to highlight that the VSC in these samples is the

consequence of an ensemble effect: each cavity mode (that is resonant with the polarization of the material) coherently couples to a large number of molecules. This coupling leads to two polaritonic modes and a macroscopic set of quasi-degenerate dark (subradiant) modes that, to a good approximation, should feature chemical dynamics that is indistinguishable from that of the bare molecular modes [113]. This picture could potentially change as a consequence of ultrastrong coupling effects; however, these effects should not be significant for modest Rabi splittings as those observed in the experiments [71, 74, 77, 78].

From the population of vibrationally excited states at thermal equilibrium, a tiny fraction would be allocated to the polariton modes, with the overwhelming majority residing in the dark-state reservoir [67, 81, 82, 114], unless the temperature is low enough for the lower polariton to overtake the predominant population second to that of the ground state. It is thus puzzling and remarkable that differences in the chemical kinetics can be detected in macroscopic systems under VSC at room temperature. This article provides a possible rationale for these observations. By studying a VSC version of the well-established Marcus-Levich-Jortner (MLJ) TA electron transfer model [97–99], we find a parameter range where, even if the number of dark-state channels massively outweigh the few polaritonic ones, the latter dictate the kinetics of the reaction given their smaller activation energies. The present model does not feature the complexity of the experimentally studied systems; however, it provides a minimalistic conceptual framework to develop qualitative insights on general TA VSC processes. We believe that this mechanism of polaritonic activation barrier reduction might be a widespread feature among such processes.
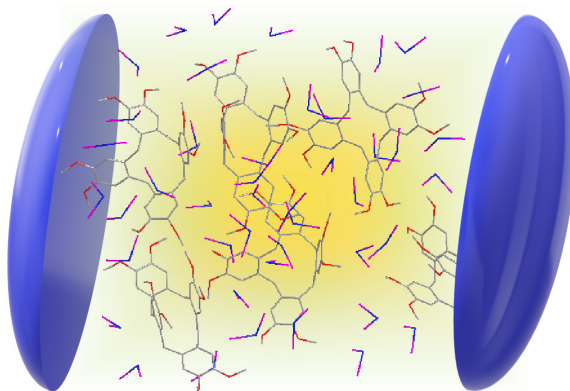
Figure 4.1: Depiction of a microcavity. A large number of molecules can undergo a chemical reaction (e.g., electron-transfer induced conformational transformation [130]) and support a high-frequency vibrational mode that can strongly couple to a confined optical mode; these molecules are in a solvated environment (blue/purple moieties). The reaction of concern is mediated by that intramolecular mode and a low-frequency collective configuration of the solvation sphere. The optical mode is typically confined by two dielectric mirrors (blue structures) separated by a spacer that is saturated with the reaction mixture.

4.2 Theoretical framework

According to MLJ theory, the rate coefficient of charge-transfer from a reactant (R) to a product (P) electronic state, at constant temperature T, is given by [97–99]

$$k_{\text{R}\to\text{P}} = \sqrt{\frac{\pi}{\lambda_{\text{S}} k_{\text{B}} T}} \frac{|J_{\text{RP}}|^2}{\hbar} e^{-S} \sum_{v=0}^{\infty} \frac{S^v}{v!} \exp\left(-\frac{(\Delta E + \lambda_{\text{S}} + v\hbar\omega_{\text{P}})^2}{4\lambda_{\text{S}} k_{\text{B}} T}\right),$$

(4.1)

where J_{RP} is the non-adiabatic coupling between electronic states, λ_{S} is the outer-sphere reorganization energy related to the low-frequency (classical) degrees of freedom of the solvent, ω_{P} is the frequency of a high-frequency intramolecular (quantum) mode with quantum number labeled by v, $S = \lambda_{\text{P}}/\hbar\omega_{\text{P}}$ is a Huang-Rhys parameter with λ_{P} the reorganization energy of the quantum mode, ΔE is the difference in energy between the equilibrium configurations of the R and P potential energy surfaces, and k_{B} is the Boltzmann constant. The MLJ rate can be thought of as a generalization of Marcus theory to include a sum over channels with different quanta v in the high-frequency mode of the product.

To gauge the effects of VSC, we consider the interaction between a single microcavity mode and an ensemble of M molecules that undergo electron transfer. For simplicity, we assume that VSC occurs via the high-frequency mode of P (since the MLJ rate only accounts for transitions originated in the ground state of the reactants, the case where this coupling also happens through R shares features with the current one that we shall discuss later). This constraint implies a drastic change in molecular geometry upon charge transfer so that the vibrational transition dipole moment goes from negligible to perceptible. This rather unusual behavior can be observed in molecular actuators. [130, 131] The Hamiltonian for such system is

$$\hat{H} = \hat{H}_{\mathrm{ph}} + \sum_{i=1}^{M} \left[\hat{H}_{\mathrm{R}}^{(i)} \, |R_i\rangle \, \langle R_i| + \left(\hat{H}_{\mathrm{P}}^{(i)} + \hat{\mathcal{V}}_{\mathrm{int}}^{(i)} \right) |P_i\rangle \, \langle P_i| + J_{\mathrm{RP}} \left(|R_i\rangle \, \langle P_i| + |P_i\rangle \, \langle R_i| \right) \right], \quad (4.2)$$

where $\hat{H}_{\mathrm{ph}} = \hbar\omega_0 \left(\hat{a}_0^\dagger \hat{a}_0 + \frac{1}{2} \right)$ is the Hamiltonian of the electromagnetic mode with frequency ω_0, $|R_i\rangle$ and $|P_i\rangle$ denote the electronic (reactant/product) states of the i-th molecule, $\hat{H}_{\mathrm{R}}^{(i)} = \hbar\omega_{\mathrm{R}} \hat{\mathcal{D}}_i^\dagger \hat{\mathcal{S}}_i^\dagger \left(\hat{a}_i^\dagger \hat{a}_i + \frac{1}{2} \right) \hat{\mathcal{S}}_i \hat{\mathcal{D}}_i + \hat{H}_{\mathrm{S}}(\hat{\mathbf{q}}_{\mathrm{S}}^{(i)} + \mathbf{d}_{\mathrm{S}})$ and $\hat{H}_{\mathrm{P}}^{(i)} = \hbar\omega_{\mathrm{P}} \left(\hat{a}_i^\dagger \hat{a}_i + \frac{1}{2} \right) + \hat{H}_{\mathrm{S}}(\hat{\mathbf{q}}_{\mathrm{S}}^{(i)}) + \Delta E$ are the bare Hamiltonians of the i-th reactant/product with quantum mode frequency ω_{R} and ω_{P}, respectively. $\hat{\mathcal{V}}_{\mathrm{int}}^{(i)} = \hbar g \left(\hat{a}_i^\dagger \hat{a}_0 + \hat{a}_0^\dagger \hat{a}_i \right)$ is the light-matter interaction under the rotating wave approximation [132] with single-molecule coupling $g = -\mu \sqrt{\frac{\hbar\omega_0}{2V\varepsilon_0}}$, transition dipole moment μ, and cavity mode volume V, $\hat{a}_i^\dagger / \hat{a}_i$ are creation/annihilation operators acting on the quantum mode of the i-th molecule ($i = 0$ denotes the cavity mode), $\hat{\mathcal{S}}_i = \exp \left[\frac{1}{2} \ln \left(\sqrt{\frac{\omega_{\mathrm{P}}}{\omega_{\mathrm{R}}}} \right) (\hat{a}_i^{\dagger 2} - \hat{a}_i^2) \right]$ and $\hat{\mathcal{D}}_i = \exp \left[\frac{1}{\sqrt{2}} (\hat{a}_i^\dagger - \hat{a}_i) D_{\mathrm{P}} \right]$ are squeezing and displacement operators [132], $\hat{H}_{\mathrm{S}}(\hat{\mathbf{q}}_{\mathrm{S}}^{(i)}) = \sum_\ell \frac{1}{2} \hbar\omega_{\mathrm{S}}^{(\ell)} \left(\hat{p}_{\mathrm{S}}^{(i,\ell)2} + \hat{q}_{\mathrm{S}}^{(i,\ell)2} \right)$ is the Hamiltonian of the classical modes with frequencies $\omega_{\mathrm{S}}^{(\ell)}$, $\hat{\mathbf{p}}_{\mathrm{S}}^{(i)}$ and $\hat{\mathbf{q}}_{\mathrm{S}}^{(i)}$ are the set of rescaled classical momenta and positions associated with the i-th quantum mode, and D_{P} and $\mathbf{d}_{\mathrm{S}}$ are the rescaled (dimensionless) distances between equilibrium configurations of the reactant and product along the quantum and classical mode coordinates, respectively. We shall point out that, since it only considers coupling to a single cavity mode, the Hamiltonian in equation (4.2) entails coarse-graining; therefore, M is not the total number of molecules in the cavity volume, but the

57

average number of molecules coupled per cavity mode [81]. While polaritonic effects in electron transfer processes have been studied in the pioneering work of [49] (see also [53]), we note that they were considered in the *electronic* strong coupling regime; as we shall see, the vibrational counterpart demands a different formalism and offers conceptually different phenomenology.

4.2.1 Relation between reactant and product harmonic oscillator operators.

Let us consider the vibrational Hamiltonians for the single-molecule reactant and product electronic states (we omit label (i) for simplicity hereafter),

$$\hat{H}_R = \frac{\hat{p}^2}{2m} + \frac{m\omega_R^2 \hat{x}^2}{2} = \hbar\omega_R \left(\hat{a}_R^\dagger \hat{a}_R + \frac{1}{2} \right), \tag{4.3}$$

$$\hat{H}_P = \frac{\hat{p}^2}{2m} + \frac{m\omega_P^2 (\hat{x} - d_P)^2}{2} + \Delta E = \hbar\omega_P \left(\hat{a}_P^\dagger \hat{a}_P + \frac{1}{2} \right) + \Delta E, \tag{4.4}$$

where m is the reduced mass of the mode, ω_A is the frequency of the mode in each electronic state ($A = R, P$), d_P is the difference between nuclear equilibrium configurations, ΔE is the energy difference between the electronic states, and $\hat{p}$ and $\hat{x}$ are the momentum and position operators for the described mode; therefore, the harmonic oscillator potential energy surface for P is a displaced-distorted version of that for R. The creation and annihilation operators are defined in terms of position and momentum ($d_R = 0$),

$$\begin{aligned}
\hat{a}_A^\dagger &= \sqrt{\frac{\omega_A m}{2\hbar}} (\hat{x} - d_A) - \frac{i\hat{p}}{\sqrt{2\hbar\omega_A m}}, \\
\hat{a}_A &= \sqrt{\frac{\omega_A m}{2\hbar}} (\hat{x} - d_A) + \frac{i\hat{p}}{\sqrt{2\hbar\omega_A m}};
\end{aligned} \tag{4.5}$$

conversely, the position-momentum representation is written in terms of the creation and annihilation operators as

$$\hat{x} - d_A = \sqrt{\frac{\hbar}{2\omega_A m}} \left(\hat{a}_A^\dagger + \hat{a}_A \right),$$
$$\hat{p} = \sqrt{\frac{\hbar \omega_A m}{2}} i \left(\hat{a}_A^\dagger - \hat{a}_A \right). \tag{4.6}$$

Equation (4.6) implies

$$\frac{\hat{a}_R^\dagger + \hat{a}_R}{\sqrt{\omega_R}} = \frac{\hat{a}_P^\dagger + \hat{a}_P + \tilde{d}_P}{\sqrt{\omega_P}},$$
$$\sqrt{\omega_R} \left(\hat{a}_R^\dagger - \hat{a}_R \right) = \sqrt{\omega_P} \left(\hat{a}_P^\dagger - \hat{a}_P \right), \tag{4.7}$$

where $\tilde{d}_P = \sqrt{2m/\hbar} \, d_P$; therefore, the reactant operators are written in terms of product ones as

$$\hat{a}_R^\dagger = \frac{1}{2} \left(\sqrt{\frac{\omega_R}{\omega_P}} + \sqrt{\frac{\omega_P}{\omega_R}} \right) \hat{a}_P^\dagger + \frac{1}{2} \left(\sqrt{\frac{\omega_R}{\omega_P}} - \sqrt{\frac{\omega_P}{\omega_R}} \right) \hat{a}_P + \sqrt{\frac{\omega_R}{\omega_P}} \frac{\tilde{d}_P}{2},$$
$$\hat{a}_R = \frac{1}{2} \left(\sqrt{\frac{\omega_R}{\omega_P}} - \sqrt{\frac{\omega_P}{\omega_R}} \right) \hat{a}_P^\dagger + \frac{1}{2} \left(\sqrt{\frac{\omega_R}{\omega_P}} + \sqrt{\frac{\omega_P}{\omega_R}} \right) \hat{a}_P + \sqrt{\frac{\omega_R}{\omega_P}} \frac{\tilde{d}_P}{2}. \tag{4.8}$$

These transformations can be written in terms of a squeezing and a displacement operator [132]:

$$\hat{S}_P(r) = \exp\left[\frac{r}{2} (\hat{a}_P^2 - \hat{a}_P^{\dagger 2}) \right], \tag{4.9}$$

$$\hat{D}_P(\alpha) = \exp\left[\alpha (\hat{a}_P^\dagger - \hat{a}_P) \right], \tag{4.10}$$

with actions given by

$$\hat{S}_P^\dagger(r) \hat{a}_P^\dagger \hat{S}_P(r) = \hat{a}_P^\dagger \cosh r - \hat{a}_P \sinh r, \tag{4.11}$$

$$\hat{D}_P^\dagger(\alpha) \hat{a}_P \hat{D}_P(\alpha) = \hat{a}_P + \alpha. \tag{4.12}$$

Therefore,

$$\hat{a}_{\text{R}}^{\dagger} = \hat{\mathcal{D}}_{\text{P}}^{\dagger}(\alpha)\hat{\mathcal{S}}_{\text{P}}^{\dagger}(r)\hat{a}_{\text{P}}^{\dagger}\hat{\mathcal{S}}_{\text{P}}(r)\hat{\mathcal{D}}_{\text{P}}(\alpha)$$

$$\hat{a}_{\text{R}} = \hat{\mathcal{D}}_{\text{P}}^{\dagger}(\alpha)\hat{\mathcal{S}}_{\text{P}}^{\dagger}(r)\hat{a}_{\text{P}}\hat{\mathcal{S}}_{\text{P}}(r)\hat{\mathcal{D}}_{\text{P}}(\alpha),$$

(4.13)

for

$$r = \ln\sqrt{\frac{\omega_{\text{R}}}{\omega_{\text{P}}}},$$

(4.14)

$$\alpha = \tilde{d}_{\text{P}}.$$

(4.15)

4.2.2 Rate in terms of polariton moldes

As a consequence of VSC, the system is best described in terms of collective normal modes defined by the operators [38, 133]

$$\hat{a}_{+(N)} = \cos\theta_N\hat{a}_0 - \sin\theta_N\hat{a}_{\text{B}(N)},$$

$$\hat{a}_{-(N)} = \sin\theta_N\hat{a}_0 + \cos\theta_N\hat{a}_{\text{B}(N)},$$

$$\hat{a}_{\text{D}(N)}^{(k)} = \sum_{i=1}^{N} c_{ki}\hat{a}_i; \quad 2 \le k \le N$$

(4.16)

where $0 \le N \le M$ is the number of molecules in the P state at a given stage in the reaction. These operators correspond to the upper and lower polaritons (UP,LP), and dark (D) modes, respectively. Note that the operators $\hat{a}_{\text{D}(N)}^{(k)}$ are defined only for $N \ge 2$, and the coefficients c_{ki} fulfill $\sum_{i=1}^{N} c_{ki} = 0$ and $\sum_{i=1}^{N} c_{k'i}^* c_{ki} = \delta_{k'k}$. In equation (4.16), $\theta_N = \frac{1}{2}\arctan\frac{2g\sqrt{N}}{\Delta}$ is the mixing angle, where $\Delta = \omega_0 - \omega_{\text{P}}$ is the light-matter detuning, and $\hat{a}_{\text{B}(N)} = \frac{1}{\sqrt{N}}\sum_{i=1}^{N}\hat{a}_i$ corresponds to

the so-called bright (superradiant) mode. These modes have associated frequencies

$$\omega_{\pm(N)} = \frac{\omega_0 + \omega_P}{2} \pm \frac{\Omega_N}{2},$$

$$\omega_D = \omega_P,$$

(4.17)

where $\Omega_N = \sqrt{4g^2N + \Delta^2}$ is the effective Rabi splitting; equivalent definitions can be made for the creation operators. Note that there is no free-lunch: the superradiantly enhanced VSC with the bright mode occurs at the expense of the creation of a macroscopic number of dark modes that –under the context of this model– do not mix with light. (Inhomogeneous broadening results in small but experimentally observable light-like character for these modes [133–136]. This effect is negligible for the phenomena considered in this work given that the density of molecular excitations is much larger than that of the photon modes.)

Inside of the cavity, the reaction R $\longrightarrow$ P becomes

$$R + UP_{N-1} + LP_{N-1} + \sum_{k=2}^{N-1} D_{N-1}^{(k)} \longrightarrow UP_N + LP_N + \sum_{k=2}^{N} D_N^{(k)},$$

(4.18)
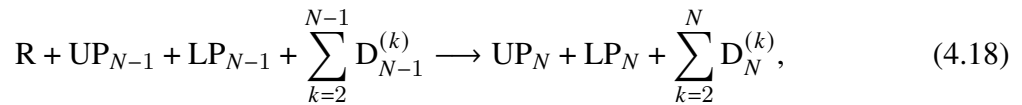
where the subscripts indicate the number of molecules that participate in VSC (from equation (4.16) it can be seen that UP_0 corresponds to the uncoupled photon mode, and LP_0 and $D_0^{(k)}$ are nonexistent). This reaction implies that each time a molecule transforms into the product, it becomes part of the ensemble that couples to light (see 4.2.3 for additional insight). Electron transfer occurs as a result of a vibronic transition between diabatic states; this feature makes it similar to Raman scattering. A study of the latter under VSC [63] took advantage of the massive degeneracy of the dark modes to introduce a judicious basis [137],

$$\hat{a}_D^{(k)} = \frac{1}{\sqrt{k(k-1)}} \left(\sum_{i=1}^{k-1} \hat{a}_i - (k-1)\hat{a}_k \right),$$

(4.19)

that enables calculations for an arbitrary number of molecules, and will prove to be convenient for
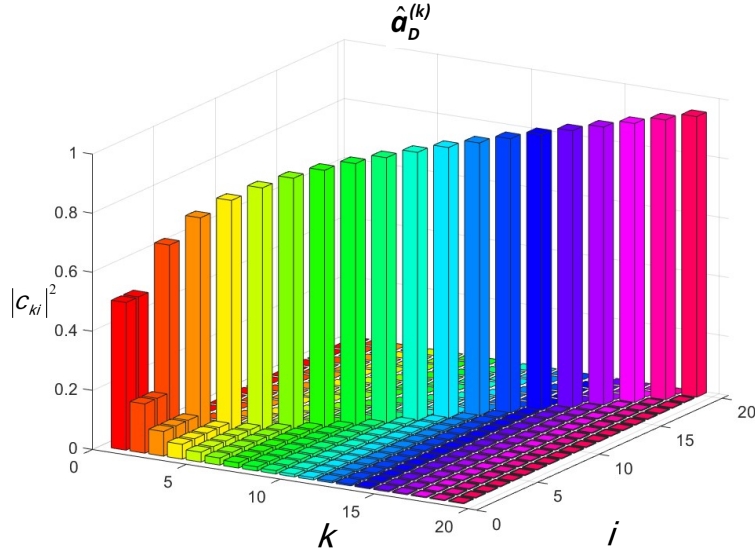
Figure 4.2: Probability coefficients for each molecular mode in the quasi-localized basis of dark modes defined in equation (4.19). As the dark mode index, k, increases, it becomes more localized in the k-th molecule, leaving a long tail behind it [63].

our purposes. Notice that the mode $\hat{a}_{\mathrm{D}}^{(k)}$ is highly localized at $\hat{a}_k$ but has a long tail for $\hat{a}_{1 \le i \le k-1}$ (fig. 4.2); furthermore, it is fully characterized by the index k, and thus does not depend explicitly on N. In terms of these dark modes, the reaction in equation (4.18) can be drastically simplified from an $N+1$ to a three-body process,

$$\mathrm{R} + \mathrm{UP}_{N-1} + \mathrm{LP}_{N-1} \longrightarrow \mathrm{UP}_N + \mathrm{LP}_N + \mathrm{D}_N^{(N)}, \tag{4.20}$$

where, without loss of generality, we have considered that the N-th molecule is the one that undergoes the reaction (notice that, in accordance with the notation introduced in equation (4.19), the mode $\mathrm{D}_N^{(N)}$ is highly localized in P_N for sufficiently large N). Furthermore, we can identify the normal modes of the photon ($\hat{a}_0$), the N-th molecule ($\hat{a}_N$), and the bright state that excludes it ($\hat{a}_{\mathrm{B}(N-1)}$) as natural degrees of freedom of the problem since the modes in reactants and products

can be written as Duschinsky transformations [138] of these. Explicitly, for the reactants we have

$$
\begin{pmatrix} \hat{a}_{+(N-1)} \\ \hat{a}_{-(N-1)} \end{pmatrix} = \begin{pmatrix} \cos\theta_{N-1} & -\sin\theta_{N-1} \\ \sin\theta_{N-1} & \cos\theta_{N-1} \end{pmatrix} \begin{pmatrix} \hat{a}_0 \\ \hat{a}_{B(N-1)} \end{pmatrix},
\tag{4.21}
$$

$$
\hat{a}'_N = \hat{\mathcal{D}}_N^\dagger \hat{\mathcal{S}}_N^\dagger \hat{a}_N \hat{\mathcal{S}}_N \hat{\mathcal{D}}_N,
\tag{4.22}
$$

where $\hat{a}'_N$ acts on the vibrational degrees of freedom of the N-th reactant (see 4.2.1 for a derivation); while for the products

$$
\begin{pmatrix} \hat{a}_{+(N)} \\ \hat{a}_{-(N)} \\ \hat{a}_D^{(N)} \end{pmatrix} = \begin{pmatrix} \cos\theta_N & -\sin\theta_N & 0 \\ \sin\theta_N & \cos\theta_N & 0 \\ 0 & 0 & 1 \end{pmatrix} \begin{pmatrix} 1 & 0 & 0 \\ 0 & \sqrt{\frac{N-1}{N}} & \sqrt{\frac{1}{N}} \\ 0 & \sqrt{\frac{1}{N}} & -\sqrt{\frac{N-1}{N}} \end{pmatrix} \begin{pmatrix} \hat{a}_0 \\ \hat{a}_{B(N-1)} \\ \hat{a}_N \end{pmatrix}.
\tag{4.23}
$$

With the above considerations, the VSC analogue of the MLJ rate coefficient in equation (4.1) is given by a sum over possible quanta $\{v_+, v_-, v_D\}$ in the product modes UP_N, LP_N and $D_N^{(N)}$, respectively:

$$
k_{R \to P}^{VSC} = \sqrt{\frac{\pi}{\lambda_S k_B T}} \frac{|J_{RP}|^2}{\hbar} \sum_{v_+=0}^{\infty} \sum_{v_-=0}^{\infty} \sum_{v_D=0}^{\infty} W_{v_+, v_-, v_D},
\tag{4.24}
$$

where $W_{v_+, v_-, v_D} = |F_{v_+, v_-, v_D}|^2 \exp\left(-\frac{E_{v_+, v_-, v_D}^\ddagger}{k_B T}\right)$, and

$$
\begin{aligned}
|F_{v_+, v_-, v_D}|^2 &= |\langle 0_{+(N-1)} 0_{-(N-1)} 0_R | v_+ v_- v_D \rangle|^2 \\
&= \left(\frac{\sin^2\theta_N}{N}\right)^{v_+} \left(\frac{\cos^2\theta_N}{N}\right)^{v_-} \left(\frac{N-1}{N}\right)^{v_D} \binom{v_+ + v_- + v_D}{v_+, v_-, v_D} |\langle 0' | v_+ + v_- + v_D \rangle|^2,
\end{aligned}
\tag{4.25}
$$

is a Franck-Condon factor between the global ground state in the reactants and the excited vibrational configuration in the product [63]. Here, $|0'\rangle$ is the vibrational ground state of the N-th molecule in the reactant electronic state and $|v_+ + v_- + v_D\rangle$ is the vibrational state of the N-th

molecule with $v_+ + v_- + v_D$ in the product electronic state. The calculation in equation (4.25) (see 4.2.4 for a derivation) is reminiscent to the contemporary problem of boson sampling [139]. Using the notation from equation (4.1),

$$E^{\ddagger}_{v_+,v_-,v_D} = \frac{(E^{v_+,v_-,v_D}_P - E^0_R + \lambda_S)^2}{4\lambda_S},$$ (4.26)

is the activation energy of the channel, with $E^0_R = \frac{\hbar}{2} \left(\omega_{+(N-1)} + \omega_{-(N-1)} + \omega_R \right)$ and $E^{v_+,v_-,v_D}_P = \Delta E + \hbar \left[\omega_{+(N)} \left(v_+ + \frac{1}{2} \right) + \omega_{-(N)} \left(v_- + \frac{1}{2} \right) + \omega_P \left(v_D + \frac{1}{2} \right) \right]$. equation (4.25) affords a transparent physical interpretation: the state $|v_+ v_- v_D\rangle$ is accessed by creating $v_+ + v_- + v_D$ excitations in the high-frequency oscillator of the N-th product; there are $\binom{v_+ + v_- + v_D}{v_+, v_-, v_D}$ ways to do so; $\left(\frac{\sin^2 \theta_N}{N} \right)$, $\left(\frac{\cos^2 \theta_N}{N} \right)$, and $\left(\frac{N-1}{N} \right)$ are the projections of the product normal modes on the oscillator of the N-th product; these scalings are the same as those obtained in our studies on polariton assisted energy transfer (PARET) [35].

4.2.3   Initial and final many-body vibronic states.

The rate to calculate corresponds to the stoichiometric process

$$(M - N)R + NP \longrightarrow (M - N - 1)R + (N + 1)P,$$ (4.27)
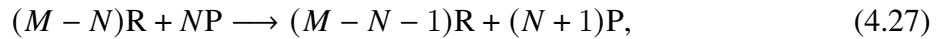
where N is the number of molecules in the product electronic state P, and $M - N$ is the number of molecules in the reactant electronic state R, such that M is the total number of molecules in the reaction vessel. Assigning labels to each molecule, without loss of generality, the transformation of the $N + 1$-th molecule can be written in the form

$$\sum_{i=N+1}^{M} R_i + \sum_{j=1}^{N} P_j \longrightarrow \sum_{i=N}^{M} R_i + \sum_{j=1}^{N+1} P_j,$$ (4.28)

which reduces to

$$R_{N+1} \longrightarrow P_{N+1}. \tag{4.29}$$

The charge transfer is ruled by the adiabatic coupling $\hat{J} = J_{RP} \sum_{i=1}^{M} (|R_i\rangle \langle P_i| + |P_i\rangle \langle R_i|)$; then, the matrix element that describes the process of our focus is

$$\langle M - N, N| \hat{J} |M - N - 1, N + 1\rangle = J_{RP} \langle M - N, N|R_{N+1}\rangle \langle P_{N+1}|M - N - 1, N + 1\rangle, \tag{4.30}$$

with many-body vibronic states given by

$$|X, Y\rangle = |P_1 P_2 \dots P_{Y-1} P_Y R_{Y+1} R_{Y+2} \dots R_{X+Y-1} R_{X+Y}\rangle \otimes |\Phi_X^Y\rangle, \tag{4.31}$$

where $|\Phi_X^Y\rangle$ is an eigenfunction of a vibrational Hamiltonian of the form

$$\begin{aligned}
\hat{H}_{X,Y} &= \hat{H}_{ph} + \sum_{i=1}^{Y} \left(\hat{H}_P^{(i)} + \hat{\mathcal{V}}_{int}^{(i)}\right) + \sum_{j=Y+1}^{X+Y} \hat{H}_R^{(j)} \\
&= \hat{H}_{+(Y)} + \hat{H}_{-(Y)} + \sum_{k=1}^{Y-1} \hat{H}_{D(Y)}^{(k)} + \sum_{i=1}^{Y} \hat{H}_S(\hat{q}_S^{(i)}) + Y\Delta E + \sum_{j=Y+1}^{X+Y} \hat{H}_R^{(j)}.
\end{aligned} \tag{4.32}$$

In equation (4.32), we have used the notation introduced in equation (4.2), and $\hat{H}_{\pm(Y)} = \hbar\omega_{\pm} \left(\hat{a}_{\pm(Y)}^{\dagger} \hat{a}_{\pm(Y)} + \frac{1}{2}\right)$ and $\hat{H}_{D(Y)}^{(k)} = \hbar\omega_P \left(\hat{a}_{D(Y)}^{\dagger(k)} \hat{a}_{D(Y)}^{(k)} + \frac{1}{2}\right)$ are the Hamiltonians of the upper/lower and k-th dark modes, respectively, all with creation and annihilation operators as defined in equation (4.16). Therefore, the matrix element corresponding to the transition becomes

$$\langle M - N, N| \hat{J} |M - N - 1, N + 1\rangle = J_{RP} \left\langle \Phi_{M-N}^{N} \middle| \Phi_{M-N-1}^{N+1} \right\rangle. \tag{4.33}$$

4.2.4 Dimensionally reduced Franck-Condon factor.

The non-vanishing overlaps between the vibrational ground state of the reactants and an arbitrary vibrational excitation with quantum numbers $\{v_+, v_-, v_D\}$ on the products can be written in terms of creation operators as

$$\langle 0_0 0_{B(N-1)} 0'_N \mid v_+ v_- v_D \rangle =$$

$$\langle 0_0 0_{B(N-1)} 0'_N \mid \frac{\left(\hat{a}^\dagger_{+(N)}\right)^{v_+}}{\sqrt{v_+!}} \frac{\left(\hat{a}^\dagger_{-(N)}\right)^{v_-}}{\sqrt{v_-!}} \frac{\left(\hat{a}^{(N-1)\dagger}_D\right)^{v_D}}{\sqrt{v_D!}} \left| 0_{+(N)} 0_{-(N)} 0^{(N-1)}_D \right\rangle. \quad (4.34)$$

These operators acting in the UP and LP can be written as linear combinations of the operators acting on the electromagnetic mode and the bright mode [equation (4.16)], i.e.,

$$\langle 0_0 0_{B(N-1)} 0'_N \mid v_+ v_- v_D \rangle =$$

$$\langle 0_0 0_{B(N-1)} 0'_N \mid \frac{\left(\hat{a}^\dagger_0 \cos\theta - \hat{a}^\dagger_{B(N)} \sin\theta\right)^{v_+}}{\sqrt{v_+!}}$$

$$\times \frac{\left(\hat{a}^\dagger_0 \sin\theta + \hat{a}^\dagger_{B(N)} \cos\theta\right)^{v_-}}{\sqrt{v_-!}} \frac{\left(\hat{a}^{(N-1)\dagger}_D\right)^{v_D}}{\sqrt{v_D!}} \left| 0_0 0_{B(N)} 0^{(N-1)}_D \right\rangle \quad (4.35)$$

The binomial theorem yields

$$\langle 0_0 0_{B(N-1)} 0'_N \mid v_+ v_- v_D \rangle =$$

$$\sum_{m=0}^{v_+} \sum_{n=0}^{v_-} \binom{v_+}{m}\binom{v_-}{n} \langle 0_0 0_{B(N-1)} 0'_N \mid \frac{\left(\hat{a}^\dagger_0 \cos\theta\right)^m \left(-\hat{a}^\dagger_{B(N)} \sin\theta\right)^{v_+-m}}{\sqrt{v_+!}}$$

$$\times \frac{\left(\hat{a}^\dagger_0 \sin\theta\right)^n \left(\hat{a}^\dagger_{B(N)} \cos\theta\right)^{v_--n}}{\sqrt{v_-!}} \frac{\left(\hat{a}^{(N-1)\dagger}_D\right)^{v_D}}{\sqrt{v_D!}} \left| 0_0 0_{B(N)} 0^{(N-1)}_D \right\rangle. \quad (4.36)$$

Since $[\hat{a}_0, \hat{a}_{B(N)}] = 0$, the only non-vanishing terms are those with $m = n = 0$, otherwise the overlap in the photonic mode would be between non-displaced states with different excitations;

66

therefore,

$$\langle 0_0 0_{B(N-1)} 0'_N \mid \nu_+ \nu_- \nu_D \rangle =$$

$$\langle 0_{B(N-1)} 0'_N \mid \frac{\left(-\hat{a}^{\dagger}_{B(N)} \cos\theta\right)^{\nu_+}}{\sqrt{\nu_+!}} \frac{\left(\hat{a}^{\dagger}_{B(N)} \sin\theta\right)^{\nu_-}}{\sqrt{\nu_-!}} \frac{\left(\hat{a}^{(N-1)\dagger}_{D}\right)^{\nu_D}}{\sqrt{\nu_D!}} \left| 0_{B(N)} 0^{(N-1)}_{D} \right\rangle. \quad (4.37)$$

Moreover, the creation operators acting on the bright and dark modes can be expressed as linear combinations of operators acting on the N-th molecule and the bright mode that excludes it [equation (4.19)], i.e.,

$$\langle 0_0 0_{B(N-1)} 0'_N \mid \nu_+ \nu_- \nu_D \rangle = \frac{(-\cos\theta)^{\nu_+} (\sin\theta)^{\nu_-}}{\sqrt{\nu_+! \nu_-! \nu_D!}} \langle 0_{B(N-1)} 0'_N \mid \left(\hat{a}^{\dagger}_{B(N-1)} \sqrt{\tfrac{N-1}{N}} + \hat{a}^{\dagger}_N \sqrt{\tfrac{1}{N}} \right)^{\nu_+}$$

$$\times \left(\hat{a}^{\dagger}_{B(N-1)} \sqrt{\tfrac{N-1}{N}} + \hat{a}^{\dagger}_N \sqrt{\tfrac{1}{N}} \right)^{\nu_-} \left(\hat{a}^{\dagger}_{B(N-1)} \sqrt{\tfrac{1}{N}} - \hat{a}^{\dagger}_N \sqrt{\tfrac{N-1}{N}} \right)^{\nu_D} \left| 0_{B(N-1)} 0_N \right\rangle. \quad (4.38)$$

By expanding the binomials as before, and discarding the terms that excite the $B(N-1)$ mode, we arrive at

$$\langle 0_0 0_{B(N-1)} 0'_N \mid \nu_+ \nu_- \nu_D \rangle = \frac{(-\cos\theta)^{\nu_+} (\sin\theta)^{\nu_-}}{\sqrt{\nu_+! \nu_-! \nu_D!}}$$

$$\times \langle 0'_N \mid \left(-\hat{a}^{\dagger}_N \sqrt{\tfrac{1}{N}} \right)^{\nu_+} \left(\hat{a}^{\dagger}_N \sqrt{\tfrac{1}{N}} \right)^{\nu_-} \left(-\hat{a}^{\dagger}_N \sqrt{\tfrac{N-1}{N}} \right)^{\nu_D} \left| 0_N \right\rangle$$

$$= \frac{\langle 0'_N \mid \left(\hat{a}^{\dagger}_N \right)^{\nu_+ + \nu_- + \nu_D} \left| 0_N \right\rangle}{\sqrt{\nu_+! \nu_-! \nu_D!}} \left(-\frac{\cos\theta}{\sqrt{N}} \right)^{\nu_+} \left(\frac{\sin\theta}{\sqrt{N}} \right)^{\nu_-} \left(-\sqrt{\frac{N-1}{N}} \right)^{\nu_D}.$$

$$(4.39)$$

Acting the creation operator on the N-th mode allows us to write

$$\langle 0_0 0_{B(N-1)} 0'_N \mid \nu_+ \nu_- \nu_D \rangle =$$

$$\sqrt{\frac{(\nu_+ + \nu_- + \nu_D)!}{\nu_+! \nu_-! \nu_D!}} \left(-\frac{\cos\theta}{\sqrt{N}} \right)^{\nu_+} \left(\frac{\sin\theta}{\sqrt{N}} \right)^{\nu_-} \left(-\sqrt{\frac{N-1}{N}} \right)^{\nu_D} \langle 0'_N \mid (\nu_+ + \nu_- + \nu_D)_N \rangle. \quad (4.40)$$

Therefore, the square of the Franck-Condon factor in equation (4.34) is

$$
\left| \langle 0_0 0_{B(N-1)} 0'_N \mid v_+ v_- v_D \rangle \right|^2 =
$$
$$
\binom{v_+ + v_- + v_D}{v_+, v_-, v_D} \left(\frac{\cos^2 \theta}{N} \right)^{v_+} \left(\frac{\sin^2 \theta}{N} \right)^{v_-} \left(\frac{N-1}{N} \right)^{v_D} \left| \langle 0'_N \mid (v_+ + v_- + v_D)_N \rangle \right|^2. \quad (4.41)
$$

4.2.5 Conditions for rate enhancement

When $\omega_R = \omega_P$ and $N \gg 1$, the expressions for the Franck-Condon factor and activation energy simplify to

$$
|F_{v_+, v_-, v_D}|^2 = \frac{e^{-S}}{v_+! v_-! v_D!} \left(\frac{S \sin^2 \theta}{N} \right)^{v_+} \left(\frac{S \cos^2 \theta}{N} \right)^{v_-} S^{v_D}, \quad (4.42)
$$
$$
E^{\ddagger}_{v_+, v_-, v_D} = \frac{[\Delta E + \lambda_S + \hbar(v_+ \omega_+ + v_- \omega_- + v_D \omega_P)]^2}{4\lambda_S}, \quad (4.43)
$$

where we have dropped the dependence of angles and frequencies on N for brevity. For most of the experiments that have achieved VSC [54–56, 58, 67, 71, 140], the number of molecules that take part in the coupling is between $N = 10^6$ and 10^{10} per cavity mode [81]. For such orders of magnitude, at first glance, equation (4.25) would suggest that the contribution from the dark modes dominates the rate, which, according to equation (4.42), is the same as the bare case (equation (4.1)) for $v_D = 1$ and $v_+ = v_- = 0$, i.e., if the polaritons are not employed in the reaction. In fact, this was the conclusion for PARET [35], where coupling the product to transitions to the cavity led to no change in energy transfer from reactant molecules. However, the TA processes in electron transfer kinetics offers a new dimension to the problem that PARET does not feature. Careful inspection of the expressions at hand hints to the existence of parameters ΔE and λ_S for which changes in the activation energy for the polariton channels dominate the rate. To find those parameters, we need first that the contribution going to the first vibrational excitation outplay that
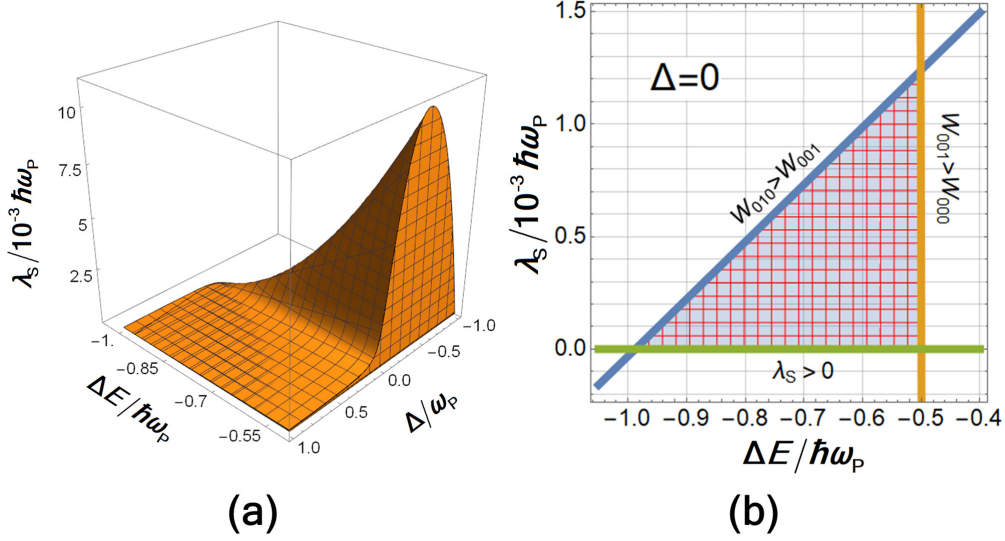
Figure 4.3: Electron transfer parameters for catalytic behavior. The lower polariton (LP) channel dominates the kinetics over the many dark (D) channels for these values of ΔE (the energy difference between product P and reactant R), λ_S (the classical reorganization energy), and Δ (the detuning between the cavity and the high-frequency mode of the product). In (a) we explore the three variables, while in (b) we show the cross section under resonant conditions. For these calculations, the high frequency modes are equal $\omega_R = \omega_P$, $k_B T = 0.2\hbar\omega_P$, $N = 10^{10}$, $S = 1$, and the Rabi splitting is $\hbar\Omega = 5 \times 10^{-2}\hbar\omega_P$.

between ground states, i.e., $W_{001} > W_{000}$, which implies

$$\frac{\lambda_P}{\hbar\omega_P} > \exp\left(\frac{\hbar\omega_P}{4\lambda_S k_B T}\left[2(\Delta E + \lambda_S) + \hbar\omega_P\right]\right). \tag{4.44}$$

Next, if the contribution from the channel where the product is formed with an excitation in the LP mode ($v_- = 1$, and $v_+ = v_D = 0$) dominates, then $W_{010} > W_{001}$, which yields

$$\frac{N}{\cos^2\theta} < \exp\left(\frac{\hbar(\Omega_N - \Delta)}{4\lambda_S k_B T}\left[\Delta E + \lambda_S + \hbar\omega_P + \frac{\hbar(\Delta - \Omega_N)}{4}\right]\right). \tag{4.45}$$

The region of parameters that satisfies these inequalities for room-temperature ($k_B T \approx 0.2\hbar\omega_P$) and typical experimental VSC Rabi-splittings $\hbar\Omega(\approx 0.1\hbar\omega_P)$ [58, 71] is illustrated in Fig. 4.3.a. The order of magnitude of the plotted ΔE values is reasonably standard for this kind of processes [141, 142], which suggests the experimental feasibility of attaining these conditions.

The effect of the electromagnetic mode and the conditions for which the enhancement of the polaritonic coupling can be achieved is illustrated in Fig. 4.4. We can understand this effect as follows; the reaction takes place as a multi-channel process consisting of an electronic transition from the reactant global ground state into the product electronic state dressed with high-frequency vibrational excitations. As shown in Fig. 4.4 and 4.5, the channel between global ground states is in the Marcus inverted regime [117, 143] and, given the small value of the classical reorganization energy, the activation energy is fairly high. On the other hand, the channel to the first excited manifold is in the normal regime with a much lower activation energy, but the range of parameters implies that the decrease in activation energy for the channel with an excitation in the LP mode is enough to overcome the elevated multiplicity of the dark modes (Fig. 4.4 and 4.5), and effectively catalyze the electron transfer process. In terms of the expression for the rate coefficient, even though the entropic pre-exponential factor of the D channel is $N - 1$ larger than that of the LP channel, the latter is associated with a larger exponential factor (lower activation energy).

In Fig. 4.3.b we also show the parameter space that produces polaritonic enhancement as a function the detuning Δ. It can be noticed that the range of admissible values for the classical reorganization energy increases as the detuning becomes negative. This can be understood from the fact that, for negative detunings, the frequency of the photon is smaller than that of the vibrational high-frequency mode and, therefore, the activation energy to LP is lower than that corresponding to D, thus providing more flexibility for parameters to fulfill the inequalities in equation (4.45). However, we must remark that this effect disappears at sufficiently large detunings, as the matter character of the LP becomes negligible to effectively mediate the electron transfer.

4.2.6 Simulation of modified kinetics

The overall effect of the cavity in the charge transfer kinetics is displayed in Fig. 4.6, where we show the ratio of the rate coefficients, calculated inside ($k_{R \to P}$) and outside ($k_{R \to P}^{VSC}$) of the cavity
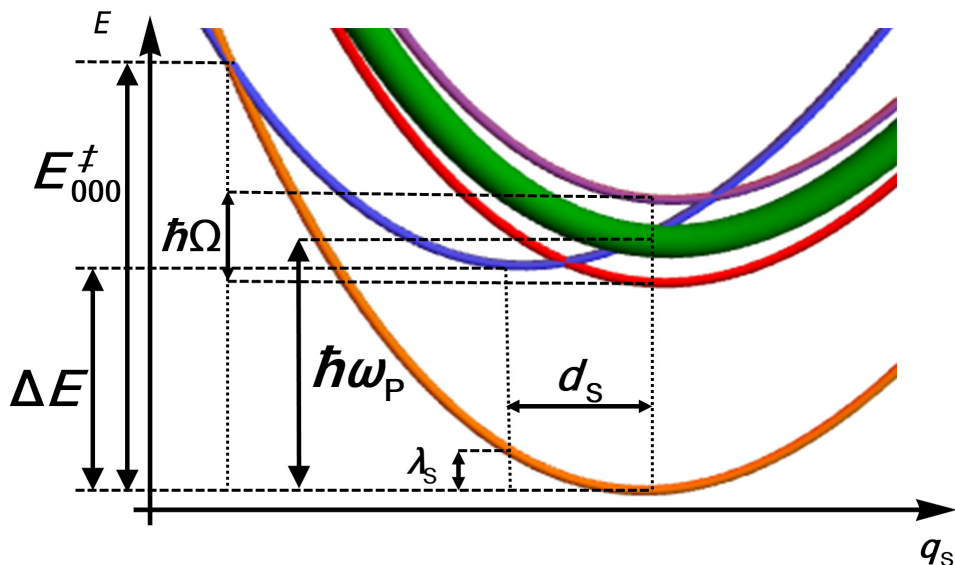
Figure 4.4: Potential energy surfaces under VSC along the slow coordinate. (Not to scale) With respect to the reactant (blue), the vibrational ground state of the product (orange) is in the Marcus inverted regime; the manifold of states with one vibrational excitation (green, red and purple) in the product is in the normal regime. While the dark states (green) outnumber the lower (red) and upper (purple) polaritons, the small activation energy associated with the lower polariton channel might make it the preferred pathway for reactivity.

as a function of the collective coupling $g\sqrt{N}/\omega_P$, for several values of detuning. The bell-shaped curves reflect the fact that, as the Rabi splitting increases, the activation energy of the LP decreases, thus making this channel the most prominent one. This trend goes on until $E_{010}^{\ddagger} = 0$, where this LP channel goes from the normal Marcus regime to the inverted one, and the activation energy starts to increase with the coupling until this pathway is rendered insignificant as compared to the transition to the D manifold, giving rise to kinetics indistinguishable from the bare molecules. The observation that larger detunings require stronger coupling to reach the maximum ratio of rate coefficients is consistent with the fact that $\hbar\Omega$ increases sublinearly with $\hbar g\sqrt{N}$; therefore, larger detunings require larger couplings to attain the same splitting. Additionally, the trend observed in the maxima, which decrease with the detuning, can be regarded as a consequence of the previous effect: the larger couplings required to reach the zero-energy-barrier are achieved with more of molecules; thus, the contribution of LP becomes less relevant than that of D, as can be seen from the pre-exponential factors. Finally, a peculiar result is the fact that the effect on the rate
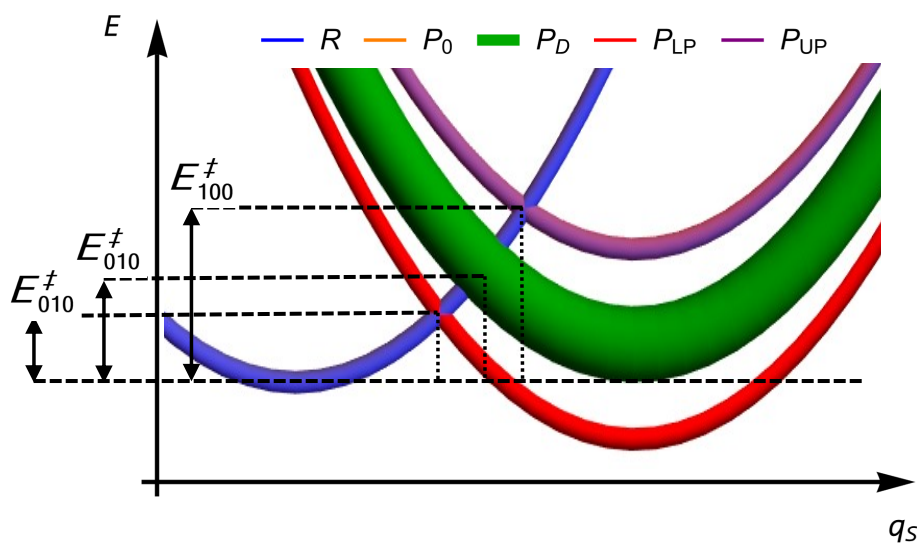
Figure 4.5: Amplification of Fig. 4.4, showing a situation where a polariton channel dominates the kinetics of a reaction starting at reactant R. The channel involving a vibrational excitation in the lower polariton of the product (P_{LP}) features a small enough activation barrier $E_{001}^{\ddagger}$ that can effectively compete against the many channels ending with a vibrational excitation in any of the dark modes, P_D, which feature corresponding activation energies $E_{001}^{\ddagger}$. These two activation energies are much smaller than $E_{000}^{\ddagger}$, the one associated with the channel leading to the global ground state of the products, P_0 (not shown in this amplified figure).
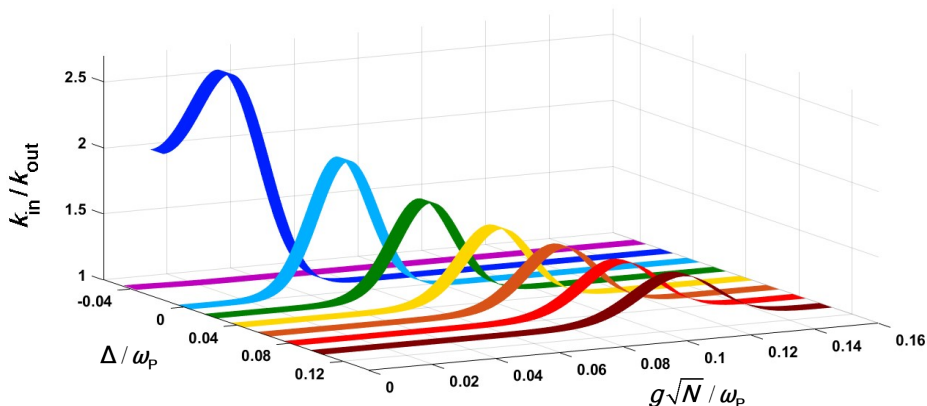
Figure 4.6: Ratio between rate coefficients inside and outside the cavity. The relation of $k_{in} = k_{R \to P}^{VSC}$ and $k_{out} = k_{R \to P}$ was calculated at several detunings Δ. For these calculations $1 \leq N \leq 10^{11}$, $\omega_R = \omega_P$, $k_B T = 0.2 \hbar \omega_P$, $S = 1$, $\hbar g = 1.6 \times 10^{-5} \hbar \omega_P$ and $E_{001}^{\ddagger} = 4.9 \hbar \omega_P$. In agreement with Marcus theory, as the lower polariton mode decreases in energy (with increasing Rabi splitting), its corresponding activation energy falls and then rises, thus dominating the kinetics and becoming irrelevant, respectively. Notice that the trend of apparent enhancement at negative detunings eventually stops at low values of $|\Delta|$.

coefficient is more prominent in a range of few molecules for slightly negative detunings. This observation should not come as surprising since, as previously mentioned, under this condition, the LP mode has a substantially decreased activation energy; therefore, for as small as it is, the light-matter coupling is enough to open a very favored channel that accelerates the reaction. This effect might end up quenched by dissipation; however, even in the absence of the latter, it becomes irrelevant for the cumulative kinetics, as we shall see next.

Up until now, we have shown that the rate coefficient depends on the number of molecules that take part in the VSC, which changes as the reaction progresses. To illustrate the cumulative effect on the kinetics, we numerically integrate the rate law

$$\frac{d\langle N_R \rangle}{dt} = -\langle k_{R \to P}^{VSC}(N_R) N_R \rangle \tag{4.46}$$

where $\langle \cdot \rangle$ indicates an average over the ensemble of reactive trajectories (see 4.2.8). We show the behavior of $N_R(t) = M - N(t)$ for several detunings in Fig. 4.7. In writing equation (4.46) we

have assumed that every electron transfer event is accompanied by a much faster thermalization of the products (largely into the global ground state in the products side) that allows us to ignore back-reactions. This assumption is well justified if we consider that, for systems with parameters close to our model molecule, the vibrational absorption linewidth is of the order of $0.01\hbar\omega_P$ [58, 67, 71], which represents a timescale suitably shorter than the reaction times estimated from the rate constant, $k_{R\to P} = 9.4 \times 10^{-6}\omega_P$, calculated with the same parameters. In Fig. 4.7 we can see that, for $\Delta \geq 0$, at early times the reactions proceed in the same way as in the bare case. However, after some molecules have been gathered in the product, the coupling is strong enough for the LP channel to open and dominate over the D ones. This effect is cumulative, and the reaction endures a steady catalytic boost. Importantly, the maximum enhancement is observed for resonant conditions where the light-matter coupling is the most intense. On the other hand, with a slightly negative detuning, $\Delta = -0.02\omega_P$, the reaction is intensified in the early stages (as explained above) but is taken over by the dark states after a relatively short amount of time. Although this off-resonant effect might look appealing, it occurs at an early stage of the reaction when VSC is not technically operative, namely, when the energetic separation between dark and polaritonic modes might be blurred by dissipative processes. These considerations are beyond the scope of the current article and will be systematically explored in future work. In conclusion, even though some off-resonant effects might be present at the rate coefficient level, the condition of resonance is essential to observe a significant cumulative acceleration of the reaction (i.e., change in reactant lifetime) with respect to the bare case.

Importantly, in the case where the high-frequency mode of the reactant molecules also couples to light, the system is under VSC before the reaction begins and the spectrum in the first excited manifold in the products remains invariant throughout the reaction. Therefore, the rate coefficient is a true rate constant evaluated at $N = M$, i.e, at the maximum coupling. We will present a detailed analysis of this problem elsewhere.
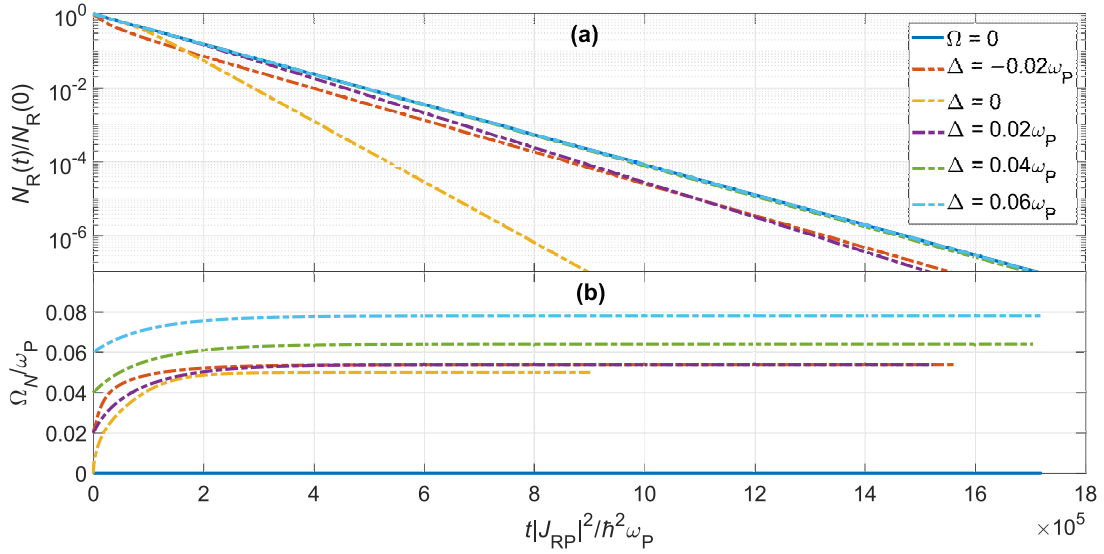
Figure 4.7: Evolution of reactant consumption. a) Integrated rate law for the reaction outside and inside of the cavity at several detunings. The departure of the VSC enhanced kinetics with respect to the bare case becomes more significant at resonance. b) Evolution of effective Rabi splittings as the reaction progresses. The effects on the kinetics are observed when the VSC regime ($\Omega_N > 0.01\omega_P$) is achieved. For these calculations $M = N_R(0) = 10^7$, $\omega_R = \omega_P$, $k_B T = 0.2\hbar\omega_P$, and $E_{001}^{\ddagger} = 3.5\hbar\omega_P$.

4.2.7 Numerical simulation

To calculate the consumption of the reactant as the polaritonic ensemble grows, we performed a finite-difference numerical integration of equation (4.46). Since the rate coefficient remains constant during a single molecule event, we assume a mean-field ansatz

$$\langle k_{R\to P}^{VSC}(N_R)N_R\rangle(t) \simeq k_{R\to P}^{VSC}(\langle N_R\rangle(t))\langle N_R\rangle(t),$$

$$\langle k_{R\to P}^{VSC}(N_R)N_R\rangle(t+\Delta t) \simeq k_{R\to P}^{VSC}(\langle N_R\rangle(t))\left(\langle N_R\rangle(t)-1\right),$$

(4.47)

which enables the stepwise integration of equation (4.46) with limits $t \to t+\Delta t$ and $N_R \to N_R - 1$, yielding

$$\Delta t(N_R) = \frac{1}{k_{R\to P}^{VSC}(N_R)} \ln \frac{N_R}{N_R - 1}.$$

(4.48)

75

We verified that this mean-field method gives numerically consistent results with the stochastic simulation algorithm (see 4.2.8 and 4.1) [144], in agreement with recent studies of mean-field solutions to polariton problems in the ensemble regime [145]. The rate coefficient $k_{R \to P}^{VSC}(N_R)$ at each step is calculated from equation (4.24) truncating the sum up to $v_+ = v_- = v_D = 2$; terms beyond these excitations do not contribute appreciably given their huge activation energies resulting from the chosen parameters. The Franck-Condon and exponential factors are calculated respectively from equation (4.25) and equation (4.26) by setting $\omega_R = \omega_P$.

4.2.8   Integration of the rate law.

Chemical Master Equation   The chemical master equation for the reaction in equation (4.20) is given by

$$\frac{\partial}{\partial t} \Pr(N_R, t \mid M, 0) = a(N_R + 1) \Pr(N_R + 1, t \mid M, 0) - a(N_R) \Pr(N_R, t \mid M, 0), \qquad (4.49)$$

where $\Pr(n, t \mid m, 0)$ is the conditional probability to observe n molecules of the donor at time t given that there were m at $t = 0$, and $a(n) = n k_{R \to P}^{VSC}(n)$ is the propensity function [144]. Since $\Pr(M + 1, t \mid M, 0) \equiv 0$, this equation can be solved exactly by successively plugging $N_R = M, M - 1, \ldots, 0$, yielding

$$\Pr(M - n, t \mid M, 0) = (-1)^n \prod_{i=0}^{n-1} a(M - i) \sum_{j=0}^{n} \frac{e^{-a(M-j)t}}{\prod_{\ell=0}^{n} \left[a(M - j) - a(M - \ell) + \delta_{j\ell} \right]}. \qquad (4.50)$$

This probability density function can be used to determine the average number of donor molecules at a given time:

$$\langle N_R(t) \rangle \doteq \sum_{n=0}^{M} (M - n) \Pr(M - n, t \mid M, 0). \qquad (4.51)$$

Taking the time derivative of this average yields equation (4.46).

However, for the number of molecules considered, $M = 10^7$, this calculation becomes

intractable; therefore, we resort to the strategy described in section 4.2.7 and corroborate its validity with the stochastic simulation algorithm [144].

Stochastic Simulation Algorithm (SSA) For the decomposition reaction in equation (4.46), we can define

$$p(\tau \mid M - n, t) = a(M - n) \exp\left[-a(M - n)\tau\right], \qquad (4.52)$$

as the conditioned probability density function for the time of the next reaction (τ) given that the number of donor molecules left is $M - n$ at t. This function enables the construction of an exact numerical realization of the reaction with the following algorithm:

1. Initialize the system at $N_R(0) = M$.

2. With the system in state $N_R(t) = M - n(t)$, evaluate $a(N_R)$.

3. Generate a value for $\tau = -\ln(r)/a(N_R)$, where R is a uniformly distributed random number.

4. Perform the next reaction by making $N_R(t + \tau) = N_R(t) - 1$.

5. Register $N_R(t)$ as needed. Return to 2 or else end the simulation.

In Table 4.1, we show the correlation (r^2) between the reaction times calculated according to the mean-field finite difference approach described in section 4.2.7 and the reaction times corresponding to the same step in the reaction with populations obtained from the mean of 100 trajectories computed with the SSA algorithm. Since these correlations are very close to the unity, we conclude that the compared methods are numerically equivalent [146]. These observations are consistent with a recent study that shows that mean-field theories provide good descriptions for polaritonic systems involving a large number of molecules [145].

Table 4.1: Correlation between methods of reaction time calculation

Ω	Δ/ω_P	r^2
0	-	0.9970
	–0.02	0.9965
	0	0.9982
≥ 0	0.02	0.9973
	0.04	0.9970
	0.06	0.9969

4.3   Discussion

We have shown that VSC can result in catalysis of TA reactions. We have presented an MLJ model to study charge transfer processes under VSC (in passing, these results suggest a VSC alternative to enhance charge conduction which has so far been only considered in the electronic strong coupling regime [32, 35, 147–149]). In this model, there is a range of molecular features where the shrinkage of the activation energy of the lower polariton channel can outcompete the rate associated with the massive number of dark-state channels. This model describes a mechanism suitable to be present in a wide variety of thermally activated nonadiabatic reactions, e.g., electron, proton and methyl transfer, among others. We have found a range of molecular parameters where the shrinkage of the activation energy of the lower polariton channel can outcompete the rate associated with the massive number of dark-state channels. We determined that these effects are most prominent under resonant conditions. This finding is relevant since such is the behavior observed in experimentally in reactions performed under VSC. We must remark, however, that the latter are presumably vibrationally adiabatic reactions and the involvement of the present mechanism is not obvious (for a recent study on possibly important off-resonant Casimir-Polder effects, we refer the reader to [83]). While a thorough understanding of the reaction pathways involved in these observations is beyond the scope of this article, we believe that the tug-of-war between the activation energy reduction from few polariton channels against the numerical advantage of the dark states could be a ubiquitous mechanism of TA polariton

chemistry under VSC, independently of whether it occurs with reactants or products. Even though there might be other subtle physical mechanisms underlying VSC TA reactions, we conclude with three important observations regarding the presently proposed catalytic mechanism. First, it does not offer a reduction of reaction rate coefficients for a broad range of parameters; after all, if the polariton channels do not provide incentives for their utilization, the dark states will still be accessible, leading to virtually unaffected reaction rates as compared with the bare case. However, an experimental suppression of reactions by VSC under TA conditions (as in [71, 74]) could correspond, microscopically, to the polaritonic modification of elementary step rates in the network of reaction pathways that comprises the mechanism. Second, it is not evident whether the conclusions associated with this mechanism are relevant in photochemical processes where nonequilibrium initialization of polariton populations is allowed. Finally, it is important to emphasize that this VSC mechanism is not guaranteed to yield changes in TA reactivity, given that particular geometric molecular conditions need to be fulfilled. Regardless, it is remarkable that TA reactions under VSC can be modified at all given the entropic limitations imposed by the dark states. It is of much interest to the chemistry community to unravel the broader class of reactions and the VSC conditions for which this mechanism is operative; this will be part of our future work.

Chapter 4, in full, is adapted from the material as it appears in "Resonant catalysis of thermally activated chemical reactions with vibrational polaritons." Campos-Gonzalez-Angulo, Jorge A.; Ribeiro, Raphael F.; Yuen-Zhou, Joel. Nature Communications, 10, 4685 (2019). The dissertation author was the primary investigator and author of this paper.

Chapter 5

Vibrational strong coupling of anharmonic oscillators

5.1 Introduction

Optical microcavities and similar devices enable the dipolar interaction between the electromagnetic (EM) field they confine and a suitable degree of freedom of quantum emitters [37–40, 42]. The coupled system, whose excitations receive the name of polaritons, is a hybrid between light and matter, and their properties have motivated extensive exploration from disciplines such as quantum optics [150], excitonic and two-dimensional materials science [151–153], and chemistry [43, 49]. In some of the systems of interest, the coupling can reach enough intensity to produce observable effects only as a consequence of the cooperative interaction of a large number of material dipoles with a single photon mode. [10, 154].

Polaritons have been produced in diverse setups and materials that require different theoretical frameworks to describe them. For instance, real spins, NV centers [155], qubits [156], SQUIDS [157], quantum dots [158, 159], and electronic transitions in organic molecules [160] are studied as two-level systems, while low vibrational transitions in molecules can be modeled with

harmonic oscillators [161, 162]. The success of these two models stems from their simplicity and the fact that conditions for the light-matter interaction can be found for which their formulations give rise to similarly simple analytical solutions.

The interest in strongly coupled systems in which the emitters have a multi-level anharmonic spectrum has recently increased. For instance, in [91, 92], Herrera and co-workers explore the role that light-matter interaction might have on chemical reactivity by studying the Rabi model with a single emitter described by a Morse oscillator. Additionally, signatures of the non-linearities present in states with two quanta have been observed experimentally [67, 69, 163], studied from theory [66, 68], and motivated revolutionary ideas for signal enhancement [70, 164].

The dynamics of the interaction between many multi-level systems and several EM modes has been discussed when non-energy conserving terms of the Hamiltonian can be neglected, i.e., under the so-called rotating wave approximation (RWA) [165–167], and it is known that analytical solutions exist for the coupling of r-level systems to $r - 1$ EM modes [168]. Regarding the problem of N molecules coupled to a single EM mode, the RWA allows separating the Hamiltonian of the system such that exact solutions can be computed numerically. However, in this kind of calculations the Hilbert space scales as the number of molecules considered, thus being suitable only for systems of relatively small size. Nonetheless, for the case of identical emitters, the permutational symmetry implies a high degree of degeneracy, which can be exploited to reduce the number of degrees of freedom of the Hamiltonian, thus increasing the computational capabilities of the model. Such an approach has been utilized to provide a formulation for open quantum systems that can be used to explore spectroscopic measurements and other processes involving relaxation [169, 170]. There is, however, little to no word about the stationary features of such systems, which are discussed in depth in the present work.

Permutational symmetry has been exploited in the few body limit to study systems such as nuclear structure [171], quantum circuits [172], magnons [173], ultra cold atoms [174], nuclear spins within molecules [175], and the one-dimensional Hubbard model [176]. In the general case,

the properties of the symmetrized quantum states have also been extensively discussed [177, 178]. However, to the best of our knowledge, there has not been an effort to present concrete results from the application of this algebraic approach to the problem of light-matter coupling in the collective regime beyond the case of two-level systems, which is widely known [177, 179, 180].

In the present work, we provide a fathomable, insightful and easily implementable procedure to simplify the Schrödinger equation for N emitters, each with r non-degenerate and non-equidistant bound states in their energy spectrum, coupled to a harmonic mode through a bilinear and excitation-conserving interaction. We identify a correlation between the symmetries of the system and the distribution of photonic component among the emerging manifolds. Of particular interest is the realization that collective states comprising excitations of distinct natures give rise to cooperative couplings that depart from the well-known factor of $\sqrt{N}$ that characterizes polaritons in the singly excited manifold. We also present the effects of anharmonicity, detuning, and intensity of collective coupling on the eigenenergies, and photon contents of the eigenstates.

This paper is organized as follows: in section 5.2 we introduce the model Hamiltonian, discuss the implied approximations and provide a layout of the algebraic structure that enables its separation. In section 5.3 we introduce the tools and concepts that enable the block-diagonalization and show the form and distribution of the diagonal elements. In section 5.4 we formulate the off-diagonal matrix elements that result from the block-diagonalization. In section 5.5 we summarize the simplification method, providing a general recipe to put it in practice. In section 5.6 we present examples for the separation for the lowest-lying excitation manifolds. In section 5.7 we explore the implications of varying parameters on properties of the eigenstates. Finally, we present the conclusions in section 5.8.

5.2 Description of the model

The Hamiltonian

$$\hat{H}_{\text{bare}}(N) = \hbar\omega\left(\hat{a}_0^\dagger\hat{a}_0 + \frac{1}{2}\right) + \sum_{i=1}^{N}\sum_{v=0}^{r}\varepsilon_v\hat{\sigma}_{v,v}^{(i)} \,, \tag{5.1}$$

describes a collection of N identical emitters with $r + 1$ states each (which could represent the lowest vibrational bound states of the ground electronic state of an anharmonic molecule) and an EM mode with frequency ω. Here, $\hat{a}_0^{(\dagger)}$ is the annihilation (creation) operator of the EM mode, ε_v is the energy of the vth state of the emitter, and $\hat{\sigma}_{v,u}^{(i)}$ is the transition operator between levels u and v in the ith emitter, i.e.,

$$\hat{\sigma}_{\alpha,\beta}^{(i)}|v_0v_1\ldots v_i\ldots v_N\rangle = \delta_{v_i\beta}|v_0v_1\ldots\alpha_i\ldots v_N\rangle\,. \tag{5.2}$$

In eq. (5.2), the eigenstates of $\hat{H}_{\text{bare}}(N)$ in eq. (5.1), henceforth pure bare-eigenstates (PBEs), are written in a collective Fock representation where the index v_i indicates the number of bosonic excitations in the ith emitter or the EM mode ($i = 0$). Hereafter, modes with $v = 0$ are considered implicitly for brevity.

The Hamiltonian describing the emitters, the EM mode, and their dipolar interactions under the RWA is

$$\hat{H}(N) = \hat{H}_{\text{bare}}(N) + \hat{H}_{\text{int}}(N), \tag{5.3}$$

where

$$\hat{H}_{\text{int}}(N) = \sum_{v=0}^{r-1}\left(g_{v,v+1}\hat{a}_0^\dagger\hat{J}_-^{(v+1,v)} + g_{v+1,v}\hat{J}_+^{(v+1,v)}\hat{a}_0\right), \tag{5.4}$$

with collective ladder operators for the emitters,

$$\hat{J}_{\pm}^{\left(v+\frac{1\pm1}{2}u,\,v-\frac{1\mp1}{2}u\right)} = \sum_{i=1}^{N}\hat{\sigma}_{v\pm u,v}^{(i)} \qquad u > 0. \tag{5.5}$$

Here, the coupling constant $g_{v\pm u, v} = \sqrt{\frac{\hbar\omega}{2\epsilon_0 \mathcal{V}}} \langle v \pm u | e\hat{x} | v \rangle$ is the product of the amplitude of the single-photon electric field, confined to a mode volume $\mathcal{V}$, and the value of the transition dipole moment between emitter states $v \pm u$ and v. Notice that the model considers coupling only between states that differ by one excitation, and therefore neglects overtone transitions.

The operator $\hat{n}_{\text{exc}} = \hat{a}_0^\dagger \hat{a}_0 + \sum_{i=1}^{N} \sum_{v=0}^{r} v \hat{\sigma}_{v,v}^{(i)}$ acts on the PBEs according to

$$\hat{n}_{\text{exc}} | v_0 v_1 \ldots v_N \rangle = \sum_{j=0}^{N} v_j | v_0 v_1 \ldots v_N \rangle, \tag{5.6}$$

thus indicating the total number of excitations of a given state; moreover, since $\left[\hat{H}(N), \hat{n}_{\text{exc}} \right] = 0$, this operator corresponds to a constant of the motion. Therefore, the Hamiltonian can be recast in the form

$$\hat{H}(N) = \sum_{n_{\text{exc}}} \hat{H}_{n_{\text{exc}}}(N), \tag{5.7}$$

in which each of the terms in the sum of the right-hand-side can be represented as block matrices spanned by PBEs of constant n_{exc}, these blocks generate the so-called *excitation manifolds*. Explicitly, we have

$$\hat{H}_0(N) = \left(\frac{\hbar\omega}{2} + N\varepsilon_0 \right) | 0 \rangle \langle 0 |, \tag{5.8a}$$

$$\hat{H}_1(N) = \left(\frac{3}{2}\hbar\omega + N\varepsilon_0 \right) | 1_0 \rangle \langle 1_0 | + \left(\frac{\hbar\omega}{2} + \varepsilon_1 + (N-1)\varepsilon_0 \right) \sum_{i=1}^{N} | 1_i \rangle \langle 1_i |$$

$$+ \sum_{i=1}^{N} \left(g_{01} | 1_0 \rangle \langle 1_i | + g_{10} | 1_i \rangle \langle 1_0 | \right), \tag{5.8b}$$

$$\hat{H}_2(N) = \left(\frac{5}{2}\hbar\omega + N\varepsilon_0 \right) | 2_0 \rangle \langle 2_0 | + \left(\frac{3}{2}\hbar\omega + \varepsilon_1 + (N-1)\varepsilon_0 \right) \sum_{i=1}^{N} | 1_0 1_i \rangle \langle 1_0 1_i |$$

$$+ \left(\frac{\hbar\omega}{2} + 2\varepsilon_1 + (N-2)\varepsilon_0 \right) \sum_{i=1}^{N-1} \sum_{j=i+1}^{N} | 1_i 1_j \rangle \langle 1_i 1_j |$$

$$+ \left(\frac{\hbar\omega}{2} + \varepsilon_2 + (N-1)\varepsilon_0 \right) \sum_{i=1}^{N} |2_i\rangle \langle 2_i|$$

$$+ \sum_{i=1}^{N} \left[\sqrt{2} g_{01} |2_0\rangle \langle 1_0 1_i| + |1_0 1_i\rangle \left(g_{12} \langle 2_i| + g_{01} \sum_{j\neq i} \langle 1_i 1_j| \right) + \text{H.c.} \right], \qquad (5.8c)$$

$$\hat{H}_3(N) = \left(\frac{7}{2}\hbar\omega + N\varepsilon_0 \right) |3_0\rangle \langle 3_0| + \left(\frac{5}{2}\hbar\omega + \varepsilon_1 + (N-1)\varepsilon_0 \right) \sum_{i=1}^{N} |2_0 1_i\rangle \langle 2_0 1_i|$$

$$+ \left(\frac{3}{2}\hbar\omega + \varepsilon_2 + (N-1)\varepsilon_0 \right) \sum_{i=1}^{N} |1_0 2_i\rangle \langle 1_0 2_i|$$

$$+ \left(\frac{3}{2}\hbar\omega + 2\varepsilon_1 + (N-2)\varepsilon_0 \right) \sum_{i=1}^{N-1} \sum_{j=i+1}^{N} |1_0 1_i 1_j\rangle \langle 1_0 1_i 1_j|$$

$$+ \left(\frac{\hbar\omega}{2} + \varepsilon_3 + (N-1)\varepsilon_0 \right) \sum_{i=1}^{N} |3_i\rangle \langle 3_i|$$

$$+ \left(\frac{\hbar\omega}{2} + \varepsilon_2 + \varepsilon_1 + (N-2)\varepsilon_0 \right) \sum_{i=1}^{N} \sum_{j\neq i} |2_i 1_j\rangle \langle 2_i 1_j|$$

$$+ \left(\frac{\hbar\omega}{2} + 3\varepsilon_1 + (N-3)\varepsilon_0 \right) \sum_{i=1}^{N-2} \sum_{j=i+1}^{N-1} \sum_{k=j+1}^{N} |1_i 1_j 1_k\rangle \langle 1_i 1_j 1_k|$$

$$+ \sum_{i=1}^{N} \left[\sqrt{3} g_{01} |3_0\rangle \langle 2_0 1_i| + \sqrt{2} |2_0 1_i\rangle \left(g_{12} \langle 1_0 2_i| + g_{01} \sum_{j\neq i} \langle 1_0 1_i 1_j| \right) + \text{H.c.} \right]$$

$$+ \sum_{i=1}^{N-1} \sum_{j=i+1}^{N} \left\{ |1_0 1_i 1_j\rangle \left[g_{12} \left(\langle 2_i 1_j| + \langle 2_j 1_i| \right) + g_{01} \sum_{k\neq i,j} \langle 1_i 1_j 1_k| \right] + \text{H.c.} \right\}$$

$$+ \sum_{i=1}^{N} \left[|1_0 2_i\rangle \left(g_{23} \langle 3_i| + g_{01} \sum_{j\neq i} \langle 2_i 1_j| \right) + \text{H.c.} \right], \qquad (5.8d)$$

$$\vdots$$

where $|0\rangle = |0_0 0_1 \dots 0_N\rangle$ is the global ground state and H.c. stands for Hermitian conjugate.

While eq. (5.8a) represents a significant simplification that allows diagonalization of eq. (5.3), it is important to remark that the matrices generated with this approach can quickly become intractable as the number of molecules increases. For instance, $\hat{H}_{n_{\text{exc}}}(N)$ is an operator in $\binom{N+n_{\text{exc}}}{n_{\text{exc}}}$ dimensions. Therefore, it is impractical to deal with the number of molecules required to

achieve observable ensemble strong coupling, which is usually in the order of millions [81,82,181].

5.3 Permutational symmetry

Further simplification of eq. (5.3) requires to identify the additional symmetries of the Hamiltonian. An inspection of eq. (5.8a) reveals that PBEs with the same distribution of quanta are degenerate under the action of $\hat{H}_{\text{bare}}(N)$; therefore, it becomes convenient to introduce a label that characterizes PBEs yet avoids spurious identification due to accidental degeneracies. While, in principle, this characterization could be achieved with the bare energy and the collection of eigenvalues of the operators

$$\hat{J}_0^{(u,v)} = \frac{1}{2}\left[\hat{J}_+^{(u,v)}, \hat{J}_-^{(u,v)}\right] \qquad 0 \le v < u \le r, \tag{5.9}$$

which commute with $\hat{H}_{\text{bare}}(N)$, a much simpler approach is the description of the distribution of quanta itself. Let us define the *spectral configuration*:

$$\tilde{\mu} = \prod_{v=0}^{r} v^{n_{\tilde{\mu}}(v)}, \tag{5.10}$$

a notation device that indicates the number of emitters $n_{\tilde{\mu}}(v)$ in the vth excited state. See table 5.1 for usage examples.

The spectral configuration labels not only PBEs, but also any bare eigenstate (BE) resulting from linear combinations of PBEs with the same distribution of quanta. The BEs can thus be partially characterized with three labels: the excitation manifold (n_{exc}), the spectral configuration ($\tilde{\mu}$), and a basis-dependent degeneracy index (y). These states fulfill

$$\hat{H}_{\text{bare}}(N) |n_{\text{exc}}, \tilde{\mu}; y\rangle = \varepsilon_{n_{\text{exc}}}^{(\tilde{\mu})} |n_{\text{exc}}, \tilde{\mu}; y\rangle, \tag{5.11}$$

Table 5.1: Examples of spectral configurations, partitions, and Young diagrams corresponding to selected PBEs.

PBE	$\tilde{\mu}$	μ	ν	Young diagram
$|0\rangle$	0^N	$[N]$	$[0]$	
$|1_i\rangle$	$0^{N-1}1^1$	$[N-1,1]$	$[1]$	
$|1_i1_j\rangle$	$0^{N-2}1^2$	$[N-2,2]$	$[1,1]$	
$|2_i\rangle$	$0^{N-1}2^1$	$[N-1,1]$	$[2]$	
$|2_i4_j5_k\rangle$	$0^{N-3}2^14^15^1$	$[N-3,1,1,1]$	$[5,4,2]$	
$|1_i1_j2_k2_\ell2_m4_n\rangle$	$1^22^34^1$	$[3,2,1]$	$[4,2,2,2,1,1]$	

$N = 6$

where

$$\varepsilon_{n_{\text{exc}}}^{(\tilde{\mu})} = \hbar\omega\left(v_0^{(n_{\text{exc}},\tilde{\mu})} + \tfrac{1}{2}\right) + \sum_{v=0}^{n_{\text{exc}}} n_{\tilde{\mu}}(v)\varepsilon_v \tag{5.12}$$

is the characteristic bare energy for states with those labels, and $v_0^{(n_{\text{exc}},\tilde{\mu})} = n_{\text{exc}} - \sum_{v=1}^{n_{\text{exc}}} vn_{\tilde{\mu}}(v)$ is the corresponding number of quanta in the EM mode.

Since $\sum_{v=0}^{r} n_{\tilde{\mu}}(v) = N$ for a given $\tilde{\mu}$, the spectral configuration corresponds to a partition of the total number of emitters. For reasons that will become apparent, it is convenient to write these partitions in its regular (non-increasing) form, i.e.,

$$\mu = [\mu_1, \mu_2, \ldots, \mu_{r+1}] \tag{5.13}$$

where $\mu_i = n_{\tilde{\mu}}(v_i)$ under the constraint that $\mu_i \leq \mu_{i'}$ for $i > i'$ [182]. In what follows, all the empty elements, $\mu_i = 0$, will be omitted for brevity, as illustrated in table 5.1. Furthermore, the spectral configurations can be identified as partitions of the number of excitations distributed among the emitters, i.e. for every $\tilde{\mu}$ there exists a regular partition $\nu(\tilde{\mu})$ such that

$$\nu(\tilde{\mu}) = \{v^{(i)} : 1 \leq v \leq r, 0 \leq i \leq n_{\tilde{\mu}}(v)\}, \tag{5.14}$$

Table 5.2: Spectral configurations, EM mode excitations and degeneracies for the first five excitation manifolds.

$\tilde{\mu}$	n_{exc} 0	1	2	3	4	$\dim(M^\mu)$	$\dim(S^\lambda)$
			$v_0^{(n_{\text{exc}},\tilde{\mu})}$				
0^N	0	1	2	3	4	1	1
$0^{N-1}1^1$		0	1	2	3	N	$N-1$
$0^{N-2}1^2$			0	1	2	$N(N-1)/2$	$N(N-3)/2$
$0^{N-1}2^1$			0	1	2	N	
$0^{N-3}1^3$				0	1	$N(N-1)(N-2)/6$	$N(N-1)(N-5)/6$
$0^{N-2}1^12^1$				0	1	$N(N-1)$	$(N-1)(N-2)/2$
$0^{N-1}3^1$				0	1	N	
$0^{N-4}1^4$					0	$N(N-1)(N-2)(N-3)/24$	$N(N-1)(N-2)(N-7)/24$
$0^{N-3}1^22^1$					0	$N(N-1)(N-2)/2$	$N(N-2)(N-4)/3$
$0^{N-2}2^2$					0	$N(N-1)/2$	
$0^{N-2}1^13^1$					0	$N(N-1)$	
$0^{N-1}4^1$					0	N	
$\lvert\tilde{\mu}_{n_{\text{exc}}}\rvert$	1	2	4	7	12		
$\lvert\lambda_{n_{\text{exc}}}\rvert$	1	2	3	5	7		

$\lambda = \mu$ when applicable.

as illustrated in table 5.1. Because of the latter, the number of possible spectral configurations within a given manifold is

$$\lvert\tilde{\mu}_{n_{\text{exc}}}\rvert = \sum_{n=0}^{n_{\text{exc}}} p(n), \tag{5.15}$$

where $p(n)$ is the number of partitions of the integer n. These numbers can be extracted from the expansion [183]

$$\prod_{k=1}^{m}\left(1-x^k\right)^{-1} = \sum_{n=0}^{m} p(n)x^n + \mathcal{O}\left(x^{m+1}\right). \tag{5.16}$$

Since the emitters are considered as identical, $\hat{H}(N)$ is invariant under the action of the symmetric group of degree N, S_N, whose elements are the $N!$ possible permutations of labels of the emitters. In other words, for all permutations $\hat{\pi} \in S_N$, $\left[\hat{H}(N),\hat{\pi}\right] = 0$.

The permutation operators act on the BEs according to

$$\hat{\pi}\,\lvert n_{\text{exc}}, \tilde{\mu}; y\rangle = \lvert n_{\text{exc}}, \tilde{\mu}; y'\rangle, \tag{5.17}$$

which means that BEs with common n_{exc} and $\tilde{\mu}$ can be used to form a representation of S_N. For instance,

$$\hat{\pi}() = |1_1\rangle\langle 1_1| + |1_2\rangle\langle 1_2| + |1_3\rangle\langle 1_3|, \tag{5.18}$$

$$\hat{\pi}(12) = |1_1\rangle\langle 1_2| + |1_2\rangle\langle 1_1| + |1_3\rangle\langle 1_3|, \tag{5.19}$$

$$\hat{\pi}(23) = |1_1\rangle\langle 1_1| + |1_2\rangle\langle 1_3| + |1_3\rangle\langle 1_2|, \tag{5.20}$$

$$\hat{\pi}(31) = |1_1\rangle\langle 1_3| + |1_2\rangle\langle 1_2| + |1_3\rangle\langle 1_1|, \tag{5.21}$$

$$\hat{\pi}(123) = |1_1\rangle\langle 1_3| + |1_2\rangle\langle 1_1| + |1_3\rangle\langle 1_2|, \tag{5.22}$$

$$\hat{\pi}(132) = |1_1\rangle\langle 1_2| + |1_2\rangle\langle 1_3| + |1_3\rangle\langle 1_1|, \tag{5.23}$$

are the six elements of S_3 in the basis of PBEs with $\tilde{\mu} = 1^1$.

The representations of S_N identified with a partition $\boldsymbol{\mu}$ are, in general, reducible; they receive the name of *permutation modules* and are denoted by M^{μ} [184]. The dimension of this representation is the number of BEs with the same $\boldsymbol{\mu}$, i.e.,

$$\dim(M^{\mu}) = \frac{N!}{\displaystyle\prod_{i=1}^{r+1} \mu_i!}. \tag{5.24}$$

The permutation modules can, in turn, be decomposed in irreducible representations (irreps) according to Young's rule [185]:

$$M^{\mu} = \bigoplus_{\lambda \trianglerighteq \mu} K_{\lambda\mu} S^{\lambda}, \tag{5.25}$$

where S^{λ} symbolizes the irreps, also known as *Specht modules* [186].

The direct sum in eq. (5.25) runs over all partitions $\boldsymbol{\lambda}$ of N that *dominate* (denoted by the

symbol $\trianglerighteq$) over μ, i.e., they fulfill [185]

$$\sum_{i=1}^{j} \lambda_i \geq \sum_{i=1}^{j} \mu_i \qquad 1 \leq j \leq r. \tag{5.26}$$

For instance, consider the spectral configurations in the triply excited manifold: 0^N, $0^{N-1}1^1$, $0^{N-2}1^2$, $0^{N-1}2^1$, $0^{N-3}1^3$, $0^{N-2}1^12^1$, and $0^{N-1}3^1$. Since they correspond to the same regular partition, the spectral configurations $0^{N-1}1^1$, $0^{N-1}2^1$ and $0^{N-1}3^1$ have identical permutational properties. Let us identify how each partition relates to $[N-2,1,1]$ in terms of dominance. Following eq. (5.26), it is possible to conclude that

$$[N] \trianglerighteq [N-2,1,1],$$

$$[N-1,1] \trianglerighteq [N-2,1,1],$$

$$[N-2,2] \trianglerighteq [N-2,1,1],$$

$$[N-3,3] \ntrianglerighteq [N-2,1,1],$$

$$[N-2,1,1] \trianglerighteq [N-2,1,1]. \tag{5.27}$$

The coefficients $K_{\lambda\mu}$ in eq. (5.25) are known as *Kostka numbers* [187]; they indicate the number of times a permutation module contains a Specht module. While obtaining a closed analytical expression to calculate them remains an open problem [188, 189], these coefficients can be found through their combinatorial interpretation: the number of semi-standard Young tableaux (SSYT) of shape λ and content μ [185]. A Young diagram (YD) of size N and shape μ is a collection of N cells arranged in r left-justified rows with μ_i cells on the ith row. The present work uses the English notation, which is consistent with the regular form of the partitions (see table 5.1 for selected examples). A SSYT of shape λ and content μ is obtained by filling in the cells of a λ-shaped YD with a collection of ordered symbols partitioned according to μ in such a manner that the rows do not decrease to the right and the columns increase to the bottom [185].

For instance, the SSYT of shape $[N - 1, 1]$ and content $[N - 2, 1, 1]$ are

$$
\begin{array}{|c|c|c|c|c|}
\hline 0 & 0 & \cdots & 0 & 1 \\
\hline 2 \\
\cline{1-1}
\end{array}
\quad \text{and} \quad
\begin{array}{|c|c|c|c|c|}
\hline 0 & 0 & \cdots & 0 & 2 \\
\hline 1 \\
\cline{1-1}
\end{array};
\tag{5.28}
$$

therefore, $K_{[N-1,1],[N-2,1,1]} = 2$.

With the above definitions, it can be verified that the representation of S_N in the basis of all BEs with $\tilde{\mu} = 0^{N-2}1^1 2^1$ fulfills

$$
M^{[N-2,1,1]} = S^{[N]} \oplus 2S^{[N-1,1]} \oplus S^{[N-2,2]} \oplus S^{[N-2,1,1]}.
\tag{5.29}
$$

The dimension of the Specht modules corresponds to the number of standard Young tableaux (SYT) of shape λ, i.e., the number of ways in which the sequence $[1, 2, \ldots, N]$ fills a λ-shaped YD such that the entries increase across rows and columns [185]. For instance, the SYTs for $\lambda = [3, 2]$ are

$$
\begin{array}{|c|c|c|}
\hline 1 & 2 & 3 \\
\hline 4 & 5 \\
\cline{1-2}
\end{array},
\begin{array}{|c|c|c|}
\hline 1 & 2 & 4 \\
\hline 3 & 5 \\
\cline{1-2}
\end{array},
\begin{array}{|c|c|c|}
\hline 1 & 2 & 5 \\
\hline 3 & 4 \\
\cline{1-2}
\end{array},
\begin{array}{|c|c|c|}
\hline 1 & 3 & 4 \\
\hline 2 & 5 \\
\cline{1-2}
\end{array},
\text{ and }
\begin{array}{|c|c|c|}
\hline 1 & 3 & 5 \\
\hline 2 & 4 \\
\cline{1-2}
\end{array}.
\tag{5.30}
$$

This quantity is given by the hook-length formula [190]:

$$
\dim(S^\lambda) = \frac{N!}{\displaystyle\prod_{i=1}^{N} h_\lambda(i)},
\tag{5.31}
$$

where $h_\lambda(i)$ represents the number of cells in the hook of the ith cell in the λ-shaped YD, i.e. the number of cells that are either directly below of, directly to the right of, or the ith cell itself. For

example, for $\lambda = [6, 4, 3, 2, 1]$, the hook of the cell with coordinates $(2, 2)$ is

,
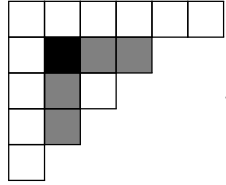
and the hook-lengths for each cell are

.
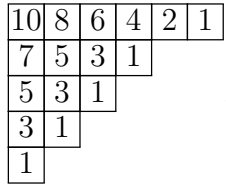
A direct result from Young's rule is that

$$\dim(M^\mu) = \sum_{\lambda \trianglerighteq \mu} K_{\lambda\mu} \dim(S^\lambda). \tag{5.32}$$

The dimensions of the permutation and Specht modules for the spectral configurations found up to $n_{\text{exc}} = 4$ are displayed in table 5.2.

The irreps identify the smallest possible subspaces that remain excluded under permutations. In other words, the space of BEs with the same $\tilde{\mu}$ can be split into sets of symmetry adapted linear combinations of BEs (SABEs) labeled by λ for which

$$\hat{\pi} \, |n_{\text{exc}}, \tilde{\mu}, \lambda; \mathbf{y}, \mathbf{w}\rangle = |n_{\text{exc}}, \tilde{\mu}, \lambda; \mathbf{y}', \mathbf{w}\rangle \, , \tag{5.33}$$

for all $\hat{\pi} \in S_n$, where the label $\mathbf{w}$ has been added to acknowledge repetition of irreps, i.e., when $K_{\lambda\mu} > 1$.

Table 5.3: Examples of standard Young tableaux and their associated indices for $N = 6$.

SYT	λ	y
$\boxed{1\,2\,3\,4\,5\,6}$	$[6]$	0
$\boxed{1\,2\,3\,4\,5}$ $\boxed{6}$	$[5,1]$	6
$\boxed{1\,2\,4\,6}$ $\boxed{3\,5}$	$[4,2]$	$(3,5)$
$\boxed{1\,2\,4}$ $\boxed{3\,5\,6}$	$[3,3]$	$(3,5,6)$
$\boxed{1\,2\,5\,6}$ $\boxed{3}$ $\boxed{4}$	$[4,1,1]$	$(3;4)$
$\boxed{1\,3\,4}$ $\boxed{2\,5}$ $\boxed{6}$	$[3,2,1]$	$(2,5;6)$

It is a well-known result from Representation Theory that

$$\left(\mathbb{C}^{r+1}\right)^{\otimes N} \cong \bigoplus_{\lambda \vdash N} \left(S^\lambda \otimes V_{r+1}^\lambda\right), \tag{5.34}$$

where $\mathbb{C}^{r+1}$ is the vector space spanned by the energy eigenstates of each molecule, and therefore $\left(\mathbb{C}^{r+1}\right)^{\otimes N}$ is the vector space spanned by the BEs. The symbol $\vdash$ reads as *partition of*, and V_{r+1}^λ is a so-called weight-space; it corresponds to an irrep of the unitary group $U(r + 1)$. This result, known as the *Schur-Weyl duality* [191, 192], implies that the SABEs are arranged in exclusive subspaces, labeled by λ, in which they are classified according to not only their behavior under permutations, but also under unitary operators. Furthermore, the decomposition in eq. (5.34) provides with the meaning of all the indices in eq. (5.33).

As previously discussed, the dimension of a Specht module corresponds with the number of SYT of shape λ, and the index $\mathbf{y}$ was used to enumerate them; therefore the indices λ and $\mathbf{y}$ uniquely define a SYT. In what remains of this paper, the index $\mathbf{y}$ will encode the elements of the Young tableaux after removal of the top row. See some examples in table 5.3. On the other hand,

Table 5.4: Examples of semistandard Young tableaux and their associated indices for $N = 6$ and $\tilde{\mu} = 0^3 1^2 2^1$.

SSYT	λ	$\mathbf{w}$
$\boxed{0\,0\,0\,1\,1\,2}$	$[6]$	0
$\begin{array}{l}\boxed{0\,0\,0\,1\,2}\\\boxed{1}\end{array}$	$[5,1]$	1^1
$\begin{array}{l}\boxed{0\,0\,0\,1\,1}\\\boxed{2}\end{array}$	$[5,1]$	2^1
$\begin{array}{l}\boxed{0\,0\,0\,1}\\\boxed{1\,2}\end{array}$	$[4,2]$	$1^1 2^1$
$\begin{array}{l}\boxed{0\,0\,0}\\\boxed{1\,1\,2}\end{array}$	$[3,3]$	$1^2 2^1$
$\begin{array}{l}\boxed{0\,0\,0\,1}\\\boxed{1}\\\boxed{2}\end{array}$	$[4,1,1]$	$(1^1, 2^1)$
$\begin{array}{l}\boxed{0\,0\,0}\\\boxed{1\,1}\\\boxed{2}\end{array}$	$[3,2,1]$	$(1^2, 2^1)$

the dimension of the irreps of $U(r + 1)$ correspond to the Kostka numbers. To be specific, the elements of the weight space V_{r+1}^{λ} can be enumerated with SSYT, and thus uniquely identified with the indices $\tilde{\mu}$, λ, and $\mathbf{w}$. In the remaining of the present work, $\mathbf{w}$ will encode the elements of the SSYT after removal of the top row. See some examples in table 5.4.

To gain some insight into the meaning of the irreps, let us consider the global groundstate of the emitters, i.e., the state with $\tilde{\mu} = 0^N$. The only partition that dominates over $[N]$ is itself, and there is a unique SSYT when the shape and content correspond to the same partition; therefore, $M^{[N]} = S^{[N]}$. These facts are consistent with the uniqueness of the state within each manifold where all the excitations reside in the EM mode, which is denoted by $\left|n_{\text{exc}}, 0^N, [N]; 0, 0\right\rangle$.

Since $\left[\hat{\pi}, \hat{J}_+^{(u,v)}\right] = 0$, the states $|n_{\text{exc}}, \tilde{\mu}, \lambda; \mathbf{y}, \mathbf{w}\rangle$ behave identically to $\hat{a}_0 \hat{J}_+^{u,v} |n_{\text{exc}}, \tilde{\mu}, \lambda; \mathbf{y}, \mathbf{w}\rangle$ under permutations. This means that, even though the operator $\hat{a}_0 \hat{J}_+^{(u,v)}$ modifies the spectral configuration, the states it couples carry the same irrep. Consequently

$$\hat{a}_0 \hat{J}_+^{(u,0)} \left|n_{\text{exc}}, 0^N, [N]; 0, 0\right\rangle \propto \left|n_{\text{exc}}, 0^{N-1} u^1, [N]; 0, 0\right\rangle . \tag{5.35}$$

$$|2, 0^N, [N]; 0, 0\rangle \xrightarrow{\hat{a}_0 \hat{J}_+^{(1,0)}} |2, 0^{N-1} 1^1, [N]; 0, 0\rangle \xrightarrow{\hat{a}_0 \hat{J}_+^{(1,0)}} |2, 0^{N-2} 1^2, [N]; 0, 0\rangle$$

Figure with arrows and states:

$\hat{a}_0 \hat{J}_+^{(2,1)}$ $|2, 0^{N-1} 1^1, [N-1, 1]; k, 1^1\rangle \xrightarrow{\hat{a}_0 \hat{J}_+^{(1,0)}} |2, 0^{N-2} 1^2, [N-1, 1]; k, 1^1\rangle$ GS

$|2, 0^{N-1} 2^1, [N]; 0, 0\rangle$ $\hat{a}_0 \hat{J}_+^{(2,1)}$ $|2, 0^{N-2} 1^2, [N-2, 2]; (k', \ell), 1^2\rangle$

GS $|2, 0^{N-1} 2^1, [N-1, 1]; k, 2^1\rangle$
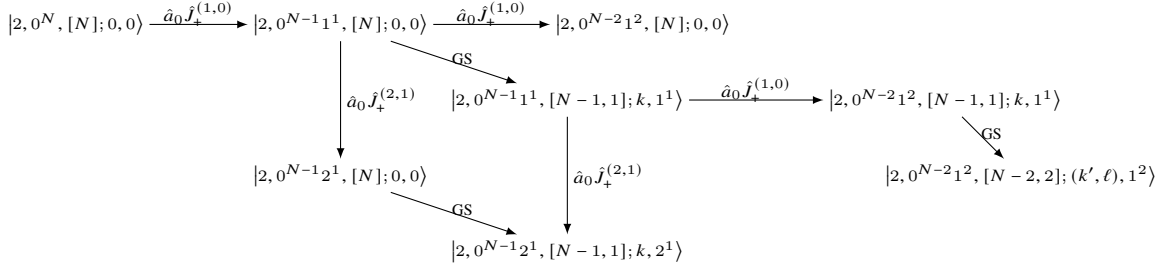
Figure 5.1: Diagram of the relations between SABEs in the doubly excited manifold. GS denotes Gram-Schmidt orthogonalization, $2 \leq k \leq N$, $2 \leq k' < \ell$, and $4 \leq \ell \leq N$.

However, $M^{[N-1,1]} = S^{[N]} \oplus S^{[N-1,1]}$, which means that the remaining SABEs with $\tilde{\mu} = 0^{N-1} u^1$ carry the irrep with $\lambda = [N-1, 1]$. These states, $|n_{\text{exc}}, 0^{N-1} u^1, [N-1, 1]; k, 1^1\rangle$ with $1 \leq k \leq N-1$, can be obtained through Gram-Schmidt orthogonalization over the basis of PBEs but with $|n_{\text{exc}}, 0^{N-1} u^1, [N]; 0, 0\rangle$ replacing one of the states and remaining fixed as seed of the procedure. The structure of the doubly excited manifold can be understood in terms of this procedure as illustrated in fig. 5.1. 5.4.1 provides with operators that allow to write the part of the emitters of all the SABEs present up to the triply excited manifold.

To exemplify how these concepts unfold, let us return to the representation in eq. (5.18). Starting from the state $|1, 0^3, [3]; 0, 0\rangle$, the action of the operator $\hat{a}_0 \hat{J}_+^{(1,0)}$ yields

$$|1, 0^2 1^1, [3]; 0, 0\rangle = \frac{1}{\sqrt{3}} (|1_1\rangle + |1_2\rangle + |1_3\rangle) . \tag{5.36}$$

The remaining two SABEs with $\tilde{\mu} = 0^2 1^1$ are

$$|1, 0^2 1^1, [2, 1]; 2, 1^1\rangle = \frac{|1_1\rangle - |1_2\rangle}{\sqrt{2}}, \tag{5.37a}$$

and

$$\left|1, 0^2 1^1, [2, 1]; 3, 1^1\right\rangle = \frac{|1_1\rangle + |1_2\rangle - 2\,|1_3\rangle}{\sqrt{6}}. \tag{5.37b}$$

The permutation operators in this basis are

$$\hat{\pi}() = |[3]; 0\rangle \langle[3]; 0| + |[2, 1]; 2\rangle \langle[2, 1]; 2| + |[2, 1]; 3\rangle \langle[2, 1]; 3|, \tag{5.38}$$

$$\hat{\pi}(12) = |[3]; 0\rangle \langle[3]; 0| - |[2, 1]; 2\rangle \langle[2, 1]; 2| + |[2, 1]; 3\rangle \langle[2, 1]; 3|, \tag{5.39}$$

$$\hat{\pi}(23) = |[3]; 0\rangle \langle[3]; 0| + \tfrac{1}{2} \left(|[2, 1]; 2\rangle \langle[2, 1]; 2| - |[2, 1]; 3\rangle \langle[2, 1]; 3|\right)$$
$$+ \tfrac{\sqrt{3}}{2} \left(|[2, 1]; 2\rangle \langle[2, 1]; 3| + |[2, 1]; 3\rangle \langle[2, 1]; 2|\right), \tag{5.40}$$

$$\hat{\pi}(31) = |[3]; 0\rangle \langle[3]; 0| + \tfrac{1}{2} \left(|[2, 1]; 2\rangle \langle[2, 1]; 2| - |[2, 1]; 3\rangle \langle[2, 1]; 3|\right)$$
$$- \tfrac{\sqrt{3}}{2} \left(|[2, 1]; 2\rangle \langle[2, 1]; 3| + |[2, 1]; 3\rangle \langle[2, 1]; 2|\right), \tag{5.41}$$

$$\hat{\pi}(123) = |[3]; 0\rangle \langle[3]; 0| - \tfrac{1}{2} \left(|[2, 1]; 2\rangle \langle[2, 1]; 2| + |[2, 1]; 3\rangle \langle[2, 1]; 3|\right)$$
$$- \tfrac{\sqrt{3}}{2} \left(|[2, 1]; 2\rangle \langle[2, 1]; 3| - |[2, 1]; 3\rangle \langle[2, 1]; 2|\right), \tag{5.42}$$

$$\hat{\pi}(132) = |[3]; 0\rangle \langle[3]; 0| - \tfrac{1}{2} \left(|[2, 1]; 2\rangle \langle[2, 1]; 2| + |[2, 1]; 3\rangle \langle[2, 1]; 3|\right)$$
$$+ \tfrac{\sqrt{3}}{2} \left(|[2, 1]; 2\rangle \langle[2, 1]; 3| - |[2, 1]; 3\rangle \langle[2, 1]; 2|\right). \tag{5.43}$$

where the notation was simplified by making implicit the common indices $n_{\text{exc}} = 1$ and $\tilde{\mu} = 0^2 1^1$, as well as by omitting the label $\mathbf{w}$. As it can be seen in eq. (5.38), the permutation operators have two clear independent subspaces labeled by $[3]$ and $[2, 1]$, respectively.

The spectral configurations, $\tilde{\mu}$, giving rise to partitions that are valid labels, λ, for the irreps fulfill

$$n_{\tilde{\mu}}(v) \geq n_{\tilde{\mu}}(v') \qquad \forall v, v' : v' > v > 0; \tag{5.44}$$

this constraint produces the so-called partitions with weakly decreasing multiplicities [193]. The

enumeration of these partitions imply that the total number of irreps in the n_{exc}th manifold is

$$|\lambda_{n_{\text{exc}}}| = \sum_{n=0}^{n_{\text{exc}}} q(n), \qquad (5.45)$$

where $q(n)$ is the number of partitions of n with weakly decreasing multiplicities as illustrated in table 5.2. These numbers can be extracted from the expansion [182, 183]

$$\prod_{k=2}^{m} \left(1 - x^{\binom{k}{2}}\right)^{-1} = \sum_{n=0}^{m} q(n)x^n + \mathcal{O}\left(x^{m+1}\right). \qquad (5.46)$$

The main result of this section is that the Hamiltonians of the excitation manifolds can be split according to

$$\hat{H}_{n_{\text{exc}}}(N) = \sum_{i=1}^{|\lambda_{n_{\text{exc}}}|} \hat{H}_{n_{\text{exc}}}^{(\lambda_i)}, \qquad (5.47)$$

where

$$\hat{H}_{n_{\text{exc}}}^{(\lambda)} = \sum_{j=1}^{\dim(S^\lambda)} \hat{H}_{n_{\text{exc}}}^{(\lambda, \mathbf{y}_j)}, \qquad (5.48)$$

with each $\hat{H}_{n_{\text{exc}}}^{(\lambda, \mathbf{y})}$ encoding the energies and interactions of spectral configurations with the same symmetry. Equation eq. (5.48) implies that the states obtained from diagonalizing $\hat{H}_{n_{\text{exc}}}^{(\lambda)}$ are $\dim(S^\lambda)$-fold degenerate. In particular, for the diagonal part of the Hamiltonian, we have

$$\hat{H}_{\text{bare}, n_{\text{exc}}}^{(\lambda)} = \sum_{\tilde{\mu} : \mu \trianglelefteq \lambda} \sum_{i=1}^{\dim(S^\lambda)} \sum_{j=1}^{K_{\lambda\mu}} \varepsilon_{n_{\text{exc}}}^{(\tilde{\mu})} \left| n_{\text{exc}}, \tilde{\mu}, \lambda; \mathbf{y}_i, \mathbf{w}_j \right\rangle \left\langle n_{\text{exc}}, \tilde{\mu}, \lambda; \mathbf{y}_i, \mathbf{w}_j \right|, \qquad (5.49)$$

Notice that

$$\dim\left(\hat{H}_{n_{\text{exc}}}^{(\lambda, y)}\right) = \sum_{\mu \trianglelefteq \lambda} K_{\lambda\mu}. \qquad (5.50)$$

The simplification achieved with this strategy is significant since, for each excitation manifold,

the problem has been reduced to the diagonalization of $|\lambda_{n_{\text{exc}}}| \sim \exp\left(An_{\text{exc}}^{1/3}\right)$ matrices with dimensions in the neighborhood of $|\tilde{\mu}_{n_{\text{exc}}}| \sim \exp\left(\sqrt{Cn_{\text{exc}}}\right)$ [194], both independent of N, which is a substantial gain over the original $\binom{N+n_{\text{exc}}}{n_{\text{exc}}}$-dimensional matrices.

A complete discussion of the structure of the Hamiltonians requires to include the couplings between spectral configurations induced by collective excitations; these will be explored in the next section.

5.4   Collective couplings.

Having determined the SABEs, the matrix elements of the interaction Hamiltonian are

$$\left\langle n'_{\text{exc}}, \tilde{\mu}', \lambda'; \mathbf{y}', \mathbf{w}' \right| \hat{H}_{\text{int}}(N) \left| n_{\text{exc}}, \tilde{\mu}, \lambda; \mathbf{y}, \mathbf{w} \right\rangle$$
$$= g_{\tilde{\mu}'\tilde{\mu}} B^{(n_{\text{exc}})}_{\tilde{\mu}',\tilde{\mu}} L^{(\lambda)}_{\tilde{\mu}',\tilde{\mu}} C^{(\lambda)}_{\tilde{\mu}',\tilde{\mu}}(\mathbf{w}', \mathbf{w}) \delta_{n'_{\text{exc}} n_{\text{exc}}} \delta_{\lambda'\lambda} \delta_{\mathbf{y}'\mathbf{y}}. \quad (5.51)$$

The notation in 5.51 highlights the fact that transitions in the EM mode produce changes in the spectral configuration. It can be shown that, for a given manifold, the number of pairings $\{\tilde{\mu}', \tilde{\mu}\}$ afforded by photonic (de)excitations is

$$n_{\text{int}}(n_{\text{exc}}) = \sum_{i=1}^{n_{\text{exc}}-1} \binom{n_{\text{exc}} - i + 2}{i + 1}. \quad (5.52)$$

The first factor at the right-hand-side of eq. (5.51) is given by

$$g_{\tilde{\mu}',\tilde{\mu}} = g_{v^*+s,v^*} \delta_{|s|,1} \delta_{n_{\tilde{\mu}'}(v^*), n_{\tilde{\mu}}(v^*)-1} \delta_{n_{\tilde{\mu}'}(v^*+s), n_{\tilde{\mu}}(v^*+s)+1}, \quad (5.53)$$

where $s = \sum_{v=1}^{n_{\text{exc}}} v[n_{\tilde{\mu}'}(v) - n_{\tilde{\mu}}(v)]$, with v^* and $v^* + s$ labeling the energy levels coupled by the

matrix element, i.e., the relevant operator acting on the emitters is $\hat{J}_{+}^{(v^*+s,v^*)}$. The coefficient

$$B_{\tilde{\mu}',\tilde{\mu}}^{(n_{\text{exc}})} = \left(v_0^{(n_{\text{exc}},\tilde{\mu})} + \delta_{s,-1}\right)^{1/2}, \tag{5.54}$$

accounts for the (de)excitation of the EM mode.

To describe the redistribution of quanta among the emitters, let's define the operators

$$\hat{J}_r^{(\tilde{\mu}',\tilde{\mu})} = \hat{J}_r^{(v^*+s,v^*)}, \tag{5.55}$$

where $r \in \{-, 0, +\}$, which generate the $\mathfrak{su}(2)$ algebra with Casimir operator

$$\hat{\mathbf{J}}_{\tilde{\mu}',\tilde{\mu}}^2 = \left(\hat{J}_0^{(\tilde{\mu}',\tilde{\mu})}\right)^2 + \tfrac{1}{2}\left(\hat{J}_+^{(\tilde{\mu}',\tilde{\mu})}\hat{J}_-^{(\tilde{\mu}',\tilde{\mu})} + \hat{J}_-^{(\tilde{\mu}',\tilde{\mu})}\hat{J}_+^{(\tilde{\mu}',\tilde{\mu})}\right). \tag{5.56}$$

These operators allow the definition of the quantities

$$M_{\tilde{\mu}',\tilde{\mu}} = \langle\tilde{\mu}|\,\hat{J}_0^{(\tilde{\mu}',\tilde{\mu})}\,|\tilde{\mu}\rangle \tag{5.57}$$

and

$$J_{\tilde{\mu}',\tilde{\mu}}^{(\lambda)}\left(J_{\tilde{\mu}',\tilde{\mu}}^{(\lambda)} + 1\right) = \langle\tilde{\mu}, \lambda|\,\hat{\mathbf{J}}_{\tilde{\mu}',\tilde{\mu}}^2\,|\tilde{\mu}, \lambda\rangle, \tag{5.58}$$

where the explicit labels in bras and kets are the only relevant ones in the calculation of the indicated matrix elements as pointed out in the study of two-level systems, where the SABEs are known as Dicke states, and $J_{\tilde{\mu}',\tilde{\mu}}^{(\lambda)}$ as the Dicke cooperation number [110]. To be specific

$$M_{\tilde{\mu}',\tilde{\mu}} = \frac{n_{\tilde{\mu}}(v^* + s) - n_{\tilde{\mu}}(v^*)}{2}, \tag{5.59}$$

and

$$J^{(\lambda)}_{\tilde{\mu}',\tilde{\mu}} = \max_{\tilde{\mu}''} \left(\langle \tilde{\mu}'', \lambda | \, \hat{J}^{(\tilde{\mu}',\tilde{\mu})}_0 \, | \tilde{\mu}'', \lambda \rangle \right). \tag{5.60}$$

According to the prescription of quantum angular momentum, the contribution of collective (de)excitations to the coupling between states is given by

$$L^{(\lambda)}_{\tilde{\mu}',\tilde{\mu}} = \left[\left(J^{(\lambda)}_{\tilde{\mu}',\tilde{\mu}} + M_{\tilde{\mu}',\tilde{\mu}} \right) \left(J^{(\lambda)}_{\tilde{\mu}',\tilde{\mu}} - M_{\tilde{\mu},\tilde{\mu}'} \right) \right]^{1/2}. \tag{5.61}$$

Couplings are said to be *superradiant* if $L^{(\lambda)}_{\tilde{\mu}',\tilde{\mu}} > 1$, and *subradiant* if $L^{(\lambda)}_{\tilde{\mu}',\tilde{\mu}} < 1$ [110]. Section 5.4.2 shows a couple of neat ways to calculate these coefficients.

The last component of eq. (5.51), the coefficient $C^{(\lambda)}_{\tilde{\mu}',\tilde{\mu}}(\mathbf{w}', \mathbf{w})$, acknowledges the fact that, since $\left[\hat{J}^{(v',v)}_+, \hat{J}^{(u',u)}_+ \right] \propto 1 - \delta_{uv}\delta_{u'v'}$, two strings of the same raising operators applied in different order to a SABE will not, in general, produce the same state. This situation creates an ambiguity when $\hat{H}^{(\lambda,\mathbf{y})}_{n_{\text{exc}}}$ requires more than one function with the same $\tilde{\mu}$, i,e, when $K_{\lambda\mu} > 1$; otherwise, $C^{(\lambda)}_{\tilde{\mu}',\tilde{\mu}}(\mathbf{w}', \mathbf{w}) = 1$. For instance, consider the state $\left| 3, 0^{N-1}1^1, [N-1,1]; 2, 1 \right\rangle = (|2_0 1_1\rangle - |2_0 1_2\rangle)/\sqrt{2}$, and apply to it consecutive excitations to get to a state with $\tilde{\mu} = 0^{N-2}1^1 2^1$. There are two possible paths:

$$\frac{|2_0 1_1\rangle - |2_0 1_2\rangle}{\sqrt{2}} \xrightarrow{\hat{a}_0 \hat{J}^{(1,0)}_+} \sum_{i=3}^{N} \frac{|1_0 1_1 1_i\rangle - |1_0 1_2 1_i\rangle}{\sqrt{2(N-2)}}$$

$$\xrightarrow{\hat{a}_0 \hat{J}^{(2,1)}_+} \sum_{i=3}^{N} \frac{|2_1 1_i\rangle - |2_2 1_i\rangle + |1_1 2_i\rangle - |1_2 2_i\rangle}{2\sqrt{N-2}}, \tag{5.62a}$$

and

$$\frac{|2_0 1_1\rangle - |2_0 1_2\rangle}{\sqrt{2}} \xrightarrow{\hat{a}_0 \hat{J}^{(2,1)}_+} \frac{|1_0 2_1\rangle - |1_0 2_2\rangle}{\sqrt{2}}$$

$$\xrightarrow{\hat{a}_0 \hat{J}_+^{(1,0)}} \frac{1}{\sqrt{2(N-1)}} \left[|2_1 1_2\rangle - |1_1 2_2\rangle + \sum_{i=3}^{N} (|2_1 1_i\rangle - |2_2 1_i\rangle) \right]. \qquad (5.62b)$$

While the identifications

$$\left|3, 0^{N-2}1^2, [N-1,1]; 2,1\right\rangle = \sum_{i=3}^{N} \frac{|1_0 1_1 1_i\rangle - |1_0 1_2 1_i\rangle}{\sqrt{2(N-2)}}, \qquad (5.63)$$

$$\left|3, 0^{N-1}2^1, [N-1,1]; 2,1\right\rangle = \frac{|1_0 2_1\rangle - |1_0 2_2\rangle}{\sqrt{2}} \qquad (5.64)$$

are immediate, the assignment of $\left|3, 0^{N-2}1^1 2^1, [N-1,1]; 2,1\right\rangle$ and $\left|3, 0^{N-2}1^1 2^1, [N-1,1]; 2,2\right\rangle$ is unclear since the two obtained states are linearly independent yet not mutually orthogonal. Bypassing this ambiguity requires the definition of an orthonormal basis spanned by the previous states, then the coefficients can be extracted from the identity

$$L_{\tilde{\mu}'\tilde{\mu}}^{(\lambda)} C_{\tilde{\mu}'\tilde{\mu}}^{(\lambda)}(\mathbf{w}', \mathbf{w}) = \langle \tilde{\mu}, \lambda; \mathbf{y}, \mathbf{w} | \hat{J}_-^{(\tilde{\mu}', \tilde{\mu})} | \tilde{\mu}', \lambda; \mathbf{y}, \mathbf{w}' \rangle. \qquad (5.65)$$

For instance, let's set

$$|A\rangle = \sum_{i=3}^{N} \frac{|2_1 1_i\rangle - |2_2 1_i\rangle + |1_1 2_i\rangle - |1_2 2_i\rangle}{2\sqrt{N-2}}, \qquad (5.66)$$

and

$$|X\rangle = \frac{|2_1 1_2\rangle - |1_1 2_2\rangle + \sum_{i=3}^{N} (|2_1 1_i\rangle - |2_2 1_i\rangle)}{\sqrt{2(N-1)}}, \qquad (5.67)$$

and compute their orthogonal complements:

$$|B\rangle = \frac{\hat{I} - |A\rangle \langle A|}{\left(1 - |\langle X|A\rangle|^2\right)^{1/2}} |X\rangle, \qquad (5.68)$$

Table 5.5: Coefficients of projected couplings involving $\tilde{\mu}' = 0^{N-2}1^1 2^1$ for repeated irreps with $\lambda = [N-1, 1]$.

$\lvert 3, \tilde{\mu}', \lambda; 2, 1\rangle$	$\lvert 3, \tilde{\mu}', \lambda; 2, 2\rangle$	$\tilde{\mu}$	$C_{\tilde{\mu}',\tilde{\mu}}^{(\lambda)}(1^1, 1^1)$	$C_{\tilde{\mu}',\tilde{\mu}}^{(\lambda)}(1^1, 2^1)$
$\lvert A\rangle$	$\lvert B\rangle$	$0^{N-2}1^2$	1	0
		$0^{N-1}2^1$	$\langle X\lvert A\rangle$	$\langle X\lvert B\rangle$
$\lvert X\rangle$	$\lvert Y\rangle$	$0^{N-2}1^2$	$\langle A\lvert X\rangle$	$\langle A\lvert Y\rangle$
		$0^{N-1}2^1$	1	0

and

$$\lvert Y\rangle = \frac{\hat{I} - \lvert X\rangle\langle X\rvert}{\left(1 - \lvert\langle X\lvert A\rangle\rvert^2\right)^{1/2}} \lvert A\rangle, \tag{5.69}$$

where $\hat{I}$ is the identity operator. The values of the coefficients calculated with both working basis are shown in table 5.5. Since the bare energies, $\varepsilon_{n_{\mathrm{exc}}}^{(\tilde{\mu})}$, are independent of the index $\mathbf{w}$, and $\sum_{t'=1}^{K_{\lambda\mu'}} \left\lvert C_{\tilde{\mu}'\tilde{\mu}}^{(\lambda)}(\mathbf{w}', \mathbf{w})\right\rvert^2 = 1$, the choice of basis is immaterial for the eigenvalues of $\hat{H}_{n_{\mathrm{exc}}}^{(\lambda, \mathbf{y})}$.

In summary, the full symmetrized blocks of the interaction Hamiltonian are given by

$$\hat{H}_{\mathrm{int}, n_{\mathrm{exc}}}^{(\lambda, \mathbf{y})} =$$

$$\sum_{\tilde{\mu}:\mu \trianglelefteq \lambda}\sum_{\tilde{\mu}':\mu' \trianglelefteq \lambda}\sum_{i=1}^{K_{\lambda\mu}}\sum_{i'=1}^{K_{\lambda\mu'}} g_{\tilde{\mu}'\tilde{\mu}} B_{\tilde{\mu}',\tilde{\mu}}^{(n_{\mathrm{exc}})} L_{\tilde{\mu}',\tilde{\mu}}^{(\lambda)} C_{\tilde{\mu}',\tilde{\mu}}^{(\lambda)}(\mathbf{w}'_{i'}, \mathbf{w}_i) \lvert n_{\mathrm{exc}}, \tilde{\mu}', \lambda; \mathbf{y}, \mathbf{w}'_{i'}\rangle \langle n_{\mathrm{exc}}, \tilde{\mu}, \lambda; \mathbf{y}, \mathbf{w}_i\rvert. \tag{5.70}$$

5.4.1 Schur-Weyl basis.

The SABEs obtained through application of the collective excitations, $\hat{J}_+^{(u,v)}$, and Gram-Schmidt orthogonalization have been discussed in the literature under the name of Schur-Weyl states [173, 195–197], or Gelfand-Tsetlin states [198–201]. Although not necessary for the block-diagonalization of the Hamiltonian, an illustration of the explicit form of the symmetrized states in terms of the PBEs might be useful for the reader. Since symmetrization only affects the portion of the Hilbert space concerning the emitters, the quantum number n_{exc}, as well as the

operators acting on the photonic mode, $\hat{a}_0^{(\dagger)}$, are not included in the following discussion, i.e., the SABEs are denoted by $|\tilde{\mu}, \lambda; \mathbf{y}, \mathbf{w}\rangle$.

If the explicit form of the SABE in terms of PBEs is known, the application of collective excitation operators gives a straightforward result. For instance, the ground-state and some of its collective excitations are

$$\left|0^N, [N]; 0, 0\right\rangle = |0\rangle, \tag{5.71a}$$

$$\left|0^{N-1}v^1, [N]; 0, 0\right\rangle = \frac{1}{\sqrt{N}} \sum_{i=1}^{N} |v_i\rangle, \tag{5.71b}$$

$$\left|0^{N-2}v^2, [N]; 0, 0\right\rangle = \binom{N}{2}^{-1/2} \sum_{i=1}^{N-1} \sum_{j=i+1}^{N} |v_i v_j\rangle, \tag{5.71c}$$

$$\left|0^{N-3}v^3, [N]; 0, 0\right\rangle = \binom{N}{3}^{-1/2} \sum_{i=1}^{N-2} \sum_{j=i+1}^{N-1} \sum_{k=j+1}^{N} |v_i v_j v_k\rangle, \tag{5.71d}$$

$$\left|0^{N-2}u^1v^1, [N]; 0, 0\right\rangle = \frac{1}{\sqrt{N(N-1)}} \sum_{i=1}^{N-1} \sum_{j=i+1}^{N} \left(|u_i v_j\rangle + |v_i u_j\rangle\right), \tag{5.71e}$$

where $\lambda = [N]$ and $\mathbf{y} = 0$ indicate the SYT $\boxed{1}\boxed{2}\ldots\boxed{N}$. This tableau implies that the wavefunction must be invariant under any permutation of all the labels. Since all emitters are in the same state in the collective ground-state, this condition is met by default. The linear combinations of the excited spectral configurations are thus totally symmetric.

The states with spectral configuration such that $\boldsymbol{\mu} = \boldsymbol{\lambda}$ cannot be generated through excitation operators, and thus require a orthogonalization strategy. Since these states are highly degenerate, the change of basis is not unique; however, there is an approach that highlights the meaning of the label $\mathbf{y}$. For a 1D array $(i_1, i_2, \ldots, i_n)$, let's define the vandermonde matrix $\hat{\mathbf{V}}(i_1, i_2, \ldots, i_n)$ with elements

$$\left[\hat{\mathbf{V}}(i_1, i_2, \ldots, i_n)\right]_{\alpha,\beta} = \hat{\sigma}_{\alpha-1,0}^{(\beta)}. \tag{5.72}$$

A given SYT can be associated to Young operators of the form

$$\hat{Y}(\lambda, \mathbf{y}) = \sum_{\psi} \prod_{j=1}^{\lambda_1} \det\left(\hat{\mathbf{V}}(\text{col}_j[\mathbf{y}'_\psi])\right), \tag{5.73}$$

where $\text{col}_j(\mathbf{A})$ extracts the jth column of array $\mathbf{A}$, and $\mathbf{y}'_\psi$ is any permutation of the elements in each row of $\mathbf{y}$ that produces downwards increasing columns. For instance, the SYT

$$\mathbf{y}'_1 = \begin{array}{|c|c|c|} \hline 1 & 3 & 4 \\ \hline 2 & 5 \\ \cline{1-2} 6 \\ \cline{1-1} \end{array}, \tag{5.74}$$

generates the arrays

$$\mathbf{y}'_2 = \begin{array}{|c|c|c|} \hline 1 & 3 & 4 \\ \hline 2 & & 5 \\ \cline{1-1}\cline{3-3} 6 \\ \cline{1-1} \end{array}, \tag{5.75a}$$

$$\mathbf{y}'_3 = \begin{array}{|c|c|c|} \hline 1 & 3 & 4 \\ \hline 2 & 5 \\ \cline{1-2} & 6 \\ \cline{2-2} \end{array}, \tag{5.75b}$$

$$\mathbf{y}'_4 = \begin{array}{|c|c|c|} \hline 1 & 3 & 4 \\ \hline 2 & & 5 \\ \cline{1-1}\cline{3-3} & & 6 \\ \cline{3-3} \end{array}. \tag{5.75c}$$

And the corresponding operator is

$$
\begin{aligned}
\hat{Y}\left([3,2,1],(2,5;6)\right) = {} & \det\left(\hat{\mathbf{V}}(1,2,6)\right) \det\left(\hat{\mathbf{V}}(3,5)\right) \det\left(\hat{\mathbf{V}}(4)\right) \\
& + \det\left(\hat{\mathbf{V}}(1,2,6)\right) \det\left(\hat{\mathbf{V}}(3)\right) \det\left(\hat{\mathbf{V}}(4,5)\right) \\
& + \det\left(\hat{\mathbf{V}}(1,2)\right) \det\left(\hat{\mathbf{V}}(3,5,6)\right) \det\left(\hat{\mathbf{V}}(4)\right) \\
& + \det\left(\hat{\mathbf{V}}(1,2)\right) \det\left(\hat{\mathbf{V}}(3)\right) \det\left(\hat{\mathbf{V}}(4,5,6)\right)
\end{aligned} \tag{5.76}
$$

If $\mu = \lambda$, the wavefunction $|\tilde{\mu}, \lambda; \mathbf{y}, \mathbf{w}\rangle$ is proportional to $\hat{Y}(\lambda, \mathbf{y}) |0^N, [N]; 0, 0\rangle$. Notice that the constraint $\mu = \lambda$ uniquely defines a SSYT, and therefore a $\mathbf{w}$.

The states orthogonal to $|0^{N-1}1^1, [N]; 0, 0\rangle$ with the same $\tilde{\mu}$ can be written as

$\left|0^{N-1}1^1, [N-1,1]; k, 1^1\right\rangle$, with $2 \leq k \leq N$. The corresponding SYT are

1	2	...	$k-1$	$k+1$	...	N
k						

,

which have associated Young operators of the form

$$\hat{Y}([N-1,1], k) = \sum_{i=1}^{k-1} \prod_{j=1}^{i-1} \hat{\sigma}_{0,0}^{(j)} \cdot \begin{vmatrix} \hat{\sigma}_{0,0}^{(i)} & \hat{\sigma}_{0,0}^{(k)} \\ \hat{\sigma}_{1,0}^{(i)} & \hat{\sigma}_{1,0}^{(k)} \end{vmatrix} \cdot \prod_{j'=i+1}^{N} \hat{\sigma}_{0,0}^{(j')}. \tag{5.77}$$

Therefore, the corresponding SABEs are

$$\left|0^{N-1}1^1, [N-1,1]; k, 1^1\right\rangle = \frac{1}{\sqrt{k(k-1)}} \left(-\sum_{i=1}^{k-1} |1_i\rangle + (k-1)\,|1_k\rangle\right). \tag{5.78}$$

The functions $\left|0^{N-1}v^1, [N-1,1]; k, v^1\right\rangle$ for $v > 1$ have an equivalent form. Furthermore, the action of the collective excitation $\hat{J}_+^{(1,0)}$ yields

$$\begin{aligned}
\left|0^{N-2}1^2, [N-1,1]; k, 1^1\right\rangle =&\frac{1}{\sqrt{(N-2)\,k\,(k-1)}} \left\{ \sum_{i=1}^{k-1}\left[(k-2)\,|1_i 1_k\rangle - \sum_{j=k+1}^{N} |1_i 1_j\rangle\right]\right. \\
&\left. + (k-1)\sum_{i=k+1}^{N} |1_k 1_i\rangle - 2\sum_{i=1}^{k-2}\sum_{j=i+1}^{k-1} |1_i 1_j\rangle\right\}
\end{aligned} \tag{5.79}$$

Following the same reasoning, the remaining states with $\tilde{\mu} = 0^{N-2}1^2$ that are orthogonal

to all the states above are

$$
\begin{aligned}
\left|0^{N-2}1^2, [N-2, 2]; (k, \ell), 1^2\right\rangle = &\frac{1}{\sqrt{k(k-1)(\ell-2)(\ell-3)}} \left\{ 2\sum_{i=1}^{k-2}\sum_{j=i+1}^{k-1} \left|1_i1_j\right\rangle \right. \\
&- (k-2)\sum_{i=1}^{k-1}\left|1_i1_k\right\rangle - \sum_{j=k+1}^{\ell-1}\left[(k-1)\left|1_k1_j\right\rangle - \sum_{i=1}^{k-1}\left|1_i1_j\right\rangle\right] \\
&\left. +(\ell-3)\left[(k-1)\left|1_k1_\ell\right\rangle - \sum_{i=1}^{k-1}\left|1_i1_\ell\right\rangle\right]\right\}
\end{aligned}
$$

(5.80)

Tables 5.6 and 5.7 show the excitation operators, $\hat{O}\{\tilde{\mu}, \lambda; \mathbf{y}, \mathbf{w}\}$ that produce the states with the same labels when applied to the global groundstate of the emitters, i.e.

$$
\hat{O}\{\tilde{\mu}, \lambda; \mathbf{y}, \mathbf{w}\}\left|0\right\rangle = \mathcal{N}^{-2}\left|\tilde{\mu}, \lambda; \mathbf{y}, \mathbf{w}\right\rangle. \tag{5.81}
$$

The nested structure of the operators responds to the fact that the higher states are obtained through either collective excitations, or Gram-Schmidt orthogonalization of the lower ones.

5.4.2 Efficient calculation of $L^{(\lambda)}_{\tilde{\mu}',\tilde{\mu}}$

In this section, we present two approaches, one analytical and other computational, to the calculation of the contribution of the collective transitions in the Hilbert space of the emitters to the couplings between states in eq. (5.51).

First, we introduce a by-hand method to compute individual instances of eq. (5.61). Taking advantage of the fact that $n_{\tilde{\mu}}(v^* + s) + n_{\tilde{\mu}}(v^*) = n_{\tilde{\mu}'}(v^* + s) + n_{\tilde{\mu}'}(v^*)$, we can write

$$
L^{(\lambda)}_{\tilde{\mu}'\tilde{\mu}} = \left\{\left[n_{\tilde{\mu}}(v^*) - \rho_J\right]\left[n_{\tilde{\mu}'}(v^* + s) - \rho_J\right]\right\}^{1/2}, \tag{5.82}
$$

where $\rho_J = [n_{\tilde{\mu}}(v^* + s) + n_{\tilde{\mu}}(v^*)]/2 - J^{(\lambda)}_{\tilde{\mu}'\tilde{\mu}}$. When $\rho_J = 0$, which is a typical situation among low

excitation manifolds, the term inside the radical has an intuitive interpretation since it can be read as the product of the number of emitters in $\tilde{\mu}$ available for excitation with the number of emitters in $\tilde{\mu}'$ available for deexcitation. Furthermore, ρ_J increases as λ becomes less dominant, i.e., strays away from $[N]$; this provides with an automatic way to determine the symmetry labels for which a given coupling is worth to calculate. table 5.8 illustrates this calculation for the couplings between $\tilde{\mu} = 0^{N-2}1^2$ and $\tilde{\mu}' = 0^{N-3}1^3$.

Second, we discuss a computational method to get not only multiple values of the sought coefficients, but also the SABEs connected by a particular raising operator. Given that

$$\hat{J}_+^{(\tilde{\mu}',\tilde{\mu})} |\tilde{\mu}, \lambda; \mathbf{y}, \mathbf{w}\rangle = L_{\tilde{\mu}',\tilde{\mu}}^{(\lambda)} C_{\tilde{\mu}',\tilde{\mu}}^{(\lambda)}(\mathbf{w}', \mathbf{w}) |\tilde{\mu}', \lambda; \mathbf{y}, \mathbf{w}'\rangle, \tag{5.83}$$

it is possible to write

$$\hat{J}_+^{(\tilde{\mu}',\tilde{\mu})} = \sum_{\lambda \trianglerighteq \mu'}^{\dim(S^\lambda)} \sum_{i=1}^{K_{\lambda\mu'}} \sum_{j'=1}^{K_{\lambda\mu}} \sum_{j=1} L_{\tilde{\mu}',\tilde{\mu}}^{(\lambda)} C_{\tilde{\mu}',\tilde{\mu}}^{(\lambda)}(\mathbf{w}', \mathbf{w}) \left|\tilde{\mu}', \lambda; \mathbf{y}_i, \mathbf{w}'_{j'}\right\rangle \left\langle\tilde{\mu}, \lambda; \mathbf{y}_i, \mathbf{w}_j\right|, \tag{5.84}$$

and define

$$\hat{U}_{\tilde{\mu}} = \sum_{\lambda \trianglerighteq \mu}^{\dim(S^\lambda)} \sum_{i=1}^{K_{\lambda\mu}} \sum_{j=1} \left|\tilde{\mu}, \lambda; \mathbf{y}_i, \mathbf{w}_j\right\rangle \left\langle\tilde{\mu}, \lambda; \mathbf{y}_i, \mathbf{w}_j\right|. \tag{5.85}$$

The latter implies that, if the raising operator is written in the basis of the PBEs, the coefficients $L_{\tilde{\mu}',\tilde{\mu}}^{(\lambda)} C_{\tilde{\mu}',\tilde{\mu}}^{(\lambda)}(\mathbf{w}', \mathbf{w})$ are its singular values, while the unitary operators $\hat{U}_{\tilde{\mu}'}$ and $\hat{U}_{\tilde{\mu}}$ correspond to the matrices of singular vectors, which provide with the changes of basis between PBEs and SABEs. In short, singular value decomposition of $\hat{J}_+^{(\tilde{\mu}',\tilde{\mu})}$ in an arbitrary basis yields the coupling coefficients as well as the symmetrized states in the subspaces of functions with the spectral configurations involved in the transition. The apparent contradiction in eq. (5.84) that there are symmetry labels such that $\lambda \trianglerighteq \mu'$ yet $\lambda \ntrianglerighteq \mu$ is solved by recognizing the set of states $\{|\tilde{\mu}', \lambda; y, t'\rangle : \lambda \ntrianglerighteq \mu\}$ as the null-space of the raising operator, i.e., $L_{\tilde{\mu}',\tilde{\mu}}^{(\lambda \ntrianglerighteq \mu)} = 0$. This feature is consistent with the fact that $\dim(M^{\mu'}) > \dim(M^\mu)$.

Table 5.6: SABEs in terms of PBEs for spectral configurations with at most three excitations in the emitters.

$\bar{\mu}$	λ	y	w	$\hat{O}\{\bar{\mu},\lambda;y,w\}$	$\mathcal{N}^{-2}$	Notes
0^N	$[N]$	0	0	1	1	
$0^{N-1}\nu^1$	$[N]$	0	0	$\displaystyle\sum_{i=1}^N \hat{\sigma}_{\nu,0}^{(i)}$	N	$\nu \in \{1,2,3\}$
	$[N-1,1]$	k	ν^1	$(k-1)\hat{\sigma}_{\nu,0}^{(k)} - \hat{O}\{0^{k-2}1^1,[k-1];0,0\}$	$k(k-1)$	$2 \le k \le N$
$0^{N-2}1^2$	$[N]$	0	0	$\displaystyle 2\sum_{i=1}^{N-1}\sum_{j=i+1}^N \hat{\sigma}_{1,0}^{(i)}\hat{\sigma}_{1,0}^{(j)}$	$2N(N-1)$	
	$[N-1,1]$	k	1^1	$(k-2)\hat{\sigma}_{1,0}^{(k)}\hat{O}\{0^{k-2}1^1,[k-1];0,1\} - \hat{O}\{0^{k-3}1^2,[k-1];0,0\}$ $\displaystyle+ \sum_{j=k+1}^N \hat{\sigma}_{1,0}^{(j)}\hat{O}\{0^{k-1}1^1,[k-1,1];k,1^1\}$	$k(k-1)(N-2)$	$2 \le k \le N$
	$[N-2,2]$	(k,ℓ)	1^2	$(\ell-3)\hat{\sigma}_{1,0}^{(\ell)}\hat{O}\{0^{k-1}1^1,[k-1,1];k,1^1\} - \hat{O}\{0^{\ell-3}1^2,[\ell-2,1];k,1^1\}$	$k(k-1)(\ell-2)(\ell-3)$	$4 \le \ell \le N$ $2 \le k < \ell$
$0^{N-3}1^3$	$[N]$	0	0	$\displaystyle 6\sum_{h=1}^{N-2}\sum_{i=h+1}^{N-1}\sum_{j=i+1}^N \hat{\sigma}_{1,0}^{(h)}\hat{\sigma}_{1,0}^{(i)}\hat{\sigma}_{1,0}^{(j)}$	$6N(N-1)(N-2)$	
	$[N-1,1]$	k	1^1	$(k-3)\hat{\sigma}_{1,0}^{(k)}\hat{O}\{0^{k-3}1^2,[k-1];0,0\} - \hat{O}\{0^{k-4}1^3,[k-1];0,0\}$ $\displaystyle+2\sum_{h=k+1}^N \hat{\sigma}_{1,0}^{(h)}\left[(k-2)\hat{\sigma}_{1,0}^{(k)}\hat{O}\{0^{k-2}1^1,[k-1];0,0\} - \hat{O}\{0^{k-3}1^2,[k-1];0,0\}\right]$ $\displaystyle+2\sum_{j=k+1}^{N-1}\sum_{h=j+1}^N \hat{\sigma}_{1,0}^{(j)}\hat{\sigma}_{1,0}^{(h)}\hat{O}\{0^{k-1}1^1,[k-1,1];k,1^1\}$	$2k(k-1)N(N-1)$	$2 \le k \le N$
	$[N-2,2]$	(k,ℓ)	1^2	$(\ell-4)\hat{\sigma}_{1,0}^{(\ell)}\hat{O}\{0^{\ell-3}1^2,[\ell-2,1];k,1^1\} + \displaystyle\sum_{h=\ell+1}^N \hat{\sigma}_{1,0}^{(h)}\hat{O}\{0^{\ell-3}1^2,[\ell-3,2];(k,\ell),1^2\}$ $-\hat{O}\{0^{\ell-4}1^3,[\ell-2,1];k,1^1\}$	$k(k-1)(\ell-2)(\ell-3)(N-4)$	$4 \le \ell \le N$ $2 \le k < \ell$
	$[N-3,3]$	(k,ℓ,m)	1^3	$(m-5)\hat{\sigma}_{1,0}^{(m)}\hat{O}\{0^{\ell-3}1^2,[\ell-3,2];(k,\ell),1^2\} + \hat{O}\{0^{m-4}1^3,[m-3,2];(k,\ell),1^2\}$	$k(k-1)(\ell-2)(\ell-3)(m-4)(m-5)$	$6 \le m \le N$ $4 \le \ell < m$ $2 \le k < \ell$

Table 5.7: SABEs in terms of PBEs with $\tilde{\mu} = 0^{N-2}1^12^1$.

$\tilde{\mu}$	λ	y	$\mathbf{w}$	$\hat{O}\{\tilde{\mu},\lambda;\mathbf{y},\mathbf{w}\}$	$\mathcal{N}^{-2}$	Notes
$0^{N-2}1^12^1$	$[N]$	0	0	$2\sum_{i=1}^{N-1}\sum_{j=i+1}^{N}\left(\hat{\sigma}_{2,0}^{(i)}\hat{\sigma}_{1,0}^{(j)}+\hat{\sigma}_{2,0}^{(j)}\hat{\sigma}_{1,0}^{(i)}\right)$	$4N(N-1)$	
	$[N-1,1]$	k	1^1	$(k-2)\left(\hat{\sigma}_{2,0}^{(k)}\hat{O}\{0^{k-2}1^1,[k-1];0,0\}+\hat{\sigma}_{1,0}^{(k)}\hat{O}\{0^{k-2}2^1,[k-1];0,0\}\right)$ $-\sum_{j=k+1}^{N}\left(\hat{\sigma}_{1,0}^{(j)}\hat{O}\{0^{k-2}2^1,[k-1];0,0\}+\hat{\sigma}_{2,0}^{(j)}\hat{O}\{0^{k-2}1^1,[k-1];0,0\}\right)$ $+(k-1)\sum_{j=k+1}^{N}\left(\hat{\sigma}_{2,0}^{(k)}\hat{\sigma}_{1,0}^{(j)}+\hat{\sigma}_{1,0}^{(k)}\hat{\sigma}_{2,0}^{(j)}\right)-\hat{O}\{0^{k-3}1^12^1,[k-1],0,0\}$	$2k(k-1)(N-2)$	$2\le k\le N$
			2^1	$k\left(\hat{\sigma}_{2,0}^{(k)}\hat{O}\{0^{k-2}1^1,[k-1];0,0\}-\hat{\sigma}_{1,0}^{(k)}\hat{O}\{0^{k-2}2^1,[k-1];0,0\}\right)$ $+\sum_{j=k+1}^{N}\left(\hat{\sigma}_{2,0}^{(j)}\hat{O}\{0^{k-2}1^1,[k-1];0,0\}-\hat{\sigma}_{1,0}^{(j)}\hat{O}\{0^{k-2}2^1,[k-1];0,0\}\right)$ $+(k-1)\sum_{j=k+1}^{N}\left(\hat{\sigma}_{2,0}^{(k)}\hat{\sigma}_{1,0}^{(j)}+\hat{\sigma}_{1,0}^{(k)}\hat{\sigma}_{2,0}^{(j)}\right)$	$2k(k-1)N$	$2\le k\le N$
	$[N-2,2]$	(k,ℓ)	1^12^1	$(\ell-3)\left(\hat{\sigma}_{1,0}^{(\ell)}\hat{O}\{0^{k-2}1^2,[k-1,1];k,2^1\}+\hat{\sigma}_{2,0}^{(\ell)}\hat{O}\{0^{k-1}1^1,[k-1,1];k,1^1\}\right)$ $-\hat{O}\{0^{\ell-3}1^12^1,[\ell-2,1];k,1^1\}$	$2k(k-1)(\ell-2)(\ell-3)$	$4\le\ell\le N$ $2\le k<\ell$
	$[N-2,1,1]$	$(k;\ell)$	$(1^1,2^1)$	$(\ell-2)\left(\hat{\sigma}_{2,0}^{(k)}\hat{\sigma}_{1,0}^{(\ell)}+\hat{\sigma}_{1,0}^{(k)}\hat{\sigma}_{2,0}^{(\ell)}\right)+\sum_{i=k+1}^{\ell-1}\left[\left(\hat{\sigma}_{2,0}^{(k)}-\hat{\sigma}_{2,0}^{(\ell)}\right)\hat{\sigma}_{1,0}^{(i)}+\left(\hat{\sigma}_{1,0}^{(\ell)}+\hat{\sigma}_{1,0}^{(k)}\right)\hat{\sigma}_{2,0}^{(i)}\right]$ $+\left(\hat{\sigma}_{2,0}^{(k)}-\hat{\sigma}_{2,0}^{(\ell)}\right)\hat{O}\{0^{k-1}1^1,[k-1];0,0\}+\left(\hat{\sigma}_{1,0}^{(\ell)}-\hat{\sigma}_{1,0}^{(k)}\right)\hat{O}\{0^{k-1}2^1,[k-1];0,0\}$	$2\ell(\ell-1)$	$3\le\ell\le N$ $2\le k<\ell$

Table 5.8: Contribution of transitions in emitter space to the coupling coefficients between $\tilde{\mu} = 0^{N-2}1^2$ and $\tilde{\mu}' = 0^{N-3}1^3$. Notice that $n_{\tilde{\mu}}(0) = N - 2$ and $n_{\tilde{\mu}'}(1) = 3$.

λ	$J^{(\lambda)}_{0^{N-3}1^3,0^{N-2}1^2}$	ρ_J	$L^{(\lambda)}_{0^{N-3}1^3,0^{N-2}1^2}$
$[N]$	$\frac{N}{2}$	0	$\sqrt{3(N-2)}$
$[N-1,1]$	$\frac{N}{2} - 1$	1	$\sqrt{2(N-3)}$
$[N-2,2]$	$\frac{N}{2} - 2$	2	$\sqrt{N-4}$
$[N-3,3]$	$\frac{N}{2} - 3$	3	0

To conclude, we work the example of the coupling, in a system with $N = 4$, between $\tilde{\mu} = 0^3 1^1$ and $\tilde{\mu}' = 0^2 1^2$. The subspaces and couplings are given by

$$
\begin{pmatrix} |1_1\rangle \\ |1_2\rangle \\ |1_3\rangle \\ |1_4\rangle \end{pmatrix}
\underset{\hat{J}_-^{(1,0)}}{\overset{\hat{J}_+^{(1,0)}}{\rightleftharpoons}}
\begin{pmatrix} |1_1 1_2\rangle \\ |1_1 1_3\rangle \\ |1_1 1_4\rangle \\ |1_2 1_3\rangle \\ |1_2 1_4\rangle \\ |1_3 1_4\rangle \end{pmatrix}
\tag{5.86}
$$

In this basis, the raising operator is

$$
\mathbf{J}_+^{(0^2 1^2, 0^3 1^1)} =
\begin{pmatrix}
1 & 1 & 0 & 0 \\
1 & 0 & 1 & 0 \\
1 & 0 & 0 & 1 \\
0 & 1 & 1 & 0 \\
0 & 1 & 0 & 1 \\
0 & 0 & 1 & 1
\end{pmatrix}.
\tag{5.87}
$$

Its singular value decomposition yields

$$
\mathbf{U}_{0^3 1^1} = \frac{1}{2}
\begin{pmatrix}
1 & -\sqrt{3} & 0 & 0 \\
1 & \frac{1}{\sqrt{3}} & -\sqrt{\frac{8}{3}} & 0 \\
1 & \frac{1}{\sqrt{3}} & \sqrt{\frac{2}{3}} & -\sqrt{2} \\
1 & \frac{1}{\sqrt{3}} & \sqrt{\frac{2}{3}} & \sqrt{2}
\end{pmatrix},
\tag{5.88}
$$

$$
\mathbf{U}_{0^2 1^2} = \frac{1}{\sqrt{6}}
\begin{pmatrix}
1 & -1 & -\sqrt{2} & 0 & -\frac{1}{\sqrt{2}} & \sqrt{\frac{3}{2}} \\
1 & -1 & \frac{1}{\sqrt{2}} & -\sqrt{\frac{3}{2}} & \sqrt{2} & 0 \\
1 & -1 & \frac{1}{\sqrt{2}} & \sqrt{\frac{3}{2}} & -\frac{1}{\sqrt{2}} & -\sqrt{\frac{3}{2}} \\
1 & 1 & -\frac{1}{\sqrt{2}} & -\sqrt{\frac{3}{2}} & -\frac{1}{\sqrt{2}} & -\sqrt{\frac{3}{2}} \\
1 & 1 & -\frac{1}{\sqrt{2}} & \sqrt{\frac{3}{2}} & \sqrt{2} & 0 \\
1 & 1 & \sqrt{2} & 0 & -\frac{1}{\sqrt{2}} & \sqrt{\frac{3}{2}}
\end{pmatrix},
\tag{5.89}
$$

$$
\mathbf{S}_{0^3 1^1}^{0^2 1^2} =
\begin{pmatrix}
\sqrt{6} & 0 & 0 & 0 \\
0 & \sqrt{2} & 0 & 0 \\
0 & 0 & \sqrt{2} & 0 \\
0 & 0 & 0 & \sqrt{2} \\
0 & 0 & 0 & 0 \\
0 & 0 & 0 & 0
\end{pmatrix},
\tag{5.90}
$$

where $\mathbf{S}_{\tilde{\mu}}^{\tilde{\mu}'} = \mathbf{U}_{\tilde{\mu}'}^{\dagger} \mathbf{J}_{+}^{(\tilde{\mu}',\tilde{\mu})} \mathbf{U}_{\tilde{\mu}}$ is the matrix whose diagonal lists the singular values of $\mathbf{J}_{+}^{(\tilde{\mu}',\tilde{\mu})}$. Notice that these values correspond with the expected $\sqrt{2(N-1)}$ and $\sqrt{N-2}$ with degeneracy degrees of 1 and $N-1$ respectively; furthermore, the null-space has dimension $N(N-3)/2$.

5.5   Algorithm for Hamiltonian separation

In this section we lay out the specific steps to write the block diagonalized Hamiltonian of a given excitation manifold.

1. Define n_{exc}, the manifold.

2. List all relevant $\tilde{\mu}$, the spectral configurations.

   (a) Enumerate all the partitions, $\boldsymbol{\nu} = [\nu_1, \nu_2, \ldots, \nu_k]$, of integers from 0 to n_{exc}. These must amount to $|\tilde{\mu}_{n_{\text{exc}}}|$ as calculated with eq. (5.15) and eq. (5.16).

   (b) Gather the unique elements in each partition and their corresponding multiplicities. These are the excited levels, $1 \le \nu \le r$, and their populations, $n_{\tilde{\mu}}(\nu)$, respectively.

   (c) Write the spectral configurations according to eq. (5.10), taking into account that

   $$n_{\tilde{\mu}}(0) = \begin{cases} N & \text{if } \boldsymbol{\nu} = [0] \\ N - k & \text{otherwise} \end{cases}. \tag{5.91}$$

3. Calculate all the relevant bare energies, $\varepsilon_{n_{\text{exc}}}^{(\tilde{\mu})}$, with eq. (5.12).

4. List all the allowed $\boldsymbol{\lambda}$, the symmetry defining partitions.

   (a) Enumerate the spectral configurations as $\boldsymbol{\mu}$, i.e., as partitions in regular form.

   (b) Discard redundancies. The remaining partitions are the possible $\boldsymbol{\lambda}$. Their number must add up to $|\lambda_{n_{\text{exc}}}|$ as calculated with eq. (5.45) and eq. (5.46).

5. Determine the composition of each $\tilde{\mu}$ in terms of $\boldsymbol{\lambda}$ according to Young's rule [eq. (5.25)].

   (a) Find out the dominance relations among partitions according to Eq eq. (5.26).

   (b) Compute the pertinent Kostka numbers $(K_{\lambda\mu})$.

6. Write the diagonal of $\hat{H}_{n_{\text{exc}}}^{(\lambda)}$.

   (a) Write the diagonal of $\hat{H}_{n_{\text{exc}}}^{(\lambda,1)}$.

      i. Identify all the $\tilde{\mu}$ to which $\boldsymbol{\lambda}$ contributes.

ii. Collect the bare energies with the $\tilde{\mu}$ identified above and list each of them $K_{\lambda\mu}$ times.

(b) Calculate the dimension of the representation, $\dim(S^\lambda)$, according to the hook-length formula eq. (5.31).

(c) By following

$$\mathbf{H}_{n_{\text{exc}}}^{(\lambda)} = \mathbf{1}_{\dim(S^\lambda)} \otimes \mathbf{H}_{n_{\text{exc}}}^{(\lambda,1)}, \tag{5.92}$$

register the blocks of the Hamiltonian.

7. Calculate the couplings.

(a) Among the available spectral configurations, determine all pairings $\{\tilde{\mu}', \tilde{\mu}\}$ such that

$$\left| \sum_{v=1}^{n_{\text{exc}}} v \left[n_{\tilde{\mu}'}(v) - n_{\tilde{\mu}}(v) \right] \right| = 1. \tag{5.93}$$

The number of pairings inside a given manifold must be $n_{\text{int}}(n_{\text{exc}})$ as calculated with eq. (5.52).

(b) For each pair

i. Identify the the levels involved in the transition, v^* and $v^* + s$, as well as the respective transition dipole moment, and calculate $g_{\tilde{\mu}',\tilde{\mu}}$ with eq. (5.53).

ii. Compute the contribution from the transition in the EM mode, $B_{\tilde{\mu}',\tilde{\mu}}^{n_{\text{exc}}}$, with eq. (5.54).

(c) Write the off-diagonal terms of $\hat{H}_{n_{\text{exc}}}^{(\lambda,1)}$. For each pair $\{\tilde{\mu}', \tilde{\mu}\}$ within each block of symmetry λ:

i. Evaluate the contributions from the transition in the space of emitters, $L_{\tilde{\mu}',\tilde{\mu}}^{(\lambda)}$, according to eq. (5.61). This can be accomplished by brute-force computation of eq. (5.59) and eq. (5.60), or with the strategies described in Appendix 5.4.2.

Table 5.9: Relevant partitions, spectral configurations, excitations in the EM mode, bare energies, and module dimensions calculated in the block diagonalization of $\hat{H}_3(N)$.

n	$p(n)$	ν	$\tilde{\mu}$	$\nu_0^{(3,\tilde{\mu})}$	$\varepsilon_3^{(\tilde{\mu})}$	μ	$q(n)$	λ	$\dim(S^\lambda)$
0	1	[0]	0^N	3	$\frac{7}{2}\hbar\omega + N\varepsilon_0$	$[N]$	1	$[N]$	1
1	1	[1]	$0^{N-1}1^1$	2	$\frac{5}{2}\hbar\omega + (N-1)\varepsilon_0 + \varepsilon_1$	$[N-1,1]$	1	$[N-1,1]$	$N-1$
2	2	[2]	$0^{N-1}2^1$	1	$\frac{3}{2}\hbar\omega + (N-1)\varepsilon_0 + \varepsilon_2$	$[N-1,1]$	1	-	-
		[1,1]	$0^{N-2}1^2$	1	$\frac{3}{2}\hbar\omega + (N-2)\varepsilon_0 + 2\varepsilon_1$	$[N-2,2]$		$[N-2,2]$	$N(N-3)/2$
3	3	[3]	$0^{N-1}3^1$	0	$\frac{\hbar\omega}{2} + (N-1)\varepsilon_0 + \varepsilon_3$	$[N-1,1]$	2	-	-
		[2,1]	$0^{N-2}1^1 2^1$	0	$\frac{\hbar\omega}{2} + (N-2)\varepsilon_0 + \varepsilon_1 + \varepsilon_2$	$[N-2,1,1]$		$[N-2,1,1]$	$(N-1)(N-2)/2$
		[1,1,1]	$0^{N-3}1^3$	0	$\frac{\hbar\omega}{2} + (N-3)\varepsilon_0 + 3\varepsilon_1$	$[N-3,3]$		$[N-3,3]$	$N(N-1)(N-5)/6$
$|\tilde{\mu}_3| = 7$						$|\lambda_3| = 5$			

    ii. If $K_{\lambda\mu'} > 1$

        A. Construct SABEs, $|n_{\text{exc}}, \tilde{\mu}_i, \lambda; \mathbf{y}_1, \mathbf{w}_1\rangle$, for all $\tilde{\mu}_i$ connected to $\tilde{\mu}'$ in a convenient basis.

        B. Apply $\hat{J}_+^{\tilde{\mu}',\tilde{\mu}_i}$ to generate a basis.

        C. Orthogonalize the basis.

        D. Apply $\hat{J}_-^{\tilde{\mu}',\tilde{\mu}_i}$ to the elements of the basis and extract the quantities $L_{\tilde{\mu}'\tilde{\mu}}^{(\lambda)} C_{\tilde{\mu}'\tilde{\mu}}^{(\lambda)}(\mathbf{w}', \mathbf{w})$ using eq. (5.65).

    iii. Calculate the coupling matrix element according to eq. (5.51).

  8. Collect the calculated couplings in their respective blocks.

5.6 Worked examples

5.6.1 The triply excited manifold

In this section we illustrate the implementation of the algorithm when dealing with the system when it holds three quanta, i.e., $n_{\text{exc}} = 3$.

table 5.9 compiles the quantities computed according to steps $1-4$ of the algorithm in the previous section, as well as the dimensions of the irreps in step 6.b.

In table 5.10, we show the Kostka numbers that indicate the composition of the spaces spanned by wavefunctions with the same $\tilde{\mu}$ in terms of symmetrized subspaces labeled by λ.

Table 5.10: Kostka numbers, $K_{\lambda\mu}$, relating the permutation and Specht modules that appear in the triply excited manifold.

λ	$[N]$	$[N-1,1]$	μ $[N-2,2]$	$[N-2,1,1]$	$[N-3,3]$
$[N]$	1	1	1	1	1
$[N-1,1]$	0	1	1	2	1
$[N-2,2]$	0	0	1	1	1
$[N-2,1,1]$	0	0	0	1	0
$[N-3,3]$	0	0	0	0	1

Notice that $K_{\lambda\mu} = 0$ implies that $\lambda \ntrianglelefteq \mu$.

The factors required to calculate the off-diagonal elements, as prescribed by step 7, up until 7.c.i, are on display in table 5.11. Step 7.c.ii was worked in detail in the discussion leading to table 5.5. What is left to this section are the explicit forms of the overlaps:

$$\langle X|A \rangle = \left(\frac{N-2}{2(N-1)} \right)^{1/2},$$

and

$$\langle X|B \rangle = \left(\frac{N}{2(N-1)} \right)^{1/2} = \langle A|Y \rangle.$$

With all these elements, the Hopfield-Bogoliubov forms of the block-diagonalized

Table 5.11: Energy levels involved and contributions from transitions in the EM and emitter modes to the couplings between spectral configurations in the triply excited manifold.

$\tilde{\mu}$	$\tilde{\mu}'$	v^*	$v^* + s$	$B^{(3)}_{\tilde{\mu}',\tilde{\mu}}$	$L^{[N]}_{\tilde{\mu}',\tilde{\mu}}$	$L^{[N-1,1]}_{\tilde{\mu}',\tilde{\mu}}$	$L^{[N-2,2]}_{\tilde{\mu}',\tilde{\mu}}$
0^N	$0^{N-1}1^1$	0	1	$\sqrt{3}$	$\sqrt{N}$		
$0^{N-1}1^1$	$0^{N-2}1^2$	0	1	$\sqrt{2}$	$\sqrt{2(N-1)}$	$\sqrt{N-2}$	
$0^{N-1}1^1$	$0^{N-1}2^1$	1	2	$\sqrt{2}$	1	1	
$0^{N-2}1^2$	$0^{N-3}1^3$	0	1	1	$\sqrt{3(N-2)}$	$\sqrt{2(N-3)}$	$\sqrt{N-4}$
$0^{N-2}1^2$	$0^{N-2}1^12^1$	1	2	1	$\sqrt{2}$	$\sqrt{2}$	$\sqrt{2}$
$0^{N-1}2^1$	$0^{N-2}1^12^1$	0	1	1	$\sqrt{N-1}$	$\sqrt{N-1}$	
$0^{N-1}2^1$	$0^{N-3}3^1$	2	3	1	1	1	

Hamiltonian are

$$\mathbf{H}_3^{[N]} = \begin{pmatrix} \end{pmatrix},$$

(5.94a)

$$\mathbf{H}_3^{[N-1,1]} = \mathbf{1}_{N-1} \otimes \begin{pmatrix} \begin{array}{c} \overline{\varepsilon_3^{(0^{N-1}1^1)}} \quad g_{10}\sqrt{2(N-1)} \\ \overline{\varepsilon_3^{(0^{N-2}1^2)}} \quad g_{10}\sqrt{2(N-2)} \\ g_{21}\sqrt{2} \quad \overline{\varepsilon_3^{(0^{N-3}1^3)}} \\ g_{21}\sqrt{2} \\ \overline{\varepsilon_3^{(0^{N-1}2^1)}} \quad g_{10}\sqrt{\frac{N}{2}-1} \quad g_{10}\sqrt{\frac{N}{2}} \\ g_{32} \qquad \underline{\varepsilon_3^{(0^{N-2}1^12^1)}} \\ \overline{\varepsilon_3^{(0^{N-1}3^1)}} \end{array} \end{pmatrix}, \tag{5.94b}$$

$$\mathbf{H}_3^{[N-2,2]} = \mathbf{1}_{N(N-3)/2} \otimes \begin{pmatrix} \begin{array}{c} \overline{\varepsilon_3^{(0^{N-2}1^2)}} \quad g_{10}\sqrt{2(N-2)} \\ g_{21}\sqrt{2} \quad \overline{\varepsilon_3^{(0^{N-3}1^3)}} \\ \overline{\varepsilon_3^{(0^{N-2}1^12^1)}} \end{array} \end{pmatrix}, \tag{5.94c}$$

$$\mathbf{H}_3^{[N-3,3]} = \mathbf{1}_{N(N-1)(N-5)/6} \otimes \left(\varepsilon_3^{(0^{N-3}1^3)} \right), \tag{5.94d}$$

and

$$\mathbf{H}_3^{[N-2,1,1]} = \mathbf{1}_{(N-1)(N-2)/2} \otimes \left(\varepsilon_3^{(0^{N-2}1^12^1)} \right), \tag{5.94e}$$

where $\mathbf{1}_n$ is the $n \times n$ identity matrix. The matrices above are displayed in a diagrammatic form such that the horizontal lines represent energy levels, and therefore their labels correspond to diagonal elements, while the double-headed arrows indicate the couplings with their labels corresponding to off-diagonal matrix elements. In constructing eq. (5.94b), the couplings involving the states with $\tilde{\mu} = 0^{N-2}1^12^1$ were worked out with the basis $\{|A\rangle, |B\rangle\}$.

In the case of the totally symmetric subspace, we can recognize a ladder of four super-radiantly coupled levels, corresponding to the Dicke states. These are weakly connected to a

117

two-level superradiant interaction between the SABEs with one excitation in $v = 2$. In turn, this interaction connects weakly with the remaining SABE in which the third excited state is populated. For the $N-1$-degenerate subspace with $\lambda = [N-1, 1]$, the superradiantly connected Dicke states form a three-level system in Ξ configuration. They weakly couple to a Λ three-level system produced by the degeneracy introduced by the two-fold contribution of $\tilde{\mu} = 0^{N-2}1^{1}2^{1}$ to this symmetry. As in the case above, the remaining SABE interacts only weakly with this array. For the symmetry $\lambda = [N-2, 2]$ the subspace corresponds to a three-level system with configuration Λ and degeneracy degree of $N(N-3)/2$. However, only one of the couplings is superradiant while the other is weak. The remaining subspaces with symmetries $[N-3, 3]$ and $[N-2, 1, 1]$ are dark, and therefore there are no interactions among the states with degeneracy degrees $N(N-1)(N-5)/6$ and $(N-1)(N-2)/2$, respectively.

5.6.2   Matrices for lower manifolds

Finally, we present the Hopfield Bogoliubov form of the Hamiltonian operators for $0 \le n_{\text{exc}} \le 2$. Their properties have been exhaustively discussed elsewhere.

$$\mathbf{H}_0^{[N]} = \left(\varepsilon_0^{(0^N)} \right), \tag{5.95}$$

$$\mathbf{H}_1^{[N]} = \begin{pmatrix} \varepsilon_1^{(0^N)} & g_{10}\sqrt{N} \\ g_{01}\sqrt{N} & \varepsilon_1^{(0^{N-1}1^1)} \end{pmatrix}, \tag{5.96a}$$

$$\mathbf{H}_1^{[N-1,1]} = \mathbf{1}_{N-1} \otimes \left(\varepsilon_1^{(0^{N-1}1^1)} \right), \tag{5.96b}$$

$$\mathbf{H}_2^{[N]} = \begin{pmatrix} \varepsilon_2^{(0^N)} & g_{10}\sqrt{2N} & 0 & 0 \\ g_{01}\sqrt{2N} & \varepsilon_2^{(0^{N-1}1^1)} & g_{10}\sqrt{2(N-1)} & g_{21} \\ 0 & g_{01}\sqrt{2(N-1)} & \varepsilon_2^{(0^{N-2}1^2)} & 0 \\ 0 & g_{12} & 0 & \varepsilon_2^{(0^{N-1}2^1)} \end{pmatrix}, \tag{5.97a}$$

$$\mathbf{H}_2^{[N-1,1]} = \mathbf{1}_{N-1} \otimes \begin{pmatrix} \varepsilon_2^{(0^{N-1}1^1)} & g_{10}\sqrt{N-2} & g_{21} \\ g_{01}\sqrt{N-2} & \varepsilon_2^{(0^{N-2}1^2)} & 0 \\ g_{12} & 0 & \varepsilon_2^{(0^{N-1}2^1)} \end{pmatrix} \tag{5.97b}$$

$$\mathbf{H}_2^{[N-2,2]} = \mathbf{1}_{N(N-3)/2} \otimes \left(\varepsilon_2^{0^{N-2}1^2} \right). \tag{5.97c}$$

5.7 Properties of eigenstates.

To showcase the usefulness of the formalism, in this section, we analyze the behavior of the energy spectrum and photon content of the eigenstates as a function of parameters in the Hamiltonian, such as anharmonicity, intensity of coupling and detuning.

In the harmonic case, we can define

$$\hat{a}_i = \hat{\sigma}_{v-1,v}^{(i)} \qquad v > 0, \tag{5.98}$$

and the eigenstates can be represented as excitations of the polariton modes:

$$|v(\text{UP})v(\text{LP})v(\text{D}_1)\ldots v(\text{D}_{N-1})\rangle = (a_+^\dagger)^{v(\text{UP})}(a_-^\dagger)^{v(\text{LP})} \prod_{k=1}^{N-1} (\hat{a}_{\text{D}(k)})^{v(\text{D}_k)} |0\rangle, \tag{5.99}$$

where

$$\hat{a}_\pm^\dagger = \frac{1}{\sqrt{2\Omega_{10}}} \left(\pm\sqrt{\Omega_{10} \pm \Delta}\,\hat{a}_0^\dagger + \sqrt{\frac{\Omega_{10} \mp \Delta}{N}} \sum_{i=1}^{N} \hat{a}_i^\dagger \right), \tag{5.100a}$$

$$\hat{a}_{D(k)} = \frac{1}{\sqrt{k}} \left(\sqrt{k-1}\hat{a}_k^\dagger - \frac{1}{\sqrt{k-1}} \sum_{i=1}^{k-1} \hat{a}_i^\dagger \right). \tag{5.100b}$$

The quantities $\Delta = \omega - (\varepsilon_1 - \varepsilon_0)/\hbar$, and $\Omega_{10} = [\Delta^2 + 4(g_{10}/\hbar)^2 N]^{1/2}$ are the detunning and Rabi frequency, respectively, and the labels UP, LP and D stand for *upper*, *lower* and *dark polaritons*, respectively.

When anharmonicity is considered, the excitations in the polaritonic modes are no longer good quantum numbers; however, the actual eigenstates are similar enough to those in the harmonic case that the labels introduced in eq. (5.99) can still be consistent with some of the features displayed by these states. We introduce anharmonicities by considering the emitters as Morse oscillators [93], i.e., the single-emitter Hamiltonians include a potential energy function of the form

$$V(R) = D_e \left(1 - e^{-a(R-R_e)} \right)^2, \tag{5.101}$$

where R is the mass-scaled length of the oscillator with value at equilibrium R_e, $D_e = V(\infty) - V(R_e)$ is the dissociation energy, and

$$a^2 = \frac{1}{2D_e} \left. \frac{d^2 V(R)}{dR^2} \right|_{R_e}. \tag{5.102}$$

The corresponding eigenenergies are given by

$$\varepsilon_v = \hbar a \left(v + \frac{1}{2} \right) \left[\sqrt{2D_e} - \frac{\hbar a}{2} \left(v + \frac{1}{2} \right) \right] \qquad \varepsilon_v \le D_e, \tag{5.103}$$

with the implication that the number of bound-states is $\lfloor r_{MO} \rfloor$, where

$$r_{MO} = \frac{\sqrt{2D_e}}{\hbar a} - \frac{1}{2}; \tag{5.104}$$

therefore, the potential becomes harmonic as $D_e \to \infty$ ($a \to 0$) [202]. This model introduces a mechanical anharmonicity characterized by $-a^2$, as well as an electric anharmonicity, which

stems from the fact that

$$\frac{g_{v+1,v}^{\text{MO}}}{g_{v+1,v}^{\text{HO}}} = \frac{2}{2(r_{\text{MO}} - v) - 1} \left[2\frac{\sqrt{2D_e}}{\hbar a} \frac{(r_{\text{MO}} - v)(r_{\text{MO}} - v - 1)}{(2r_{\text{MO}} - v)} \right]^{1/2}, \qquad (5.105)$$

where the labels MO and HO indicate Morse and harmonic oscillators, respectively [203].

Figure 5.2 compares the eigenenergies as functions of the Rabi splitting, $\hbar\Omega_{10} = 2g_{10}\sqrt{N}$, of systems with different anharmonicities in which the frequency of the EM mode is resonant with the transition $0 \rightarrow 1$ of the emitters. As expected, the slope of the energy as a function of the coupling intensity is proportional to the number of quanta in the non-dark modes, with the sign of the contribution being positive for UP, and negative for LP. The introduction of anharmonicity lifts the degeneracy of states with multiple excitations in the dark modes, which has some remarkable consequences.

In the harmonic case, the quantum numbers facilitate the identification of the symmetry of a state just by inspection of its multiplicity. For instance, the state $|3_+\rangle$ is unique in regards of its spectral configuration; therefore, it belongs to $\lambda = [N]$. On the other hand, states of the form $|1_+1_-1_{\text{D}(k)}\rangle$ have multiplicity of $N - 1$ and symmetry $\lambda = [N - 1, 1]$. Also, from the $(N - 1)(N - 2)/2$ states of the form $|1_-1_{\text{D}(k)}1_{\text{D}(k')}\rangle$, one has symmetry $\lambda = [N]$ while the remaining $N(N - 3)/2$ are of the $\lambda = [N - 2, 2]$ kind. In contrast, when anharmonicities are involved, the harmonic states of reference are those with the appropriate energetics. As a consequence, a state with labels $|1_+2_{\text{D}(k)}\rangle$, which accounts for BEs with $\tilde{\mu} = 0^{N-1}2^1$, now has symmetry $\lambda = [N]$ despite belonging to a multiplet of size $N - 1$. The lift in degeneracy, together with the diversity in slopes with which the eigenenergies depend on the coupling strength generate situations in which the ordering of levels changes for different coupling intensities. This might result in interesting spectroscopic observations for samples with different concentrations of emitters.

In fig. 5.3 the energy of the eigenstates is plotted against the number of coupled molecules
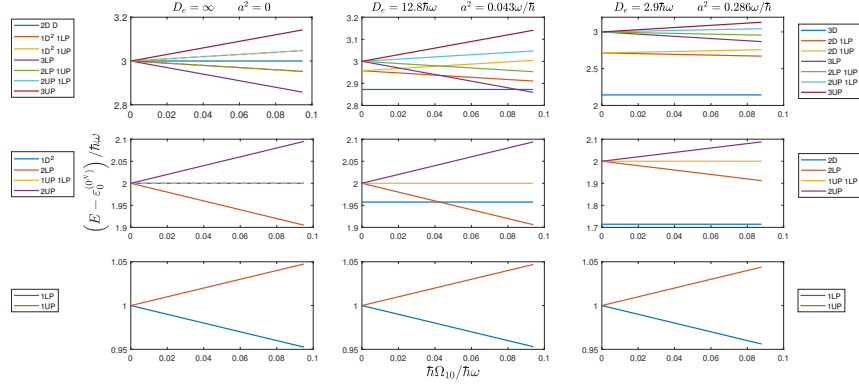
(a) $\boldsymbol{\lambda} = [N]$
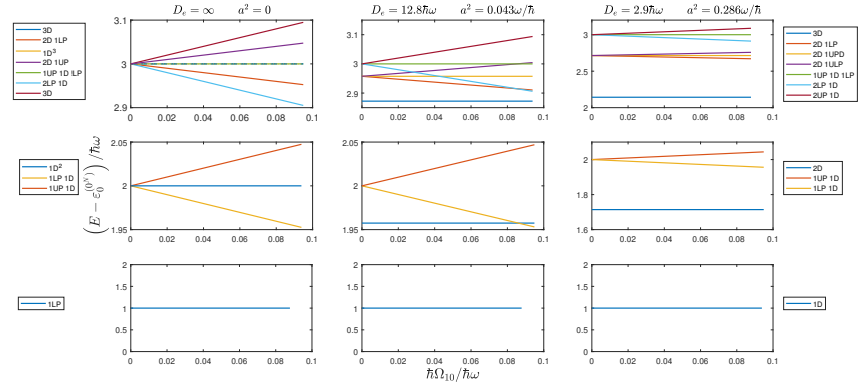
(b) $\boldsymbol{\lambda} = [N-1, 1]$
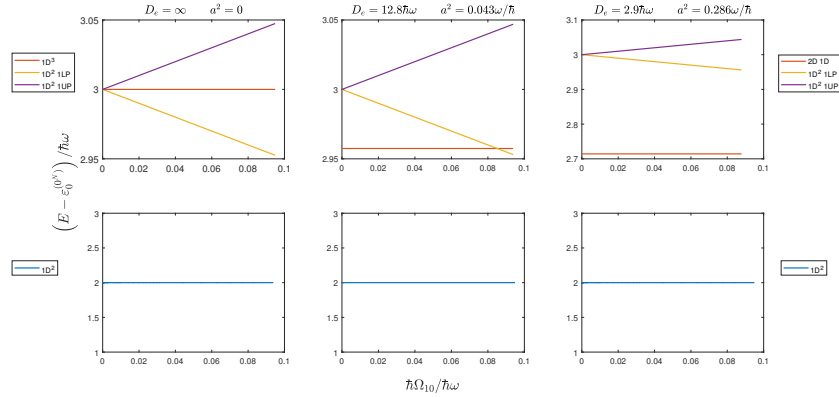
(c) $\boldsymbol{\lambda} = [N-2, 2]$

Figure 5.2: Energy spectra of emitters with various anharmonicities coupled to a harmonic EM mode as a function of coupling intensity in the weak-to-strong regime. The parameters of the Morse potential are such that the number of bound states, r_{MO}, are ∞, 24 and 4, respectively, for each of the displayed columns. The legend to the left shows the labels of states in the harmonic case, while the legend to the right labels states in the anharmonic regime.
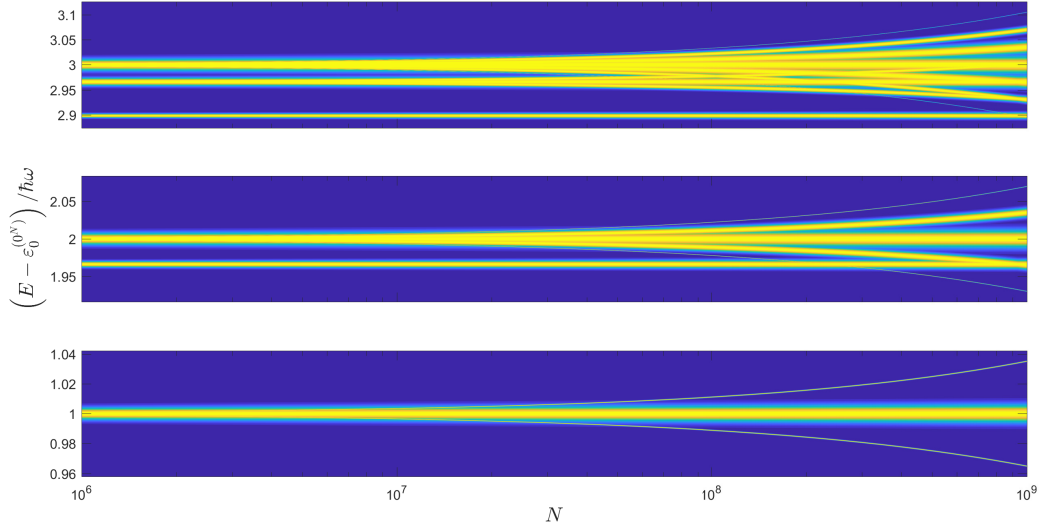
Figure 5.3: Energy spectra of anharmonic emitters coupled to a harmonic EM mode with illustrated degeneracies. The Morse potential parameters are $D_e = 15.25\hbar\omega$ and $a^2 = 0.034\omega/\hbar$. The thickness of the lines are proportional to $\log[\dim(S^\lambda)]$.

with the thickness of the lines illustrating the degeneracy of each energy level. In each case, the thickness corresponds to $\log[\dim(S^\lambda)]$ and should not be mistaken by any broadening mechanism such as dissipation or disorder. It can be seen that both, degeneracy and energy separation, increase with the number of molecules. Furthermore the most degenerate levels are those with constant energy, which are presumably dark. This observation informs that light-matter coupling might not impact processes that engage the matter component, such as chemical reactions, even when anharmonicities are taken into account. Moreover, the resolution in energies also suggests that naturally occurring broadenings shall smear the energy levels making them effectively indistinguishable.

The formalism presented in this work also allows to calculate observables associated with operators for which the permutational symmetry holds. One clear example is the photon number operator, $\hat{v}_0 = \hat{a}_0^\dagger \hat{a}_0$, which measures the photon contents of a given state. In the symmetrized
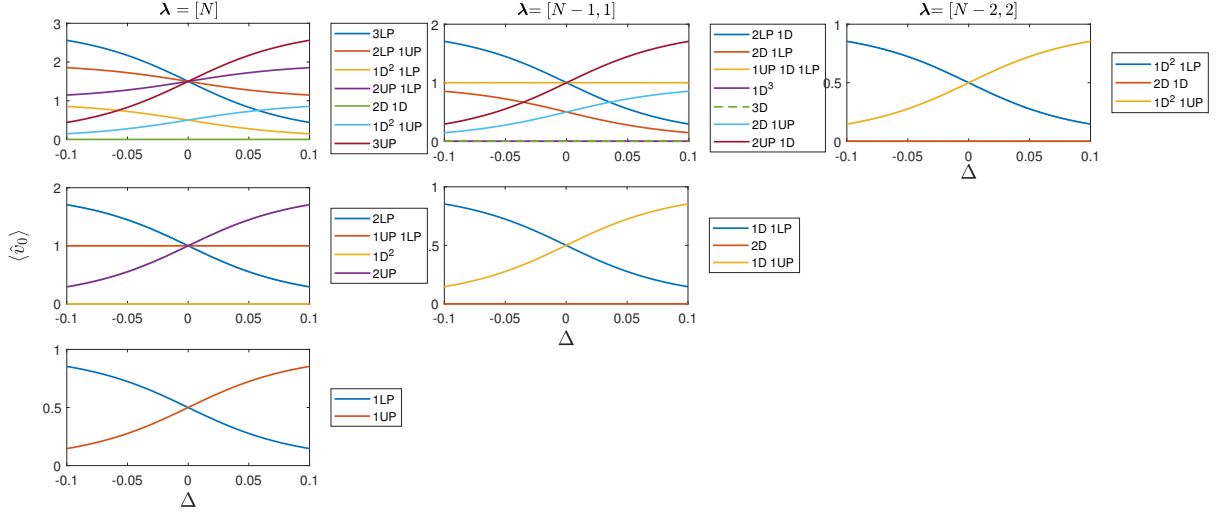
Figure 5.4: Photon content of harmonic eigenstates as a function of detuning.

basis, this operator is diagonal and has the form

$$
\hat{v}_0 = \sum_{\tilde{\mu}:\mu\trianglelefteq\lambda} \sum_{i=1}^{\dim(S^\lambda)} \sum_{j=1}^{K_{\lambda\mu}} v_0^{(n_{\mathrm{exc}},\tilde{\mu})} \left| n_{\mathrm{exc}}, \tilde{\mu}, \lambda; \mathbf{y}_i, \mathbf{w}_j \right\rangle \left\langle n_{\mathrm{exc}}, \tilde{\mu}, \lambda; \mathbf{y}_i, \mathbf{w}_j \right|. \tag{5.106}
$$

In fig. 5.4 the photon content of the eigenstates is plotted as a function of the detunning for a fixed value of the collective coupling. The inclusion of anharmonicity should be inconsequential except for the change in the labeling of eigenstates.

5.8 Conclusions.

In this paper, we address the problem of the coupling between N identical dipoles, each with an arbitrary spectral structure, and a harmonic electromagnetic mode confined in a cavity. We have introduced tools from Group Theory that capitalize from the permutational symmetry of the system to simplify the Schrödinger equation. In the symmetry-adapted basis, the Hamiltonian breaks down into manageable matrices whose dimension is independent of the number of emitters

and grows only subexponentially with the number of excitations. And while the total number of these matrices does depend polynomially on the number of emitters, they encode highly degenerate subspaces; therefore, the effective number of matricses to diagonalize is actually small. Since the method here presented does not rely on the explicit form of the basis transformation, the off-diagonal matrix elements are constructed by taking advantage of the fact that the structure of the Hilbert space also displays the symmetry of the special unitary group, and therefore can be described with the tools from angular momentum theory. This procedure exhibits the (super)radiant character of the transitions. We have also explored the immediate implications of including anharmonicities on the energetic and combinatorial characterization of the eigenstates. Finally, we have calculated the photon content of the eigenstates to exemplify the utility of the method in the calculation of observables associated with symmetry-preserving operators.

Chapter 5, in full is currently being prepared for submission for publication of the material. "Generalization of the Tavis-Cummings model for multi-level anharmonic systems". Campos-Gonzalez-Angulo, Jorge A.; Ribeiro, Raphael F.; Yuen-Zhou, Joel. The dissertation author was the primary investigator and author of this material.

Chapter 6

Conclusions and outlook.

This dissertation presents a review of the phenomenon of vibrational strong coupling and explores its implications for chemical reactivity from a theoretical point of view. It is a fact that the kinetics of several reactions have been observed to experience modification due to resonant coupling to confined electromagnetic fields. Nevertheless, a simple analysis of cavity quantum electrodynamics (CQED), the theory that successfully has helped to understand the optical properties of coupled systems, suggests that such an effect should not be observed. Even more elaborated arguments, including considerations of chemical dynamics, have been put forward, exhibiting the incapability of the theory in its current state to explain the observed phenomena [102]. Transition state theory (TST) is the main tool to explain the rates of reactions in which cavity effects have been observed. Galego and collaborators [83, 84] formalized the incorporation of CQED to TST in an attempt to explain the rate modifications. While they presented changes in the energetic landscape of a single molecule, the consideration of more realistic situations leads to conclude that their effort actually supports the idea that cavity-induced modifications should not happen. This dissertation adapted their formalism to the language of polaritons to simplify the understanding of the absence of resonant effects and illustrate how this theory is incompatible with the experimental observations in the collective regime. A possible

reason for the failure of TST to explain rate modifications is the fact that, as a classical theory, it cannot incorporate the structure of the quantized energy spectrum of polaritons. In contrast, the modification of Levich and Jortner to Marcus' rate theory of electron transfer provides a playground in which the insertion of polariton energies is straightforward. This dissertation highlights that in this framing, it is possible to conceptualize rate modification in terms of the opening of reaction channels with activation energies determined by the Rabi splitting that can be more favored than the default channel. By being consistent with the polaritonic picture, this approach relates the extent of the modification to the number of coupled reactants and finds its maximal prominence in the neighborhood of the resonant condition. Although there are arguments against the operativity of this line of reasoning in realistic situations [100], this approach has set the basis for further approaches with a higher potential of success [101, 115]. In an attempt to understand the implications of anharmonicities for VSC, beyond the single-molecule case [91], this work presents how to address the quantum problem of an arbitrary number of identical emitters coupled to a cavity mode. Given the large number of molecules required to observe strong-light matter coupling, a brute-force approach to this problem cannot proceed since the dimension of the Hilbert space renders the problem intractable. Conveniently, the permutational symmetry introduced by the uniformity of the oscillators allows us to approach the problem with group-theoretical tools that notably reduce its complexity. The present work discusses the application of such tools to reduce the dimensionality of the problem and presents the method to compute the symmetry dependent couplings for each excitation manifold. Once the problem has been simplified, it is possible to obtain the energy spectrum and characterize the eigenstates in their photon content and their similarities to polaritonic eigenstates. Since the only meaningful observables with the considered characterizations are those that preserve permutational invariance, the locality of an event such as a chemical reaction, which breaks this symmetry, makes it unlikely that an anharmonic oscillator would remain as a part of the collective coupling while it transforms. Through VSC and chemical reactivity, this experience leaves the lesson that there is still much to

figure out about how to combine chemical dynamics and quantum optics. The consistent failure of traditional theories to explain a confirmed phenomenon illustrates their limitations and the need for innovative considerations that will hopefully be informed by the findings in this work. Since classical theories at quasi-equilibrium had been arguably discarded, the next approaches need to incorporate non-equilibrium considerations and possibly acknowledge more directly the quantum spectrum of polariton modes.

Bibliography

[1] J. Jortner, R.D. Levine, and A. Pullman. *Mode Selective Chemistry: Proceedings of the Twenty-Fourth Jerusalem Symposium on Quantum Chemistry and Biochemistry Held in Jerusalem, Israel, May 20–23, 1991*. Jerusalem Symposia. Springer Netherlands, 2012.

[2] M. Shapiro and P. Brumer. *Quantum Control of Molecular Processes*. Wiley, 2012.

[3] Willis E. Lamb and Robert C. Retherford. Fine structure of the hydrogen atom by a microwave method. *Phys. Rev.*, 72:241–243, Aug 1947.

[4] E. M. Purcell. Proceedings of the american physical society. *Phys. Rev.*, 69:674–674, Jun 1946.

[5] H. B. G. Casimir and D. Polder. The influence of retardation on the london-van der waals forces. *Phys. Rev.*, 73:360–372, Feb 1948.

[6] S. Haroche, J.M. Raimond, and Oxford University Press. *Exploring the Quantum: Atoms, Cavities, and Photons*. Oxford Graduate Texts. OUP Oxford, 2006.

[7] C. Cohen-Tannoudji, J. Dupont-Roc, and G. Grynberg. *Photons and Atoms: Introduction to Quantum Electrodynamics*. Wiley, 1989.

[8] I. I. Rabi. On the process of space quantization. *Phys. Rev.*, 49:324–328, Feb 1936.

[9] I. I. Rabi. Space quantization in a gyrating magnetic field. *Phys. Rev.*, 51:652–654, Apr 1937.

[10] J. J. Hopfield. Theory of the Contribution of Excitons to the Complex Dielectric Constant of Crystals. *PR*, 112(5):1555–1567, 1958.

[11] M. G. Raizen, R. J. Thompson, R. J. Brecha, H. J. Kimble, and H. J. Carmichael. Normal-mode splitting and linewidth averaging for two-state atoms in an optical cavity. *Phys. Rev. Lett.*, 63:240–243, Jul 1989.

[12] Kerry J. Vahala. Optical microcavities. *Nature*, 424(6950):839–846, 2003.

[13] A. Kavokin, J.J. Baumberg, G. Malpuech, and F.P. Laussy. *Microcavities*. Series on Semiconductor Science and Technology. OUP Oxford, 2011.

[14] M. S. Tame, K. R. McEnery, Ş. K. Özdemir, J. Lee, S. A. Maier, and M. S. Kim. Quantum plasmonics. *Nature Physics*, 9(6):329–340, 2013.

[15] S. M. Dutra and P. L. Knight. Spontaneous emission in a planar fabry-pérot microcavity. *Phys. Rev. A*, 53:3587–3605, May 1996.

[16] Kyriacos Georgiou, Paolo Michetti, Lizhi Gai, Marco Cavazzini, Zhen Shen, and David G. Lidzey. Control over energy transfer between fluorescent bodipy dyes in a strongly coupled microcavity. *ACS Photonics*, 5(1):258–266, January 2018.

[17] D L Mills and E Burstein. Polaritons: the electromagnetic modes of media. *Reports on Progress in Physics*, 37(7):817–926, jul 1974.

[18] Gregory H. Wannier. The structure of electronic excitation levels in insulating crystals. *Phys. Rev.*, 52:191–197, Aug 1937.

[19] J. P. Reithmaier, G. Sęk, A. Löffler, C. Hofmann, S. Kuhn, S. Reitzenstein, L. V. Keldysh, V. D. Kulakovskii, T. L. Reinecke, and A. Forchel. Strong coupling in a single quantum dot-semiconductor microcavity system. *Nature*, 432(7014):197–200, 2004.

[20] A. Gruber, A. Dräbenstedt, C. Tietz, L. Fleury, J. Wrachtrup, and C. von Borczyskowski. Scanning confocal optical microscopy and magnetic resonance on single defect centers. *Science*, 276(5321):2012–2014, 1997.

[21] V. Bouchiat, D. Vion, P. Joyez, D. Esteve, and M. H. Devoret. Quantum coherence with a single cooper pair. *Physica Scripta*, T76(1):165, 1998.

[22] A. K. Geim and I. V. Grigorieva. Van der waals heterostructures. *Nature*, 499(7459):419–425, 2013.

[23] V.M. Agranovich and G. Czajkowski. *Excitations in Organic Solids*. International Series of Monogr. OUP Oxford, 2009.

[24] Paolo Michetti, Leonardo Mazza, and Giuseppe C. La Rocca. *Strongly Coupled Organic Microcavities*, pages 39–68. Springer Berlin Heidelberg, Berlin, Heidelberg, 2015.

[25] J. Kasprzak, M. Richard, S. Kundermann, A. Baas, P. Jeambrun, J. M. J. Keeling, F. M. Marchetti, M. H. Szymańska, R. André, J. L. Staehli, V. Savona, P. B. Littlewood, B. Deveaud, and Le Si Dang. Bose-einstein condensation of exciton polaritons. *Nature*, 443(7110):409–414, 2006.

[26] Alexandre Blais, Ren-Shou Huang, Andreas Wallraff, S. M. Girvin, and R. J. Schoelkopf. Cavity quantum electrodynamics for superconducting electrical circuits: An architecture for quantum computation. *Phys. Rev. A*, 69:062320, Jun 2004.

[27] S. Kéna-Cohen and S. R. Forrest. Room-temperature polariton lasing in an organic single-crystal microcavity. *Nature Photonics*, 4(6):371–375, 2010.

[28] Denis Sannikov, Timur Yagafarov, Kyriacos Georgiou, Anton Zasedatelev, Anton Baranikov, Lizhi Gai, Zhen Shen, David Lidzey, and Pavlos Lagoudakis. Room temperature broadband polariton lasing from a dye-filled microcavity. *Advanced Optical Materials*, 7(17):1900163, 2019.

[29] Fábio Barachati, Simone De Liberato, and S. Kéna-Cohen. Generation of rabi-frequency radiation using exciton-polaritons. *Phys. Rev. A*, 92:033828, Sep 2015.

[30] Fábio Barachati, Janos Simon, Yulia A. Getmanenko, Stephen Barlow, Seth R. Marder, and Stéphane Kéna-Cohen. Tunable third-harmonic generation from polaritons in the ultrastrong coupling regime. *ACS Photonics*, 5(1):119–125, January 2018.

[31] T. Schwartz, J. A. Hutchison, C. Genet, and T. W. Ebbesen. Reversible switching of ultrastrong light-molecule coupling. *Phys. Rev. Lett.*, 106:196405, May 2011.

[32] E. Orgiu, J. George, J. A. Hutchison, E. Devaux, J. F. Dayen, B. Doudin, F. Stellacci, C. Genet, J. Schachenmayer, C. Genes, G. Pupillo, P. Samorì, and T. W. Ebbesen. Conductivity in organic semiconductors hybridized with the vacuum field. *Nature Materials*, 14(11):1123–1129, 2015.

[33] Xiaolan Zhong, Thibault Chervy, Lei Zhang, Anoop Thomas, Jino George, Cyriaque Genet, James A. Hutchison, and Thomas W. Ebbesen. Energy transfer between spatially separated entangled molecules. *Angewandte Chemie International Edition*, 56(31):9034–9038, 2017.

[34] Luis A. Martínez-Martínez, Matthew Du, Raphael F. Ribeiro, Stéphane Kéna-Cohen, and Joel Yuen-Zhou. Polariton-assisted singlet fission in acene aggregates. *J. Phys. Chem. Lett.*, 9(8):1951–1957, April 2018.

[35] Matthew Du, Luis A. Martínez-Martínez, Raphael F. Ribeiro, Zixuan Hu, Vinod M. Menon, and Joel Yuen-Zhou. Theory for polariton-assisted remote energy transfer. *Chem Sci*, 9(32):6659–6669, 2018.

[36] Matthew Du, Raphael F. Ribeiro, and Joel Yuen-Zhou. Remote control of chemistry in optical cavities. *Chem*, 5(5):1167 – 1181, 2019.

[37] Thomas W. Ebbesen. Hybrid Light-Matter States in a Molecular and Material Science Perspective. *Acc Chem Res*, 49(11):2403–2412, Nov 2016.

[38] Raphael F. Ribeiro, Luis A. Martínez-Martínez, Matthew Du, Jorge Campos-Gonzalez-Angulo, and Joel Yuen-Zhou. Polariton chemistry: controlling molecular dynamics with optical cavities. *Chem Sci*, 9(30):6325–6339, 2018.

[39] Johannes Feist, Javier Galego, and Francisco J. Garcia-Vidal. Polaritonic Chemistry with Organic Molecules. *ACS Photonics*, 5(1):205–216, January 2018.

[40] Johannes Flick, Nicholas Rivera, and Prineha Narang. Strong light-matter coupling in quantum chemistry and quantum photonics. *Nanophotonics*, 7(9):1479, 2018.

[41] Stéphane Kéna-Cohen and Joel Yuen-Zhou. Polariton chemistry: Action in the dark. *ACS Cent. Sci.*, 5(3):386–388, March 2019.

[42] Felipe Herrera and Jeffrey Owrutsky. Molecular polaritons for controlling chemistry with quantum optics. *J. Chem. Phys.*, 152(10):100902, 2020.

[43] Kenji Hirai, James A. Hutchison, and Hiroshi Uji-i. Recent progress in vibropolaritonic chemistry. *ChemPlusChem*, 85(9):1981–1988, 2020.

[44] James A. Hutchison, Tal Schwartz, Cyriaque Genet, Eloïse Devaux, and Thomas W. Ebbesen. Modifying chemical landscapes by coupling to vacuum fields. *Angewandte Chemie International Edition*, 51(7):1592–1596, 2012.

[45] Battulga Munkhbat, Martin Wersäll, Denis G. Baranov, Tomasz J. Antosiewicz, and Timur Shegai. Suppression of photo-oxidation of organic chromophores by strong coupling to plasmonic nanoantennas. *Sci Adv*, 4(7):eaas9552, July 2018.

[46] Kati Stranius, Manuel Hertzog, and Karl Börjesson. Selective manipulation of electronically excited states through strong light-matter interactions. *Nature Communications*, 9(1):2273, 2018.

[47] Elad Eizner, Luis A. Martínez-Martínez, Joel Yuen-Zhou, and Stéphane Kéna-Cohen. Inverting singlet and triplet excited states using strong light-matter coupling. *Science Advances*, 5(12), 2019.

[48] Javier Galego, Francisco J. Garcia-Vidal, and Johannes Feist. Cavity-induced modifications of molecular structure in the strong-coupling regime. *Phys. Rev. X*, 5:041022, Nov 2015.

[49] Felipe Herrera and Frank C. Spano. Cavity-controlled chemistry in molecular ensembles. *Phys Rev Lett*, 116(23):238301, June 2016.

[50] Luis A. Martínez-Martínez, Raphael F. Ribeiro, Jorge Campos-González-Angulo, and Joel Yuen-Zhou. Can ultrastrong coupling change ground-state chemical reactions? *ACS Photonics*, 5(1):167–176, January 2018.

[51] Johannes Flick, Heiko Appel, Michael Ruggenthaler, and Angel Rubio. Cavity Born-Oppenheimer approximation for correlated electron-nuclear-photon systems. *J Chem Theory Comput*, 13(4):1616–1625, April 2017.

[52] Johannes Flick, Michael Ruggenthaler, Heiko Appel, and Angel Rubio. Atoms and molecules in cavities, from weak to strong coupling in quantum-electrodynamics (qed) chemistry. *Proc. Natl. Acad. Sci. U.S.A.*, 114(12):3026–3034, 2017.

[53] Alexander Semenov and Abraham Nitzan. Electron transfer in confined electromagnetic fields. *J. Chem. Phys.*, 150(17):174122, June 2019.

[54] J. P. Long and B. S. Simpkins. Coherent coupling between a molecular vibration and Fabry-Perot optical cavity to give hybridized states in the strong coupling limit. *ACS Photonics*, 2(1):130–136, January 2015.

[55] A. Shalabney, J. George, J. Hutchison, G. Pupillo, C. Genet, and T. W. Ebbesen. Coherent coupling of molecular resonators with a microcavity mode. *Nat Commun*, 6:5981, January 2015.

[56] Robrecht M. A. Vergauwe, Jino George, Thibault Chervy, James A. Hutchison, Atef Shalabney, Vladimir Y. Torbeev, and Thomas W. Ebbesen. Quantum strong coupling with protein vibrational modes. *J. Phys. Chem. Lett.*, 7(20):4159–4164, October 2016.

[57] B. S. Simpkins, Kenan P. Fears, Walter J. Dressick, Bryan T. Spann, Adam D. Dunkelberger, and Jeffrey C. Owrutsky. Spanning strong to weak normal mode coupling between vibrational and fabry-pérot cavity modes through tuning of vibrational absorption strength. *ACS Photonics*, 2(10):1460–1467, October 2015.

[58] Shaelyn R. Casey and Justin R. Sparks. Vibrational Strong Coupling of Organometallic Complexes. *The Journal of Physical Chemistry C*, 120(49):28138–28143, 2016.

[59] Jino George, Atef Shalabney, James A. Hutchison, Cyriaque Genet, and Thomas W. Ebbesen. Liquid-phase vibrational strong coupling. *J. Phys. Chem. Lett.*, 6(6):1027–1031, March 2015.

[60] J. A. Mason, G. Allen, V. A. Podolskiy, and D. Wasserman. Strong coupling of molecular and mid-infrared perfect absorber resonances. *IEEE Photonics Technology Letters*, 24(1):31–33, Jan 2012.

[61] Atef Shalabney, Jino George, Hidefumi Hiura, James A. Hutchison, Cyriaque Genet, Petra Hellwig, and Thomas W. Ebbesen. Enhanced raman scattering from vibro-polariton hybrid states. *Angewandte Chemie International Edition*, 54(27):7971–7975, 2015.

[62] Javier del Pino, Johannes Feist, and F. J. Garcia-Vidal. Signatures of vibrational strong coupling in Raman scattering. *J. Phys. Chem. C*, 119(52):29132–29137, December 2015.

[63] Artem Strashko and Jonathan Keeling. Raman scattering with strongly coupled vibron-polaritons. *Phys Rev A*, 94(2):023843, August 2016.

[64] Merav Muallem, Alexander Palatnik, Gilbert D. Nessim, and Yaakov R. Tischler. Strong light-matter coupling and hybridization of molecular vibrations in a low-loss infrared microcavity. *J. Phys. Chem. Lett.*, 7(11):2002–2008, June 2016.

[65] Vivian F. Crum, Shaelyn R. Casey, and Justin R. Sparks. Photon-mediated hybridization of molecular vibrational states. *Phys. Chem. Chem. Phys.*, 20:850–857, 2018.

[66] Prasoon Saurabh and Shaul Mukamel. Two-dimensional infrared spectroscopy of vibrational polaritons of molecules in an optical cavity. *J. Chem. Phys.*, 144(12):124115, 2018-11.

[67] Bo Xiang, Raphael F. Ribeiro, Adam D. Dunkelberger, Jiaxi Wang, Yingmin Li, Blake S. Simpkins, Jeffrey C. Owrutsky, Joel Yuen-Zhou, and Wei Xiong. Two-dimensional infrared spectroscopy of vibrational polaritons. *Proceedings of the National Academy of Sciences*, 115(19):4845–4850, 2018.

[68] Raphael F. Ribeiro, Adam D. Dunkelberger, Bo Xiang, Wei Xiong, Blake S. Simpkins, Jeffrey C. Owrutsky, and Joel Yuen-Zhou. Theory for Nonlinear Spectroscopy of Vibrational Polaritons. *J. Phys. Chem. Lett.*, 9(13):3766–3771, 2018.

[69] Bo Xiang, Raphael F. Ribeiro, Yingmin Li, Adam D. Dunkelberger, Blake B. Simpkins, Joel Yuen-Zhou, and Wei Xiong. Manipulating optical nonlinearities of molecular polaritons by delocalization. *Science Advances*, 5(9), 2019.

[70] Raphael F Ribeiro, Jorge A Campos-Gonzalez-Angulo, Noel C Giebink, Wei Xiong, and Joel Yuen-Zhou. Enhanced optical nonlinearities under strong light-matter coupling. Preprint, 2020.

[71] Anoop Thomas, Jino George, Atef Shalabney, Marian Dryzhakov, Sreejith J. Varma, Joseph Moran, Thibault Chervy, Xiaolan Zhong, Eloïse Devaux, Cyriaque Genet, James A. Hutchison, and Thomas W. Ebbesen. Ground-state chemical reactivity under vibrational coupling to the vacuum electromagnetic field. *Angew Chem Int Ed*, 55(38):11462–11466, February 2016.

[72] Anoop Thomas, Lucas Lethuillier-Karl, Joseph Moran, and Thomas Ebbesen. Comment on "on the sn2 reactions modified in vibrational strong coupling experiments: Reaction mechanisms and vibrational mode assignments", Sep 2020.

[73] Anoop Thomas, Anjali Jayachandran, Lucas Lethuillier-Karl, Robrecht M.A. Vergauwe, Kalaivanan Nagarajan, Eloise Devaux, Cyriaque Genet, Joseph Moran, and Thomas W. Ebbesen. Ground state chemistry under vibrational strong coupling: dependence of thermodynamic parameters on the rabi splitting energy. *Nanophotonics*, 9(2):249 – 255, 2020.

[74] A. Thomas, L. Lethuillier-Karl, K. Nagarajan, R. M. A. Vergauwe, J. George, T. Chervy, A. Shalabney, E. Devaux, C. Genet, J. Moran, and T. W. Ebbesen. Tilting a ground-state reactivity landscape by vibrational strong coupling. *Science*, 363(6427):615, February 2019.

[75] Kenji Hirai, Rie Takeda, James A. Hutchison, and Hiroshi Uji-i. Modulation of prins cyclization by vibrational strong coupling. *Angewandte Chemie International Edition*, 59(13):5332–5335, 2020.

[76] Robrecht M. A. Vergauwe, Anoop Thomas, Kalaivanan Nagarajan, Atef Shalabney, Jino George, Thibault Chervy, Marcus Seidel, Eloïse Devaux, Vladimir Torbeev, and Thomas W. Ebbesen. Modification of enzyme activity by vibrational strong coupling of water. *Angewandte Chemie International Edition*, 58(43):15324–15328, 2019.

[77] Hidefumi Hiura, Atef Shalabney, and Jino George. Vacuum-field catalysis: Accelerated reactions by vibrational ultra strong coupling, Nov 2018.

[78] Jyoti Lather, Pooja Bhatt, Anoop Thomas, Thomas W. Ebbesen, and Jino George. Cavity catalysis by cooperative vibrational strong coupling of reactant and solvent molecules. *Angewandte Chemie International Edition*, 58(31):10635–10638, 2019.

[79] Yantao Pang, Anoop Thomas, Kalaivanan Nagarajan, Robrecht M. A. Vergauwe, Kripa Joseph, Bianca Patrahau, Kuidong Wang, Cyriaque Genet, and Thomas W. Ebbesen. On the role of symmetry in vibrational strong coupling: The case of charge-transfer complexation. *Angewandte Chemie International Edition*, 59(26):10436–10440, 2020.

[80] Blake Simpkins. Vibration-cavity coupling: Modulation of coupling strength and ground state reaction rates. YouTube.

[81] Javier del Pino, Johannes Feist, and Francisco J Garcia-Vidal. Quantum theory of collective strong coupling of molecular vibrations with a microcavity mode. *New J Phys*, 17(5):053040, May 2015.

[82] Konstantinos S. Daskalakis, Stefan A. Maier, and Stéphane Kéna-Cohen. *Polariton Condensation in Organic Semiconductors*, pages 151–163. Springer International Publishing, Cham, 2017.

[83] Javier Galego, Clàudia Climent, Francisco J. Garcia-Vidal, and Johannes Feist. Cavity Casimir-Polder Forces and Their Effects in Ground-State Chemical Reactivity. *Phys Rev X*, 9:021057, June 2019.

[84] Clàudia Climent, Javier Galego, Francisco J. Garcia-Vidal, and Johannes Feist. Plasmonic Nanocavities Enable Self-Induced Electrostatic Catalysis. *Angew Chem Int Ed*, 58(26):8698–8702, 2019.

[85] Vladimir P. Zhdanov. Vacuum field in a cavity, light-mediated vibrational coupling, and chemical reactivity. *Chemical Physics*, page 110767, 2020.

[86] Jorge A. Campos-Gonzalez-Angulo and Joel Yuen-Zhou. Polaritonic normal modes in transition state theory. *The Journal of Chemical Physics*, 152(16):161101, 2020.

[87] Xinyang Li, Arkajit Mandal, and Pengfei Huo. Resonance theory of vibrational strong couplings in polariton chemistry, Sep 2020.

[88] H.A. Kramers. Brownian motion in a field of force and the diffusion model of chemical reactions. *Physica*, 7(4):284 – 304, 1940.

[89] Richard F. Grote and James T. Hynes. The stable states picture of chemical reactions. ii. rate constants for condensed and gas phase reaction models. *The Journal of Chemical Physics*, 73(6):2715–2732, 1980.

[90] Eli Pollak. Theory of activated rate processes: A new derivation of kramers' expression. *The Journal of Chemical Physics*, 85(2):865–867, 1986.

[91] Federico J. Hernández and Felipe Herrera. Multi-level quantum rabi model for anharmonic vibrational polaritons. *The Journal of Chemical Physics*, 151(14):144116, 2019.

[92] Johan F. Triana, Federico J. Hernández, and Felipe Herrera. The shape of the electric dipole function determines the sub-picosecond dynamics of anharmonic vibrational polaritons. *The Journal of Chemical Physics*, 152(23):234111, 2020.

[93] Philip M. Morse. Diatomic molecules according to the wave mechanics. ii. vibrational levels. *Phys. Rev.*, 34:57–64, Jul 1929.

[94] Norah M. Hoffmann, Lionel Lacombe, Angel Rubio, and Neepa T. Maitra. Effect of many modes on self-polarization and photochemical suppression in cavities. *The Journal of Chemical Physics*, 153(10):104103, 2020.

[95] Christian Schäfer, Michael Ruggenthaler, Vasil Rokaj, and Angel Rubio. Relevance of the quadratic diamagnetic and self-polarization terms in cavity quantum electrodynamics. *ACS Photonics*, 7(4):975–990, April 2020.

[96] Jorge A. Campos-Gonzalez-Angulo, Raphael F. Ribeiro, and Joel Yuen-Zhou. Resonant catalysis of thermally activated chemical reactions with vibrational polaritons. *Nat Commun*, 10(1):4685, October 2019.

[97] R. A. Marcus. Chemical and electrochemical electron-transfer theory. *Annu Rev Phys Chem*, 15(1):155–196, February 1964.

[98] VG Levich. Present state of the theory of oxidation-reduction in solution (bulk and electrode reactions). *Advances in electrochemistry and electrochemical engineering*, 4:249–371, 1966.

[99] Joshua Jortner. Temperature dependent activation energy for electron transfer between biological molecules. *J Chem Phys*, 64(12):4860–4867, February 1975.

[100] Igor Vurgaftman, Blake S. Simpkins, Adam D. Dunkelberger, and Jeffrey C. Owrutsky. Negligible effect of vibrational polaritons on chemical reaction rates via the density of states pathway. *J. Phys. Chem. Lett.*, 11(9):3557–3562, May 2020.

[101] Matthew Du, Jorge A. Campos-Gonzalez-Angulo, and Joel Yuen-Zhou. Nonequilibrium effects of cavity leakage and vibrational dissipation in thermally-activated polariton chemistry, 2020.

[102] Tao E. Li, Abraham Nitzan, and Joseph E. Subotnik. On the origin of ground-state vacuum-field catalysis: Equilibrium consideration. *The Journal of Chemical Physics*, 152(23):234107, 2020.

[103] Daniel A Steck. Classical and modern optics. course notes available online.

[104] Daniel A Steck. Quantum and atom optics, 2007.

[105] Nur Ismail, Cristine Calil Kores, Dimitri Geskus, and Markus Pollnau. Fabry-Pérot resonator: spectral line shapes, generic and related Airy distributions, linewidths, finesses, and performance at low or frequency-dependent reflectivity. *Optics Express*, 24(15):16366–16389, Jul 2016.

[106] R. Lemus-Casillas and L. Narvaez-Macarro. *Introducción a la teoría de representaciones de grupos con aplicaciones a sistemas moleculares y cristalinos*. Monografías de la Real Academia Sevillana de Ciencias. Real Academia Sevillana de Ciencias, 2006.

[107] E.B. Wilson, J.C. Decius, and P.C. Cross. *Molecular Vibrations: The Theory of Infrared and Raman Vibrational Spectra*. Dover Books on Chemistry. Dover Publications, 2012.

[108] K. Huber. *Molecular Spectra and Molecular Structure: IV. Constants of Diatomic Molecules*. Springer US, 2013.

[109] E. T. Jaynes and F. W. Cummings. Comparison of quantum and semiclassical radiation theories with application to the beam maser. *Proceedings of the IEEE*, 51(1):89–109, 1963.

[110] R. H. Dicke. Coherence in Spontaneous Radiation Processes. *Phys. Rev.*, 93:99–110, 1954.

[111] Michael Tavis and Frederick W. Cummings. Exact Solution for an *N*-Molecule—Radiation-Field Hamiltonian. *Phys. Rev.*, 170:379–384, 1968.

[112] Michael Ruggenthaler, Nicolas Tancogne-Dejean, Johannes Flick, Heiko Appel, and Angel Rubio. From a quantum-electrodynamical light-matter description to novel spectroscopies. *Nat. Rev. Chem.*, 2:0118, March 2018.

[113] A. D. Dunkelberger, B. T. Spann, K. P. Fears, B. S. Simpkins, and J. C. Owrutsky. Modified relaxation dynamics and coherent energy exchange in coupled vibration-cavity polaritons. *Nat Commun*, 7(1):13504, November 2016.

[114] Justin Erwin, Madeline Smotzer, and James V. Coe. Effect of strongly coupled vibration-cavity polaritons on the bulk vibrational states within a wavelength-scale cavity. *J Phys Chem B*, 123(6):1302–1306, February 2019.

[115] Nguyen Thanh Phuc, Pham Quang Trung, and Akihito Ishizaki. Controlling the nonadiabatic electron-transfer reaction rate through molecular-vibration polaritons in the ultrastrong coupling regime. *Scientific Reports*, 10(1):7318, 2020.

[116] Donald G. Truhlar, Bruce C. Garrett, and Stephen J. Klippenstein. Current status of transition-state theory. *J. Phys. Chem.*, 100(31):12771–12800, January 1996.

[117] A. Nitzan. *Chemical Dynamics in Condensed Phases: Relaxation, Transfer and Reactions in Condensed Molecular Systems*. Oxford Graduate Texts. OUP Oxford, 2006.

[118] Christophe L. Vaillant, Manish J. Thapa, Jiří Vaníček, and Jeremy O. Richardson. Semiclassical analysis of the quantum instanton approximation. *J. Chem. Phys.*, 151(14):144111, 2019.

[119] E. Wigner. The transition state method. *Trans. Faraday Soc.*, 34:29–41, 1938.

[120] Peter Hänggi, Peter Talkner, and Michal Borkovec. Reaction-rate theory: fifty years after kramers. *Rev. Mod. Phys.*, 62:251–341, April 1990.

[121] Eli Pollak and Peter Talkner. Reaction rate theory: What it was, where is it today, and where is it going? *Chaos: An Interdisciplinary Journal of Nonlinear Science*, 15(2):026116, 2005.

[122] L. Arnaut and H. Burrows. *Chemical Kinetics: From Molecular Structure to Chemical Reactivity*. Elsevier Science, 2006.

[123] N.E. Henriksen and F.Y. Hansen. *Theories of Molecular Reaction Dynamics: The Microscopic Foundation of Chemical Kinetics*. Oxford Graduate Texts. OUP Oxford, 2018.

[124] Clive Emary and Tobias Brandes. Chaos and the quantum phase transition in the dicke model. *Phys. Rev. E*, 67:066203, June 2003.

[125] M. A. Bastarrachea-Magnani, S. Lerma-Hernández, and J. G. Hirsch. Comparative quantum and semiclassical analysis of atom-field systems. ii. chaos and regularity. *Phys. Rev. A*, 89:032102, March 2014.

[126] V. M. Agranovich and A. G. Malshukov. Surface polariton spectra if the resonance with the transition layer vibrations exist. *Opt Commun*, 11(2):169–171, June 1974.

[127] Kochise Bennett, Markus Kowalewski, and Shaul Mukamel. Novel photochemistry of molecular polaritons in optical cavities. *Faraday Discuss*, 194(0):259–282, 2016.

[128] Maxim Sukharev and Abraham Nitzan. Optics of exciton-plasmon nanomaterials. *J Phys : Condens Matter*, 29(44):443003, October 2017.

[129] Denis G. Baranov, Martin Wersäll, Jorge Cuadra, Tomasz J. Antosiewicz, and Timur Shegai. Novel nanostructures and materials for strong light-matter interactions. *ACS Photonics*, 5(1):24–42, January 2018.

[130] Denan Wang, Maxim V. Ivanov, Saber Mirzaei, Sergey V. Lindeman, and Rajendra Rathore. An electron-transfer induced conformational transformation: from non-cofacial "sofa" to cofacial "boat" in cyclotetraveratrylene (cttv) and formation of charge transfer complexes. *Org Biomol Chem*, 16(31):5712–5717, 2018.

[131] Sujata M. Khopde and K. Indira Priyadarsini. Application of marcus theory of electron transfer for the reactions between hrp compound i and ii and 2,4-disubstituted phenols. *Biophysical Chemistry*, 88(1):103–109, 2000.

[132] Daniel F Walls and Gerard J Milburn. *Quantum Optics*. Springer Berlin Heidelberg, 2008.

[133] Felipe Herrera and Frank C. Spano. Dark vibronic polaritons and the spectroscopy of organic microcavities. *Phys Rev Lett*, 118(22):223601, May 2017.

[134] R. Houdré, R. P. Stanley, and M. Ilegems. Vacuum-field rabi splitting in the presence of inhomogeneous broadening: Resolution of a homogeneous linewidth in an inhomogeneously broadened system. *Phys. Rev. A*, 53:2711–2715, Apr 1996.

[135] L. Mazza, L. Fontanesi, and G. C. La Rocca. Organic-based microcavities with vibronic progressions: Photoluminescence. *Phys. Rev. B*, 80(23):235314, dec 2009.

[136] J-M. Manceau, G. Biasiol, N. L. Tran, I. Carusotto, and R. Colombelli. Immunity of intersubband polaritons to inhomogeneous broadening. *Phys. Rev. B*, 96(23):235301, dec 2017.

[137] E. J. Heller. *The Semiclassical Way to Dynamics and Spectroscopy*. Princeton University Press, 2018.

[138] Gerald M. Sando, Kenneth G. Spears, Joseph T. Hupp, and Peder Thusgaard Ruhoff. Large electron transfer rate effects from the Duschinsky mixing of vibrations. *J Phys Chem A*, 105(22):5317–5325, June 2001.

[139] Joonsuk Huh, Gian Giacomo Guerreschi, Borja Peropadre, Jarrod R. McClean, and Alán Aspuru-Guzik. Boson sampling for molecular vibronic spectra. *Nat Photonics*, 9:615, August 2015.

[140] Adam D. Dunkelberger, Roderick B. Davidson, Wonmi Ahn, Blake S. Simpkins, and Jeffrey C. Owrutsky. Ultrafast transmission modulation and recovery via vibrational strong coupling. *J Phys Chem A*, 122(4):965–971, February 2018.

[141] Fatemeh Mirjani, Nicolas Renaud, Natalie Gorczak, and Ferdinand C. Grozema. Theoretical investigation of singlet fission in molecular dimers: The role of charge transfer states and quantum interference. *J Phys Chem C*, 118(26):14192–14199, July 2014.

[142] Subhajyoti Chaudhuri, Svante Hedström, Dalvin D. Méndez-Hernández, Heidi P. Hendrickson, Kenneth A. Jung, Junming Ho, and Victor S. Batista. Electron transfer assisted by vibronic coupling from multiple modes. *J Chem Theory Comput*, 13(12):6000–6009, December 2017.

[143] R.A. Marcus and Norman Sutin. Electron transfers in chemistry and biology. *Biochimica et Biophysica Acta (BBA) - Reviews on Bioenergetics*, 811(3):265 – 322, 1985.

[144] Daniel T. Gillespie. Stochastic simulation of chemical kinetics. *Annu Rev Phys Chem*, 58(1):35–55, March 2007.

[145] Jonathan Keeling and Peter G. Kirton. Orientational alignment in cavity quantum electrodynamics. *Phys. Rev. A*, 97:053836, May 2018.

[146] Daniel T. Gillespie. Deterministic limit of stochastic chemical kinetics. *J Phys Chem B*, 113(6):1640–1644, February 2009.

[147] David Hagenmüller, Johannes Schachenmayer, Stefan Schütz, Claudiu Genes, and Guido Pupillo. Cavity-enhanced transport of charge. *Phys Rev Lett*, 119(22):223601, November 2017.

[148] Chiao-Yu Cheng, Rijul Dhanker, Christopher L. Gray, Sukrit Mukhopadhyay, Eric R. Kennehan, John B. Asbury, Anatoliy Sokolov, and Noel C. Giebink. Charged polaron polaritons in an organic semiconductor microcavity. *Phys Rev Lett*, 120(1):017402, January 2018.

[149] Charles Möhl, Arko Graf, Felix J. Berger, Jan Lüttgens, Yuriy Zakharko, Victoria Lumsargis, Malte C. Gather, and Jana Zaumseil. Trion-polariton formation in single-walled carbon nanotube microcavities. *ACS Photonics*, 5(6):2074–2080, June 2018.

[150] D.G. Angelakis. *Quantum Simulations with Photons and Polaritons: Merging Quantum Optics with Condensed Matter Physics*. Quantum Science and Technology. Springer International Publishing, 2017.

[151] David Alcaraz Iranzo, Sébastien Nanot, Eduardo J. C. Dias, Itai Epstein, Cheng Peng, Dmitri K. Efetov, Mark B. Lundeberg, Romain Parret, Johann Osmond, Jin-Yong Hong, Jing Kong, Dirk R. Englund, Nuno M. R. Peres, and Frank H. L. Koppens. Probing the ultimate plasmon confinement limits with a van der Waals heterostructure. *Science*, 360(6386):291, 2018-04.

[152] Junyi Lee, Victor Leong, Dmitry Kalashnikov, Jibo Dai, Alagappan Gandhi, and Leonid Krivitsky. Hybrid quantum photonics. Preprint, 2020.

[153] Nicholas V. Proscia, Harishankar Jayakumar, Xiaochen Ge, Gabriel Lopez-Morales, Zav Shotan, Weidong Zhou, Carlos A. Meriles, and Vinod M. Menon. Microcavity-coupled emitters in hexagonal boron nitride. *Nanophotonics*, 9(9):2937–2944, 2020.

[154] VM Agranovich. Dispersion of electromagnetic waves in crystals. *Sov. Phys. JETP*, 10:307–313, 1960.

[155] Y. Kubo, F. R. Ong, P. Bertet, D. Vion, V. Jacques, D. Zheng, A. Dréau, J.-F. Roch, A. Auffeves, F. Jelezko, J. Wrachtrup, M. F. Barthe, P. Bergonzo, and D. Esteve. Strong Coupling of a Spin Ensemble to a Superconducting Resonator. *PRL*, 105(14):140502, 2010-09.

[156] Robert Alicki, Michał Horodecki, Paweł Horodecki, Ryszard Horodecki, Lucjan Jacak, and Paweł Machnikowski. Optimal strategy for a single-qubit gate and the trade-off between opposite types of decoherence. *PRA*, 70(1):010501, 2004.

[157] J. M. Fink, R. Bianchetti, M. Baur, M. Göppl, L. Steffen, S. Filipp, P. J. Leek, A. Blais, and A. Wallraff. Dressed Collective Qubit States and the Tavis-Cummings Model in Circuit QED. *PRL*, 103(8):083601, 2009.

[158] Julia Kabuss, Alexander Carmele, Tobias Brandes, and Andreas Knorr. Optically Driven Quantum Dots as Source of Coherent Cavity Phonons: A Proposal for a Phonon Laser Scheme. *PRL*, 109(5):054301, 2012.

[159] Wildan Abdussalam and Paweł Machnikowski. Superradiance and enhanced luminescence from ensembles of a few self-assembled quantum dots. *PRB*, 90(12):125307, 2014-09.

[160] Marten Richter, Michael Gegg, T. Sverre Theuerholz, and Andreas Knorr. Numerically exact solution of the many emitter–cavity laser problem: Application to the fully quantized spaser emission. *PRB*, 91(3):035306, 2015.

[161] Wonmi Ahn, Igor Vurgaftman, Adam D. Dunkelberger, Jeffrey C. Owrutsky, and Blake S. Simpkins. Vibrational Strong Coupling Controlled by Spatial Distribution of Molecules within the Optical Cavity. *ACS Photonics*, 5(1):158–166, 2018.

[162] Shaul Mukamel and Yuki Nagata. Quantum field, interference, and entanglement effects in nonlinear optical spectroscopy. *Procedia Chemistry*, 3(1):132–151, 2011.

[163] Courtney A. DelPo, Bryan Kudisch, Kyu Hyung Park, Saeed-Uz-Zaman Khan, Francesca Fassioli, Daniele Fausti, Barry P. Rand, and Gregory D. Scholes. Polariton transitions in femtosecond transient absorption studies of ultrastrong light–molecule coupling. *The Journal of Physical Chemistry Letters*, 11(7):2667–2674, 2020. PMID: 32186878.

[164] Bing Gu and Shaul Mukamel. Manipulating two-photon-absorption of cavity polaritons by entangled light. *J. Phys. Chem. Lett.*, 11(19):8177–8182, October 2020.

[165] T. Skrypnyk. General integrable n-level, many-mode Jaynes-Cummings-Dicke models and classical r-matrices with spectral parameters. *Journal of Mathematical Physics*, 56(2):023511, 2015.

[166] T Skrypnyk. Generalized n-level Jaynes–Cummings and Dicke models, classical rational r-matrices and algebraic Bethe ansatz. *Journal of Physics A: Mathematical and Theoretical*, 41(47):475202, 2008.

[167] Yuan-Harng Lee, Jon Links, and Yao-Zhong Zhang. Exact solutions for a family of spin-boson systems. *Nonlinearity*, 24(7):1975, 2011.

[168] T Skrypnyk. Modified n-level, $n - 1$-mode Tavis–Cummings model and algebraic Bethe ansatz. *Journal of Physics A: Mathematical and Theoretical*, 51(1):015204, 2018.

[169] Michael Gegg and Marten Richter. Efficient and exact numerical approach for many multi-level systems in open system CQED. *New Journal of Physics*, 18(4):043037, 2016.

[170] Nathan Shammah, Shahnawaz Ahmed, Neill Lambert, Simone De Liberato, and Franco Nori. Open quantum systems with local and collective incoherent processes: Efficient numerical simulation using permutational invariance. *arXiv preprint arXiv:1805.05129*, 2018.

[171] A.N. Bohr and B.R. Mottelson. *Nuclear Structure (In 2 Volumes)*. World Scientific Publishing Company, 1998.

[172] Dave Bacon, Isaac L. Chuang, and Aram W. Harrow. Efficient quantum circuits for schur and clebsch-gordan transforms. *Phys. Rev. Lett.*, 97:170502, Oct 2006.

[173] P. Jakubczyk, Y. Kravets, and D. Jakubczyk. Entanglement of one-magnon schur-weyl states. *The European Physical Journal D*, 61(2):507–512, 2011.

[174] N. L. Harshman. One-dimensional traps, two-body interactions, few-body symmetries: I. one, two, and three particles. *Few-Body Systems*, 57(1):11–43, 2016.

[175] Hanno Schmiedt, Per Jensen, and Stephan Schlemmer. Unifying the rotational and permutation symmetry of nuclear spin states: Schur-weyl duality in molecular physics. *The Journal of Chemical Physics*, 145(7):074301, 2016.

[176] Dorota Jakubczyk. Application of the schur–weyl duality in the one-dimensional hubbard model. *Reports on Mathematical Physics*, 85(2):293 – 304, 2020.

[177] A.B. Klimov and S.M. Chumakov. *A Group-Theoretical Approach to Quantum Optics: Models of Atom-Field Interactions*. Wiley, 2009.

[178] Robert Gilmore. Geometry of symmetrized states. *Annals of Physics*, 74(2):391–463, 1972.

[179] M.O. Scully and M.S. Zubairy. *Quantum Optics*. Cambridge University Press, 1997.

[180] Marcin Dukalski and Yaroslav M Blanter. High jaynes-cummings pseudospins eigenstates in the homogeneous tavis-cummings model. Preprint, 2013.

[181] V. M. Agranovich, M. Litinskaia, and D. G. Lidzey. Cavity polaritons in microcavities containing disordered organic semiconductors. *PRB*, 67(8):085311, 2003.

[182] G.E. Andrews. *The Theory of Partitions*. Cambridge mathematical library. Cambridge University Press, 1998.

[183] M. Abramowitz and I.A. Stegun. *Handbook of Mathematical Functions with Formulas, Graphs, and Mathematical Tables*. Applied mathematics series. U.S. Government Printing Office, 1970.

[184] P.L. Meliot. *Representation Theory of Symmetric Groups*. Discrete Mathematics and Its Applications. CRC Press, 2017.

[185] B.E. Sagan. *The Symmetric Group: Representations, Combinatorial Algorithms, and Symmetric Functions*. Graduate Texts in Mathematics. Springer New York, 2013.

[186] Wilhelm Specht. Die irreduziblen darstellungen der symmetrischen gruppe. *Mathematische Zeitschrift*, 39(1):696–711, 1935.

[187] C. Kostka. Ueber den zusammenhang zwischen einigen formen von symmetrischen functionen. *Journal für die reine und angewandte Mathematik*, 1882(93):89 – 123, 1882.

[188] Mathias Lederer. A determinant-like formula for the kostka numbers. *arXiv preprint math/0501132*, 2005.

[189] Hariharan Narayanan. On the complexity of computing kostka numbers and littlewood-richardson coefficients. *Journal of Algebraic Combinatorics*, 24(3):347–354, 2006.

[190] J. S. Frame, G. de B. Robinson, and R. M. Thrall. The hook graphs of the symmetric group. *Canadian Journal of Mathematics*, 6:316–324, 1954.

[191] I. Schur. *Über eine Klasse von Matrizen, die sich einer gegebenen Matrix zuordnen lassen*. 1901.

[192] H. Weyl. *The Classical Groups: Their Invariants and Representations (PMS-1)*. Princeton Landmarks in Mathematics and Physics. Princeton University Press, 2016.

[193] The On-Line Encyclopedia of Integer Sequences: Number of partitions of n into nonzero triangular numbers.

[194] Gert Almkvist. Asymptotics of various partitions. *arXiv preprint math/0612446*, 2006.

[195] R W Haase and P H Butler. Symmetric and unitary group representations. i. duality theory. *J. Phys. A: Math. Gen.*, 17(1):61–74, 1984.

[196] P Jakubczyk, T Lulek, D Jakubczyk, and B Lulek. Fourier and schur-weyl transforms applied to XXX heisenberg magnet. *J. Phys. Conf. Ser.*, 213:012018, mar 2010.

[197] Alonso Botero and José Mejía. Universal and distortion-free entanglement concentration of multiqubit quantum states in the *w* class. *Phys. Rev. A*, 98:032326, 2018.

[198] M. D. Gould. Representation theory of the symplectic groups. i. *J. Math. Phys.*, 30(6):1205–1218, 1989.

[199] A. I. Molev. Gelfand-tsetlin basis for representations of yangians. *Lett. Math. Phys.*, 30(1):53–60, 1994.

[200] S Cordero, O Castaños, R López-Peña, and E Nahmad-Achar. A semi-classical versus quantum description of the ground state of three-level atoms interacting with a one-mode electromagnetic field. *J. Phys. A: Math. Theor.*, 46(50):505302, 2013.

[201] Vyacheslav Futorny, Luis Enrique Ramirez, and Jian Zhang. Combinatorial construction of gelfand–tsetlin modules for gln. *Advances in Mathematics*, 343:681–711, 2019.

[202] Jens Peder Dahl and Michael Springborg. The morse oscillator in position space, momentum space, and phase space. *The Journal of Chemical Physics*, 88(7):4535–4547, 1988.

[203] Emanuel F de Lima and José E M Hornos. Matrix elements for the morse potential under an external field. *Journal of Physics B: Atomic, Molecular and Optical Physics*, 38(7):815–825, mar 2005.